Mechanisms of cellular symmetry breaking in *S. cerevisiae*

By

Sarah E. Smith

Submitted to the graduate degree program in Molecular and Integrative Physiology and the Graduate Faculty of the University of Kansas in partial fulfillment of the requirements for the degree of Doctor of Philosophy.

_____
Co-Chairperson Dr. Rong Li, Ph.D.

_____
Co-Chairperson Dr. Paige C. Geiger, Ph.D.

_____
Dr. Matthew Gibson, Ph.D.

_____
Dr. Sue L. Jaspersen, Ph.D.

_____
Dr. Joel W. Schwartz, Ph.D.

_____
Dr. Charlotte M. Vines, Ph.D.

_____
Dr. Michael J. Werle, Ph.D.

Date Defended: June 21, 2013

The Dissertation Committee for Sarah E. Smith
certifies that this is the approved version of the following dissertation:

Mechanisms of cellular symmetry breaking in *S. cerevisiae*

_____
Co-Chairperson Dr. Rong Li, Ph.D.

_____
Co-Chairperson Dr. Paige C. Geiger, Ph.D.

Date approved:
September 6, 2013

ABSTRACT

Cell polarization is vital to diverse biological processes, from maintenance of stem cell identity to chemotaxis of neutrophils. The small GTPase Cdc42 has long been known to be a primary regulator of polarity, but the mechanistic details of how Cdc42 may shift from an isotropic to a polarized distribution, balancing diffusion with targeting in a dynamic system, are not well understood. Here we investigate this question using the budding yeast *S. cerevisiae* as a model system. Yeast polarize via two distinct but coupled mechanisms. Actin-dependent polarization comprises a positive feedback loop wherein Cdc42-dependent nucleation of polarized actin cables leads to a transport of Cdc42 to the polarized site. A standing question in this model was how Cdc42 could maintain concentration in the cap in the presence of membrane flux due to docking and excision of vesicles. Careful imaging revealed a spatiotemporal heterogeneity of Cdc42 distribution at the cap, with peaks corresponding to regions of high exocytosis, low endocytosis, and low diffusion of Cdc42 within the membrane. Mathematical simulation revealed that these microdomains were sufficient to support polarization via the actin pathway in the presence of membrane flux, with concentration of Cdc42 onto vesicles having a lesser impact.

We next sought to gain mechanistic insight into actin-independent polarization, which requires both the guanine nucleotide dissociation inhibitor (GDI) Rdi1, which extracts Cdc42 from the peripheral membrane into a rapidly diffusing cytosolic complex, and the adaptor molecule Bem1, which binds both active $Cdc42^{GTP}$ and its guanine nucleotide exchange factor (GEF) or activator Cdc24. It was thought that Bem1 mediated symmetry breaking through a

positive feedback loop wherein Bem1 recruited Cdc24 to sites of $Cdc42^{GTP}$, upon which Cdc24 would catalyze the activation of additional Cdc42. To critically test the proposed feedback loop, we examined the capacity of cells to undergo actin-independent polarization when specific steps in the loop were disrupted. We found that although binding of Bem1 with the GEF was required, binding of Bem1 with Cdc42 was not required and, strikingly, nor was localization of Bem1 to the polar cap. Using a Cdc42 activation biosensor, we found that Bem1 binding boosts Cdc24 GEF activity. Importantly, expression of a constitutively active GEF partially rescued actin-independent polarization in the Bem1-Cdc24 binding mutant. Wondering if polarization could occur via an Rdi1-dependent mechanism of extraction and targeted deposition in the presence of uniformly activated Cdc42, we turned to mathematical modeling. We found that polarization could indeed occur within a defined range of Rdi1/Cdc42 ratios, which we verified experimentally.

Table of Contents

Chapter 1

Introduction

Portions of this chapter were adapted from
Slaughter, B.D., S.E. Smith, and R. Li, *Symmetry Breaking in the Life Cycle of the Budding Yeast.*
Cold Spring Harbor Perspectives in Biology, 2009. **1** (3).
Only the portions written primarily by Sarah E. Smith were used.

Introduction

Cell polarization, or the establishment of a front-to-back axis, is vital for morphogenesis across a range of systems: chemotaxis of neutrophils, anterior-posterior axis establishment in *C. elegans*, and axon determination in differentiating neurons, to name a few. Although the mechanism of polarity establishment has been a subject of intense study for more than ten years, and many of the molecular players, their interactions, enzymatic activities, targets and regulators have been identified, how these players work together to generate polarity is a complex physical question that has yet to be answered. At its most basic, cell polarization involves the redistribution of cellular components from an isotropic distribution across the cell to an oriented, directional distribution, often involving a massive reorganization of cellular components including the cytoskeleton. How is this switchlike change in morphology initiated? This is the central question that drives the work presented here.

Budding yeast as a model of polarity

The budding yeast *Saccharomyces cerevisiae* presents one of the best model systems for studying cell polarity. A simple, unicellular eukaryote with remarkably tractable genetics, yeast polarize during each cell cycle and in response to pheromone, and serve as an example for the conserved pathways and broader emerging themes of polarity in higher eukaryotes. In this section, I will discuss how themes including regulation by Cdc42, capacity for self-organization through feedback, and the interplay of signaling pathways and the cytoskeleton apply to polarization in budding yeast and in higher eukaryotes. I will then follow in the next section

with a detailed discussion of our current understanding of the mechanisms of polarization in budding yeast specifically.

Cdc42 signaling directs polarization

Considered the master regulator of polarity, Cdc42, was first identified in yeast(Adams et al., 1990) and subsequently shown to be required either for cell polarization *per se* or for spatial regulation of polarity in many eukaryotic organisms(Etienne-Manneville, 2004b). A Rho family GTPase, Cdc42 is thought to act as a molecular switch, cycling between an "on," or GTP-bound state, in which it can interact with effectors, and an "off" or GDP-bound state, in which it is thought to be dormant. The native GTPase cycling rate of Cdc42 is slow, so the activation state of Cdc42 in the cell is thought to be determined by the relative activities of two types of regulators: guanine nucleotide exchange factors (GEF), which stimulate the release of GDP to promote GTP binding and activation, and GTPase activating proteins (GAPs), which accelerate hydrolysis of GTP and promote inactivation. In yeast, Cdc42 has one GEF (Cdc24), and four GAPs (Bem2, Bem3, Rga1, and Rga2). Temporal and positional control of Cdc42 signaling is often mediated through GEF and GAP activities and distribution.

Cdc42 signaling is regulated not only by its activation state but also by its localization. Due to the presence of a gernylgeranyl group at its C-terminus, Cdc42 associates with the plasma membrane, although it can also form a diffusible cytosolic complex with guanine nucleotide dissociation inhibitor (GDI, in yeast Rdi1). It is thought that Cdc42 interacts with effectors only in the membrane-bound fraction, while the GDI-bound fraction may act as a reserve or perhaps play an active role in the dynamic localization of Cdc42 (discussed further below). Total Cdc42

signaling capacity at any location on the membrane is reflective of both concentration and activation state of Cdc42 at that location; as a rule, the key step in polarization is the concentrating of Cdc42 at a specific region of the cell cortex, concurrent with an increase in Cdc42 activation in that region, frequently through coupled mechanisms. In budding yeast, as cells prepare to bud during the G1/S transition, Cdc42 shifts from an isotropic cortical distribution to a polarized cortical distribution, with the majority of Cdc42 focused in a "polar cap" at the nascent bud site. The symmetry breaking of Cdc42 is at the heart of cell polarization, as $Cdc42^{GTP}$ and its effectors direct polarization of the actin cytoskeleton, the secretory pathway, and signaling pathways leading to polarized growth (Fig 1).

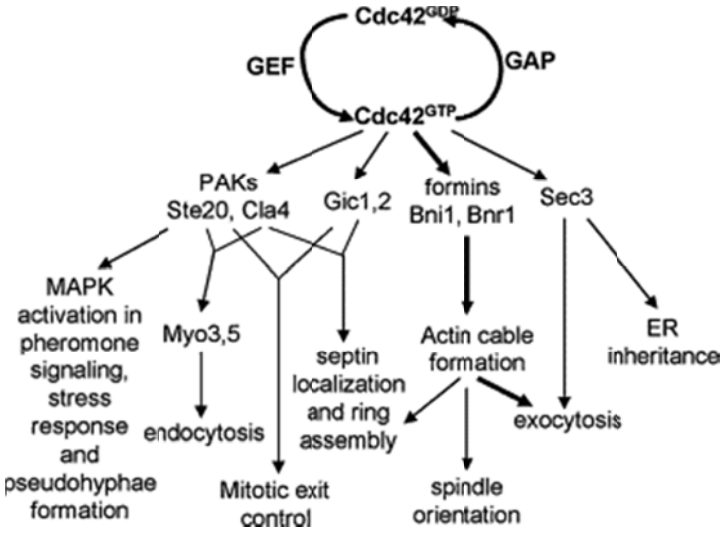

Figure 1. Effectors and downstream pathways controlled by Cdc42 signaling in budding yeast. Polarized activation of Cdc42 initiates myriad downstream events leading to polarized morphogenesis. Thick lines denote actin cable formation and exocytosis, themselves part of the core polarization machinery together with Cdc42. Figure taken from(Wedlich-Soldner and Li, 2008).

The capacity for self-organization

The status of Cdc42 as the "master regulator" of polarity positions it at the nexus of the regulatory signaling upstream and core polarization machinery downstream. It has been

postulated that that pathways for spatial cue recognition evolved convergently to harness intrinsic mechanisms of spontaneous polarization through Cdc42(Wedlich-Soldner and Li, 2008). In budding yeast, polarization and budding usually occur in a defined pattern according to cell type, but cells continue to polarize with equal efficiency (albeit in random orientations) if the spatial cues signaling the budding pattern are removed or cells lose the ability to recognize them. Spontaneous, randomly-oriented polarization is also observed in chemotactic cells such as neutrophils or the slime mold Dictyostelium when exposed to a uniform concentration of chemoattractant. Cue-independent polarization has also been postulated to occur during axon determination in hippocampal neurons *in vitro*(Da Silva and Dotti, 2002), though this hypothesis is controversial, as timelapse imaging revealed the majority of axons to originate from the first emerging neurite in each cell(Calderon de Anda et al., 2008).

The interplay of cytoskeleton and signaling

A final theme in the study of cell polarity is the interplay of cytoskeletal structures and signaling pathways. A hallmark of cell polarity is the reorganization of the actin and/or microtubule cytoskeleton into a polarized configuration directed by GTPase signaling. However, cytoskeletal dynamics likewise contribute to polarity: In *C. elegans* zygotes, the rapid contraction of the cortical actin network upon fertilization is important for anterior-posterior polarity establishment(Munro and Bowerman, 2009), while in hippocampal neurons, depolymerization of the actin network in a single neurite is sufficient to confer axonal identity(Dent et al., 2011). In budding yeast, actomyosin-dependent trafficking of vesicles bearing Cdc42 to the polarized site contributes to cdc42 localization, as discussed below.

Polarization in budding yeast

Polarization is a way of life for budding yeast: following a period of isoptropic growth in the G1 phase, each cell must polarize at the G1/S transition of each cell cycle in preparation for budding (Fig 2). Yeast also must polarize to form a mating projection in response to pheromone. Polarization during vegetative growth is accomplished via at least two coupled mechanisms: One dependent on actin structures, and one independent of actin but requiring the adaptor Bem1 and the guanine nucleotide dissociation inhibitor (GDI) Rdi1.

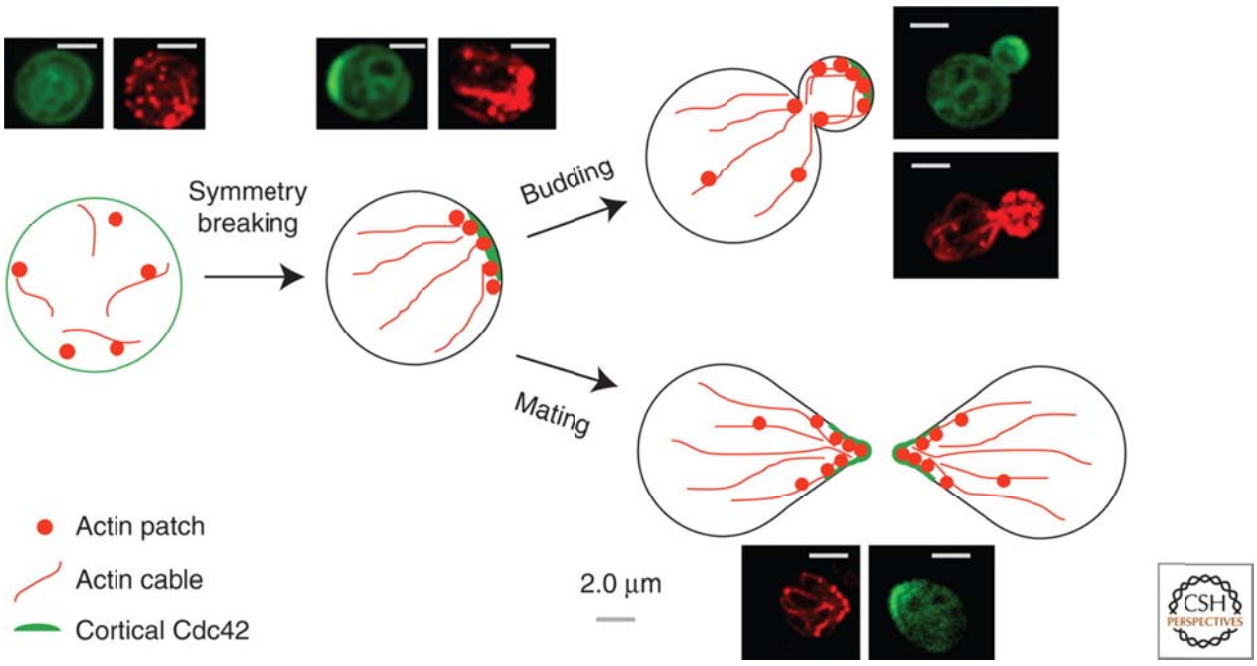

Figure 2. Symmetry breaking processes in the life cycle of budding yeast. Shown are the locations of actin patches, actin cables, and Cdc42 during polarized growth for both cycling cells and cells undergoing pheromone response. In G1 cells, Cdc42 is distributed symmetrically, and the actin cytoskeleton is not

polarized. In response to cell cycle signals or mating pheromone stimulation, Cdc42 and the actin cytoskeleton become polarized: Cdc42 forms a "polar cap" and actin cables become oriented to allow for targeted secretion. Polarized growth further leads to formation of a bud (cell cycle signal) or formation of a mating projection (pheromone signal). Images represent GFP-Cdc42 (green), and rhodamine-phalloidin staining of filamentous actin (red). Figure taken from (Slaughter et al., 2009c).

Symmetry breaking via the actin-dependent positive feedback loop

Yeast cells feature two types of actin structures which figure prominently in polarity: cables and patches(Li and Gundersen, 2008). Actin patches are endocytic structures consisting of networks of branched actin filaments nucleated by the Arp2/3 complex(Pruyne et al., 2004). Actin cables consist of long, unbranched bundles of actin filaments nucleated by formins Bni1 and Bnr1(Evangelista et al., 2002; Pruyne et al., 2004; Sagot et al., 2002). Type V myosins, which travel along actin cables unidirectionally toward actin barbed ends, transport cargoes including exocytic vesicles, mRNAs, and organelles. In this way, actin structures provide the infrastructure necessary for intracellular transport, with cables acting as the transport superhighways while patches acts as the ports where cargo is brought in from the cortex. In polarizing cells, $Cdc42^{GTP}$ works through mechanisms that are not yet well understood to positively regulate both types of actin nucleators at the polar cortex, resulting in the formation of a polarized actin network with patches concentrated near the cap and cables radiating outward from barbed ends at the site of polarized growth(Evangelista et al., 1997b).

While Cdc42 activity is required for the formation of a polarized actin network, actin in turn plays an important role in the polar localization of Cdc42 (Fig 3)(Wedlich-Soldner et al., 2004a). Depolymerization of actin structures due to treatment with the actin polymerization inhibitor Latrunculin A (LatA) results in a reduction in the efficiency and stability of Cdc42

polarization(Wedlich-Soldner et al., 2003a), while treatment with another actin inhibitor, LatB, which appears to preferentially depolymerize actin cables but not patches, results in loss of polarity, an effect that is ameliorated by introduction of defects in endocytosis(Irazoqui et al., 2005). Further, mutations disrupting factors important in cable stability or vesicle transport result in severe polarization defects(Drees et al., 1995; Gao and Bretscher, 2009; Irazoqui et al., 2005; Johnston et al., 1991; Karpova et al., 2000; Liu and Bretscher, 1992; Pruyne et al., 1998; Schott et al., 1999; Wedlich-Soldner et al., 2004a; Zajac et al., 2005). Taken together, these results suggest that the polarity of actin structures and that of their regulator Cdc42 are intimately related: actin polarization requires polarized Cdc42 to direct the formation of the actin network, while Cdc42 may be transported and recycled via actin to achieve its polarized distribution. While these observations are difficult to explain through a linear pathway mindset, they are consistent with a highly cooperative process where Cdc42 and the actin cytoskeleton are mutually enhanced through feedback interactions to achieve an asymmetric organization.

This positive feedback loop is sufficient for symmetry breaking, presumably through amplification of stochastic fluctuations in Cdc42 or actin distribution. This intrinsic mechanism can be best seen in an experimental system in which cells are held in G1 by depletion of G1 cyclins and are induced to express $Cdc42^{Q61L}$, a constitutively active mutant of Cdc42(Butty et al., 2002b; Wedlich-Soldner et al., 2003a). These cells, bypassing both temporal and spatial cues, form polar caps of Cdc42 in an actin and myosin V-dependent manner. Computational modeling further showed that a system of directed feedback (Fig 3) in which $Cdc42^{GTP}$ induced formation of actin cables on which more $Cdc42^{GTP}$ was transported to the initial site, was sufficient to polarize cells(Marco et al., 2007b; Wedlich-Soldner et al., 2003a).

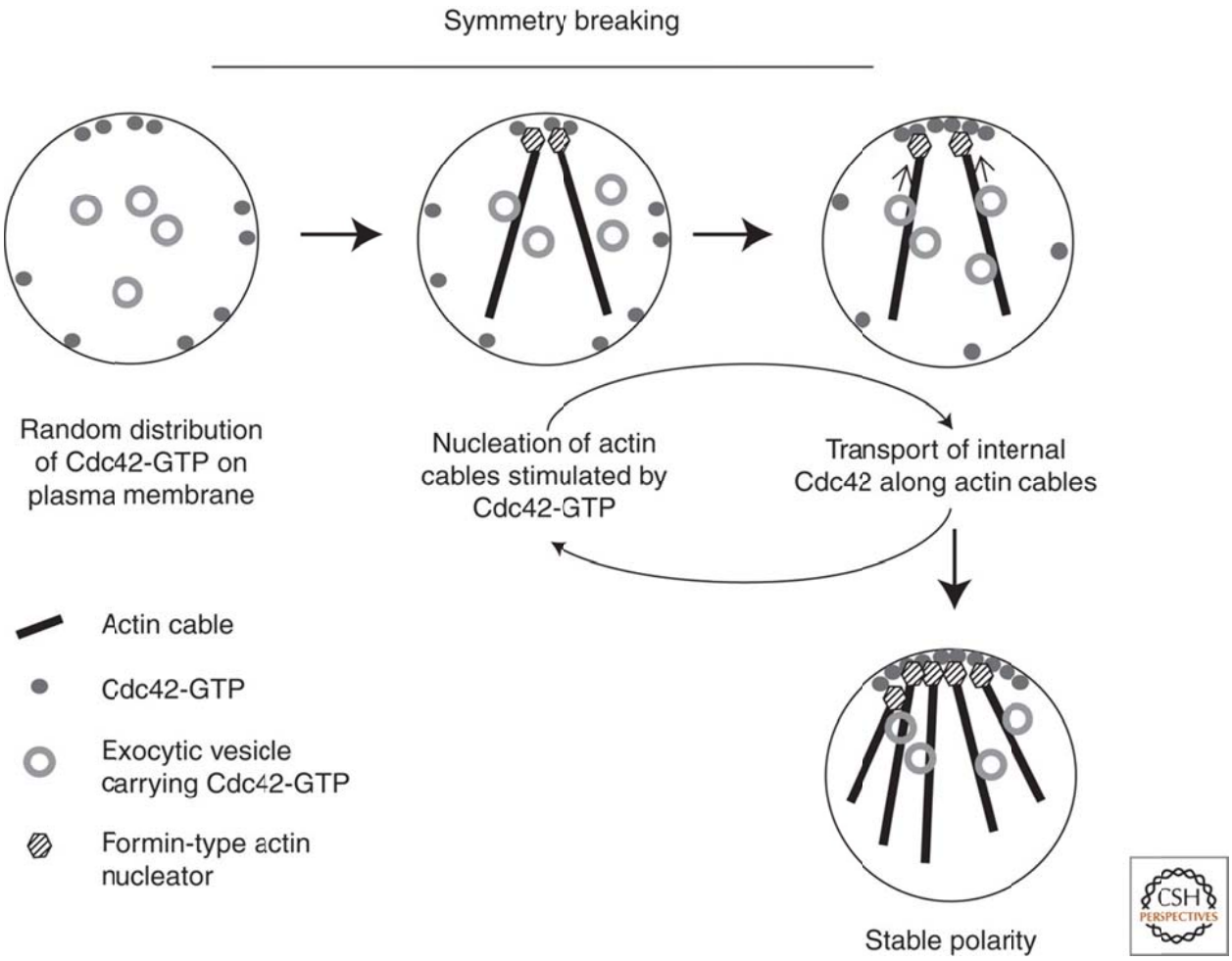

Figue 3. An intrinsic mechanism for symmetry breaking through an actin-dependent positive feedback loop. Initial stochastic accumulation of $Cdc42^{GTP}$ triggers (directly or indirectly) nucleation of actin cables by formin family proteins. This in turn leads to transport of internal Cdc42 to the polarizing site, leading to further nucleation of actin cables. Figure taken from (Slaughter et al., 2009c).

Breaking symmetry without actin

While actin structures are central to polarized cell growth, multiple studies have shown that cells polarize with only slightly reduced efficiency when actin is depolymerized(Wedlich-Soldner et al., 2003a; Wedlich-Soldner et al., 2004a), indicating that there exists a second

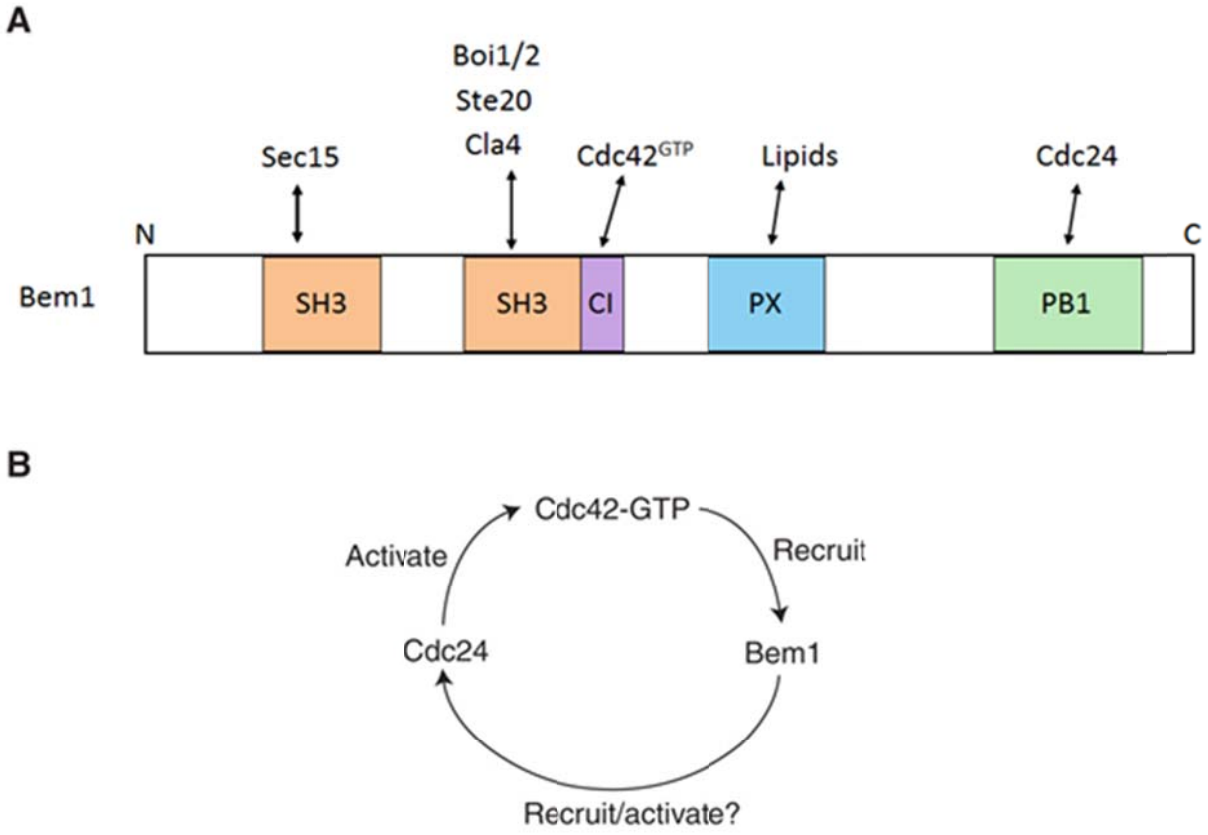

Figure 4. In the absence of actin, cells are able to polarize through a mechanism dependent upon the adaptor protein Bem1. (A) Binding domains and partners of Bem1, including Cdc24, $Cdc42^{GTP}$, and Cdc42 effectors. (B) A proposed signaling feedback loop that involves Bem1, where $Cdc42^{GTP}$ recruits Bem1, which in turn recruits and/or activates Cdc24, leading to localized conversion of $Cdc42^{GDP}$ to $Cdc42^{GTP}$. Figure adapted from (Slaughter et al., 2009c).

mechanism for symmetry breaking. This alternate pathway requires Bem1, a multidomain binding protein sharing structural similarity with the mammalian p47Phox, a component of the NADPH oxidase complex(El-Benna et al., 2009). Bem1 bears two SH3 domains, the COOH-terminal of which interacts with the PAK kinases Cla4 and Ste20(Bose et al., 2001b; Gulli et al., 2000a; Winters and Pryciak, 2005) as well as the adaptor molecules Boi1 and Boi2(Bender et al., 1996); a PX domain which interacts with phospholipids(Stahelin et al., 2007); and a PB1 domain

which interacts with Cdc24(Ito et al., 2001; Zheng et al., 1995a), the lone GEF of Cdc42 in yeast (Fig 4). Bem1 also interacts with $Cdc42^{GTP}$ through a noncanonical interaction of the second SH3 domain and an adjacent region termed the CI(Yamaguchi et al., 2007). Deletion of *BEM1* is not lethal, but *Δbem1* cells are slow growing, temperature sensitive and show significant defects in polarized growth.

Like actin-dependent polarization, Bem1-dependent polarization can occur in the absence of spatial cues, apparently through amplification of a stochastic accumulation of polar components. Dominant models for the amplification process center on the relationship among Cdc24, Bem1, and Cdc42(Butty et al., 2002b; Goryachev and Pokhilko, 2008; Gulli et al., 2000a; Howell et al., 2012; Howell et al., 2009; Irazoqui et al., 2003a; Savage et al., 2012; Shimada et al., 2004b; Yamaguchi et al., 2007). Proper localization of Cdc24 is dependent on Bem1; in cells in which the Cdc24-Bem1 interaction has been disrupted polar localization of Cdc24 is unstable and prematurely lost(Butty et al., 2002b; Gulli et al., 2000b). In turn, polar localization of Bem1 is dependent on Cdc42; Bem1 does not polarize in *cdc42* cells, even when Cdc24 has polarized in response to positional signaling. Bem1 is presumably recruited to the polar cap through its direct interaction with $Cdc42^{GTP}$, as its polarization is independent of other Cdc42 effectors. Finally, Cdc42 activation is dependent on the guanine nucleotide exchange activity of Cdc24. These findings led Butty and coworkers to propose that Cdc24, Bem1, and Cdc42 comprise a positive feedback loop in which Bem1 recruits Cdc24 to sites of active Cdc42, where additional Cdc42 is then activated (Fig 4b)(Butty et al., 2002b). This feedback loop forms the basis for many later proposed models for Bem1-dependent polarization.

Because Bem1 binds both with important members of the polarization establishment machinery and possibly with itself, it was speculated that actin-independent polarization occurs as an aggregation of polar components, with Bem1 acting as a polymeric scaffold(Irazoqui et al., 2003a). However, kinetic data gathered from fluorescence recovery after photobleaching (FRAP) experiments argued against this model(Wedlich-Soldner et al., 2004a): were Bem1 acting as a polymeric scaffold holding its interacting partners at the polarized site, one would expect that fluorescence of labeled Cdc42, Cdc24, and especially Bem1 would recover slowly after bleaching the polar cap. In fact, the opposite is true: the fluorescence recovery of each of these molecules is surprisingly quick ($t_{1/2}$ of a few seconds), with Bem1 recovering most quickly. Moreover, when an area of the cell opposite the polar cap is continuously bleached, Bem1 fluorescence in the cap is rapidly and completely lost(Wedlich-Soldner et al., 2004a). These data strongly suggest that the polar cap is a dynamic structure, with diffusion and targeting of polar components balanced in a rapid and constant flux.

The nature of Cdc24 regulation in polarity remains ambiguous

The polar localization of the GEF Cdc24 is closely tied with Bem1 function. As mentioned above, in cells deleted for Bem1, polar localization of Cdc24 is short-lived compared with wild type cells(Gulli et al., 2000b). The initial polar localization of Cdc24 in the absence of Bem1 may result from its interaction with Rsr1, a Ras-like GTPase that was discovered as part of the bud site selection machinery that links the bud scar signal with the Cdc42 polarization module, and which, like Bem1, physically interacts with Cdc24(Park et al., 1997b). Simultaneous deletion of *BEM1* and *RSR1* has been reported to result in inviability (Kozubowski

et al., 2008), suggesting that the proteins encoded by these genes encode share an essential function, perhaps related to Cdc24 regulation as explored further in this work.

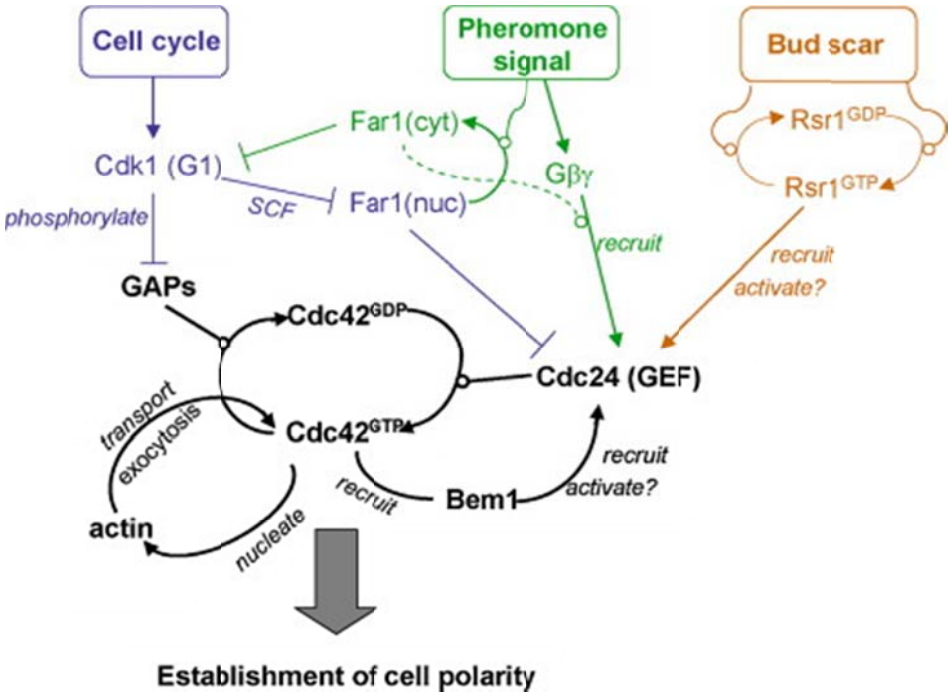

Figure 5. Cdc24 is a conduit for upstream positional and temporal signaling for Cdc42 activation. Cell cycle (purple), mating pheromone (green), and bud scar patterning (orange) signaling pathways are all thought to act on Cdc24. $Cdc42^{GTP}$ may also feed back to Cdc24 through Bem1. Figure taken from (Wedlich-Soldner and Li, 2008).

Several lines of evidence point to Cdc24 as a primary subject of regulation at the initiation of polarization (Fig 5). In haploid cells, Cdc24 is sequestered in the nucleus until the G1-S transition or pheromone response, which result in its release into the cytosol (Nern and Arkowitz, 2000; Shimada et al., 2000), but mutants of Cdc24 that are not sequestered do not prematurely activate Cdc42. In fact Cdc24 is never sequestered in diploid cells (Nern and Arkowitz, 2000), suggesting that there is some other mechanism that regulates its activity.

$Cdc42^{GTP}$, although required for Cdc24 polar localization, is not sufficient as even cytosolic Cdc24 requires cell cycle entry for localization to ectopic caps of active Cdc42 (Wedlich-Soldner et al., 2004a), suggesting that regulation of Cdc24 is upstream of Cdc42. Artificial localization of Cdc24 to the cortex by addition of a myristoylation signal likewise does not result in activity(Shimada et al., 2004c). Conversely, Cdc24 is both recruited to the cortex (albeit uniformly) and activated by expression of the constitutively active $Rsr1^{G12V}$ (Shimada et al., 2004c). Mutagenesis and deletion experiments led to the conclusion that Cdc24 exists in an autoinhibited state due to an intra-molecular interaction between the PB1 domain and the PH-adjacent domain. Since Bem1 interacts with the PB1 domain of Cdc24, this interaction might help relieve the inhibited conformation(Shimada et al., 2004c). How Rsr1 might synergize with this interaction to activate Cdc24 remains unclear: a recent study found that mutations in the NH_2-terminal region of Cdc24 abrogating its ability to bind Rsr1 also prevented binding with Bem1 as well as proper localization(Fujimura-Kamada et al., 2012), although Cdc24 localization defects have not been observed previously in either *rsr1Δ* or other mutants affecting the Rsr1-Cdc24 interaction (although these exhibit random budding)(Park et al., 1997a). Nevertheless this evidence strongly suggests GEF activation and membrane recruitment of Cdc24 are highly coupled processes that involve interactions with Bem1 and Rsr1.

Another potential mechanism of Cdc24 regulation is phosphorylation. Cdc24 is hyperphosphorylated in a cell cycle dependent manner, in a process which requires the formation of a tertiary complex containing Cdc24, Bem1, $Cdc42^{GTP}$, and Cla4, a PAK kinase(Bose et al., 2001a). The purpose of Cdc24 hyperphosphorylation is unknown, and has been proposed both to be inhibitory(Gulli et al., 2000b) and to be activating(Bose et al., 2001a). Gulli and

colleagues found that expression of a kinase-dead version of Cla4 resulted in hyperpolarized cells, that overexpression of Cla4 resulted in loss of hyperpolarization of *cdc34-2* cells, and that Bem1 bound preferentially with the unphosphorylated form of Cdc24 as detected by immunoblot and antibody staining. These and other results led them to propose a model in which phosphorylation of Cdc24 by Cla4 led to dissociation of Cdc24 from Bem1 and subsequent redistribution of Cdc24 away from the polar cortex(Gulli et al., 2000b). In contrast, Bose and colleagues found that Bem1 complexed with Cdc24 phosphoforms proportionately to those found in the cell lysate as detected by immunoblot of epitope-tagged proteins(Bose et al., 2001a). This group went on to show that the interaction of Bem1 with a functional PAK kinase was required for viability in *rsr1Δ* cells in one genetic background(Kozubowski et al., 2008), presumably due to the requirement of this complex for Cdc24 phosphorylation, and that synthetic lethality of *bem1Δ rsr1Δ* was rescued by expression of a chimeric construct of $Cdc24^{\Delta PB1}$ fused with Cla4. The latter result is difficult to interpret, however, as $Cdc24^{\Delta PB1}$ has been proposed to be constitutively active, and Cla4, as an effector of Cdc42, could function to ectopically localize the GEF to the polar cap. Phosphorylation may turn out to be a weak regulator of Cdc24 activity if at all, as identification and mutagenesis of more than 30 putative in vivo Cdc24 phosphorylation sites returned no distinguishable phenotype(Wai et al., 2009).

Rdi1, an emerging player in actin-independent polarization

Another required player in actin-independent polarization is the Cdc42 Guanine nucleotide Dissociation Inhibitor (GDI) Rdi1(Freisinger et al., 2013; Slaughter et al., 2009b). Like Rho GDIs found in mammalian cells, Rdi1 bears a hydrophobic pocket which shields the prenyl group at the C-terminus of Cdc42 during binding, preventing targeting of Cdc42 to the

membrane and maintaining it as a diffusible cytosolic complex(DerMardirossian and Bokoch, 2005; Johnson et al., 2009). GDIs are often thought of as a negative regulator of GTPase signaling, as GDI binding is generally high affinity (Kd ~ 1.6-30 nM)(Gosser et al., 1997; Nomanbhoy and Cerione, 1996), with binding sites overlapping those of GEFs, GAPs and effectors; thus the GDI-bound pool of Cdc42 could be considered an inactive reserve, held in the cytosol away from the center of Cdc42 signalling at the cortex(DerMardirossian and Bokoch, 2005). Rdi1 overexpression experiments in yeast, which lead to high levels of cytosolic Cdc42 coupled with polarization defects and poor growth, support this idea(Das et al., 2012b; Richman et al., 2004). However, recent work in yeast has shown that deletion of Rdi1, while not adversely affecting growth, dramatically reduces the rate of Cdc42 recycling at the polar cap and (as mentioned above) abrogates actin-independent polarization, suggesting that Rdi1 plays an active role in Cdc42 targeting that is parallel to the mechanism for the secretory pathway(Das et al., 2012b; Freisinger et al., 2013; Slaughter et al., 2009b). This hypothesis could explain some puzzling findings in the effort to understand GDI function in mammalian cells: Knockout of RHOGDI in mice has only a mild phenotype(Togawa et al., 1999), however, the ability of a fast cycling mutant of Cdc42 (Phe28Leu) to accumulate in the plasma membrane and induce oncogenic transformation of cells was dependent on its ability to bind GDI(Lin et al., 2003). The mechanism for how Rdi1 could contribute to targeting is not well understood. Biochemical data suggests that GDI has higher affinity for GTPases in the GDP-bound state(Johnson et al., 2009), suggesting that GDIs may passively facilitate targeting directed by GAP and GEF (this hypothesis has been incorporated into several mathematical models, as discussed in the following section). Alternatively, the existence of a GDI Dissociation Factor

(GDF) has been proposed, which would act on the GDI-Cdc42 complex to break it apart and induce membrane binding of Cdc42 in a targeted location, and could take the form of a variety of mechanisms including lipid signaling, phosphorylation, or GEF activity(Garcia-Mata et al., 2011).

Mathematical modeling, a critical tool in the study of cell polarity

Actin-independent symmetry breaking may result from a Turing-type mechanism of positive feedback

It is puzzling to consider how symmetry breaking might occur in the absence of a fixed scaffold, the directed feedback of actin, or any other type of physical marker. Such a scenario, as is found in actin-independent polarization, creates difficulty in forming an intuitive understanding of mechanistic models. In this case computational modeling has proven an invaluable tool for testing the feasibility of models and for suggesting future experiments. Recent studies have applied the basic ideas first proposed by Alan Turing in 1952(Turing, 1952), that in a dynamic system, symmetry breaking could occur as a result of a local positive feedback loop paired with global inhibition. Gorachev and Pokhilko took a bottom-up approach, generating a system of eight equations which included a range of assumptions based on experimental data(Goryachev and Pokhilko, 2008). In this model, the GTPase activity was explicitly included, and the Cdc24-Bem1-Cdc42 loop served as the central source for positive feedback (Fig 6A-D). $Cdc42^{GDP}$ but not $Cdc42^{GTP}$ was allowed to recycle through the cytosol due to an assumed differential interaction with Rdi1. Global inhibition was included in the form of a generalized GAP. Thus a stochastic accumulation of $Cdc42^{GTP}$ would recruit Bem1 and Cdc24, which in turn would

convert neighboring $Cdc42^{GDP}$ to $Cdc42^{GTP}$. This growing population of $Cdc42^{GTP}$ would be confined to diffuse slowly within the membrane, but molecules which diffused away from the central population of Cdc24 would be more likely to be converted by GAP to $Cdc42^{GDP}$ and join the quickly recycling cytosolic pool. Those cytosolic molecules which were randomly deposited at the polarized site would be quickly converted to slowly diffusing $Cdc42^{GTP}$, while those deposited elsewhere would remain part of the fast recycling pool. In this way, the polarized site acts as a sink for $Cdc42^{GDP}$, resulting in a net flux of molecules from the cytosol to the site which offsets diffusion of membrane-bound molecules away from the site. This model is appealing because it provides an explanation for the requirement for Cdc42 GTPase activity in actin-independent polarization, but the central assumption that active but not inactive Cdc42 is confined to diffuse within the membrane has yet to be experimentally confirmed. Indeed, both GDP- and GTP- locked mutants of Cdc42 show low cytosolic pools and are unable to polarize independently of actin. Subsequent work by the Lew research group(Howell et al., 2009; Savage et al., 2012) refined the Goryachev model using parameter value estimates based on in vitro assays. Comparing kinetic predictions of the model with FRAP measurements taken *in vivo*, Savage and colleagues found that the Goryachev model could only match observation if the rate of GDI-based recycling were an order of magnitude higher than measured, a difference they attributed to uncharacterized regulatory mechanisms affecting the GDI. In this work, we contrast the Goryachev model with a simple analytical model incorporating Cdc42 recycling via GDF-directed feedback.

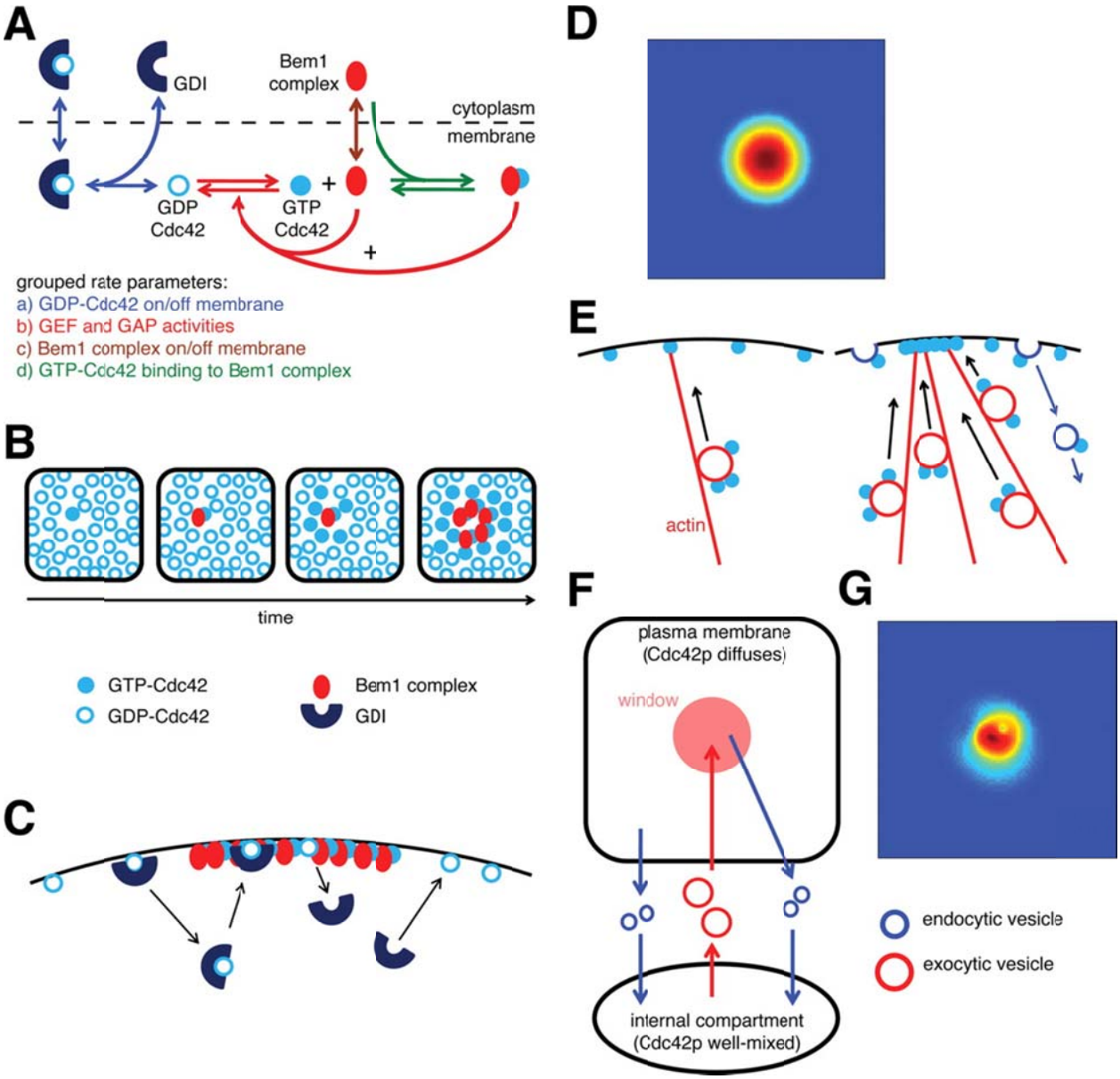

Figure 6. Model schematics for Bem1-dependent polarization (Goryachev reaction-diffusion model) and actin-dependent polarization with membrane flux (Layton model). (A) Schematic of the reaction-diffusion model. +,positive feedback. (B) Positive feedback "grows" a cluster of $Cdc42^{GTP}$. Stochastically arising $Cdc42^{GTP}$ recruits Bem1p complexes from the cytoplasm, promoting GTP loading of neighboring Cdc42, and hence more Bem1p recruitment. (C) Cytoplasmic delivery of $Cdc42^{GDP}$ to the polarity patch via GDI. GDI extracts $Cdc42^{GDP}$ from the membrane to the cytoplasm, and returns it to the membrane. If GDI delivers $Cdc42^{GDP}$ to the polarity patch, Cdc42 becomes GTP-bound and thus protected from GDI removal, so the GDI mediates a net transfer of Cdc42 from outside to inside the cluster. (D) The square represents the plasma membrane, and the color indicates Cdc42 concentration (red, high; blue, low). A simulation of the scheme shown in (A) combined with diffusion was initiated with a small $Cdc42^{GTP}$ stimulus in the center of the membrane and developed the steady-state Cdc42p distribution shown. (E) Actin-mediated feedback loop. Cdc42p at the plasma membrane can nucleate an actin cable, which delivers vesicles carrying more Cdc42p to that site. The delivered Cdc42 can nucleate more actin cables,

which deliver more vesicles containing Cdc42, growing a cluster of Cdc42. Endocytosis (blue arrows) returns Cdc42 to internal pools before it diffuses too far from the cluster. (F) Schematic of the vesicle-trafficking model. (G) A simulation of the scheme shown in (F) with traffic of vesicles carrying concentrated Cdc42p to/from a small central window yielded a fluctuating but polarized Cdc42 distribution (snapshot shown). Figure and legend taken from(Savage et al., 2012)

Modeling membrane flux in actin-dependent polarization

Mathematical modeling has highlighted a gap in our understanding of the mechanism for actin-dependent polarization: How do cells manage the flux of membrane from exocytic vesicles into the cap and out through endocytic vesicles? The original proposal for the actin-dependent mechanism included a simple conceptual model with mass-conserved Cdc42 showing the feasibility of polarization via directed feedback(Wedlich-Soldner et al., 2003a). The mechanism was supported by further modeling which incorporated parameter measurements made *in vivo*, and which made experimentally verified predictions that FRAP rate should be faster when both the actin-dependent and –independent mechanisms were functional than with either mechanism alone(Marco et al., 2007b; Slaughter et al., 2009b). A drawback to these models is that they accounted only for Cdc42 flux from vesicles, but not membrane flux. Layton and colleagues sought to remedy this omission with a model accounting for membrane flux(Layton et al., 2011a), and predicted that if Cdc42 was not concentrated on vesicles, then exocytosis would act to dilute rather than concentrate Cdc42 at the cap. Even if Cdc42 was concentrated onto vesicles, depletion of the internal pool of Cdc42 would ultimately lead to cap disruption and dissipation. Further, they predicted that the diluting effect of vesicle delivery could contribute to increased FRAP rate by effectively increasing diffusion of Cdc42 out of the cap and decreasing steady state concentration of Cdc42 at the cap(Savage et al., 2012). These findings led to the conclusion that actin-dependent recycling could not positively contribute to

polarization. However, extensive evidence supports the importance of actomyosin transport and polarized secretion in polarization, and the prediction that Cdc42 concentration in the cap should be higher when actin-dependent recycling is disrupted is contrary to experimental observation(Freisinger et al., 2013). These seemingly conflicting results indicate that there is a missing piece to the puzzle of the mechanism for actin-dependent polarization. In this work we use careful imaging to examine dynamics of Cdc42 within the cap, paired with mathematical simulation to identify the gap in our understanding.

Coupled feedback mechanisms pair responsiveness with robustness

It is somewhat surprising that two mechanisms exist for the establishment of polarity in yeast cells, when it seems that either one would be sufficient to do the job on its own. Computational modeling provides a possible explanation for this apparent redundancy (Brandman et al., 2005): Interlinked fast and slow positive feedback loops result in a bistable switchlike system that responds quickly to stimulus yet is robust against noise. This model is consistent with what is seen *in vivo*: When the Bem1 is mutated, polarization is delayed but the resulting polar caps are stable, while when the actin-dependent loop is blocked, polar caps form quickly but drift and flicker(Wedlich-Soldner et al., 2004a), or disappear(Irazoqui et al., 2005). This suggests that actin mediates a slow loop that provides stability, while the faster actin-independent loop provides responsiveness to temporal and possibly also spatial signals.

Spatial cues in bud site patterning

Polarization can be harnessed by spatial patterning cues

Although yeast cells are able to break symmetry in spontaneous orientations, endogenous polarization in yeast cells normally occurs in an ordered pattern directed by sites of previous cell division (bud scars), according to cell type. Haploid cells (of both mating types A and α) bud in an axial pattern, forming a polar cap immediately adjacent to the site of the previous cell

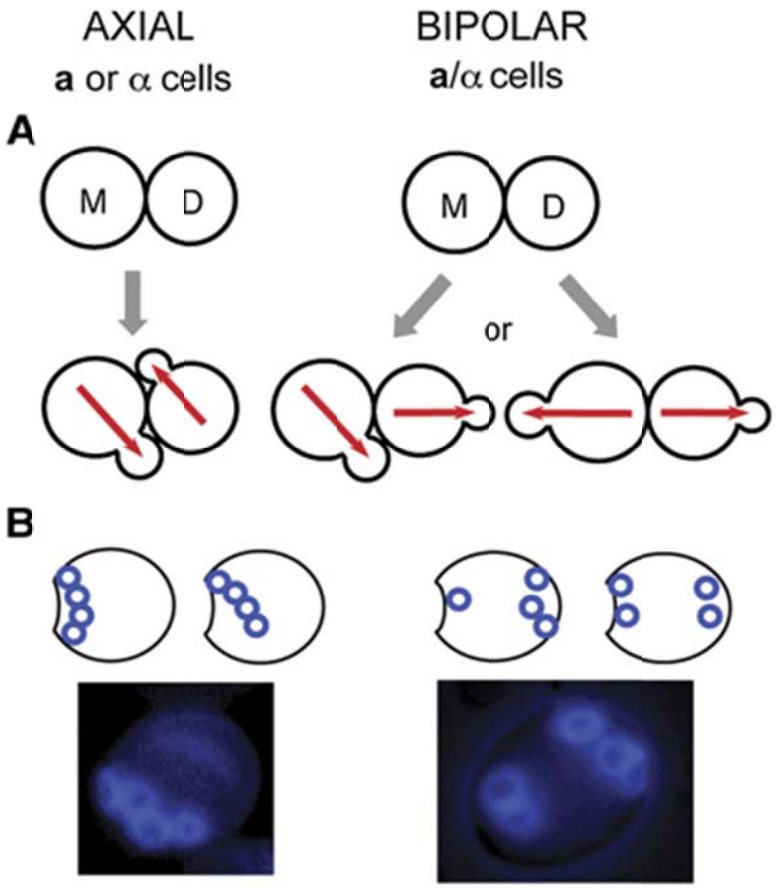

Figure 7. Modes of bud scar patterning in budding yeast. A**)** Axes of polarization (red arrows) guided by axial and bipolar patterning cues. "M" denotes mother cell and "D" daughter cell or bud. (B) Resulting patterns of bud scars (blue circles) relative to birth scars (crescent indentations on left side of cells). Below are shown images of bud scar patterns visualized by Calcofluar staining. Figure taken from (Bi and Park, 2012).

division such that bud scars frequently appear in a chain (Fig 7). Diploid (mat A/α) cells bud in a bipolar pattern, with daughter cells budding distally from the birth scar (the site of division from the mother) while mother cells bud either opposite from or proximal to the most recent bud scar.

Axial patterning

Axial and bipolar patterning each involves a unique set of membrane-associated proteins, thought to be laid down as an enduring (in bipolar patterning) or transient (in axial budding) spatial landmark of each budding cycle prior to cytokinesis. Mutations in any of the genes *BUD3*, *BUD4*, *AXL1*, or *AXL2* result in disruption of axial patterning and adoption of bipolar patterning(Chant and Herskowitz, 1991; Chant et al., 1995; Roemer et al., 1996; Sanders and Herskowitz, 1996). Of these, only Axl1 is expressed exclusively in haploid cells(Fujita et al., 1994). The peripheral membrane proteins Bud4 and Bud3, a noncanonical GTP-binding protein and GEF respectively(Kang et al., 2012), localize as a double ring encircling the mother-bud neck, persisting as single rings following cytokinesis. Bud3/4 localization is dependent on septins(Kang et al., 2013), and both Bud4-GTP and Axl1 are required for localization of Axl2, an integral membrane protein delivered to the cortex via the secretory pathway(Roemer et al., 1996). The extensive O-glycosylation on the extracellular domain of Axl2 may allow it to interact with the cell wall, limiting diffusion to maintain integrity of the landmark(Sanders et al., 1999). Axl2 associates with the Rsr1 GEF Bud5, linking the axial landmark to the polarization pathway (discussed below)(Kang et al., 2001).

Bipolar patterning

Bipolar (but not axial) patterning is disrupted by mutations in any of the genes *BUD8*, *BUD9*, *RAX1*, or *RAX2*, all encoding integral membrane membrane proteins(Fujita et al., 2004; Kang et al., 2004a; Zahner et al., 1996). Mutations in *BUD8* or *BUD9* disrupt budding only at the distal or proximal pole (relative to the birth scar), respectively, suggesting that these genes encode proteins key to spatial cues at those poles(Zahner et al., 1996). Rax1 and Rax2 localize to the bud tip (leading to demarcation of the distal pole) and as a ring at the site of cell division (marking the bud scar and proximal pole) following cytokinesis(Kang et al., 2004a). Rax1 and Rax2 are overturned slowly such that old cells with many bud scars may maintain rings of Rax1 and Rax2 at each of the scars. Rax1 is required for localization of Bud8 and Bud9 to the poles, and interacts closely with Rax2, perhaps as a complex(Kang et al., 2004a). Both Bud8 and Bud9 physically interact with Bud5(Kang et al., 2004b); it is not well understood how these molecules work in concert to direct polarization specifically toward one pole or the other.

Transmission of the landmark signal to the polarization machinery

Proper bud site patterning involves transmission of spatial signals from the site of the previous cell division to the Cdc42 polarization module, to bias cellular symmetry breaking toward a new site distinct from the origin of the signaling(Wedlich-Soldner and Li, 2008). Formation of a polar cap directly on top of existing bud scars is prevented by the Cdc42 GAP Rga1, which is thought to mitigate Cdc42 activation at those sites(Tong et al., 2007). It is not well understood how spatial signaling is translated from the bud scar landmark to the distinct site. Both axial and bipolar patterns require the Ras-like GTPase Rsr1, its GEF Bud5 and its GAP

Bud2. Deletion of any of these components, overexpression of Bud5 or expression of constitutively active $Rsr1^{G12V}$ all result in random budding. Bud5 localizes as a ring to sites of cell division and, in bipolar patterning, to a patch on the distal poles of both mother and daughter cells, while Rsr1 localizes to sites of polarized growth, persisting at the division site after cytokinesis. Upon formation of the polar cap, however, Rsr1, Bud5, and Bud2 all localize to the cap suggesting, together with the requirement for Rsr1 in both budding patterns, that Rsr1 may be key to translating the static landmark into the spatial signal for the new polarized site, albeit through unknown mechanisms.

The Rsr1 GTPase module has traditionally been considered exclusively as a member of the spatial cue signaling pathway for bud site patterning, however, several pieces of evidence suggest it may have a larger role in polarization *per se* (Bi and Park, 2012). Rsr1 interacts directly with Cdc42 as well as Cdc24 and Bem1(Kozminski et al., 2003; Park et al., 1997a); Overexpression of Rsr1 suppresses the temperature-sensitive growth of the Cdc24 mutant cdc24-4(Bender and Pringle, 1989) or the Cdc42 mutant cdc42-118(Kozminski et al., 2003); and cells lacking Rsr1 as well as the Cdc42 effectors Gic1 and Gic2 fail to form a bud(Kawasaki et al., 2003). Further, timelapse imaging has revealed that loss of Rsr1 results in caps that are unstable, fluctutating in space and in time(Howell et al., 2012; Ozbudak et al., 2005).

The distinction of whether Rsr1 is involved in polarization or simply in spatial patterning is important because RSR1 deletion is commonly used as a background for the study of cellular symmetry breaking in the absence of spatial cues. Numerous studies have interpreted lethal genetic interactions of rsr1Δ with mutations in BEM1 as being indicative of a requirement for Bem1 in spatial cue-independent polarization(Howell et al., 2012; Irazoqui et al., 2003a;

Kozubowski et al., 2008). If Rsr1 has a role in polarization, it is possible the synthetic interaction is due to a deficiency in polarization rather than in spatial signaling. In this work we compare polarization phenotypes in cells with *RSR1* deleted with cells with deleted for the upstream spatial landmarks *AXL2* and *RAX1*.

Goals of this work

Upon beginning my thesis study, it was clear that polarization in yeast was accomplished via two concurrent mechanisms, one dependent on actin structures and one actin-independent. Both mathematical modeling and experimental evidence supported the existence of an actin-dependent feedback loop for Cdc42 polarization wherein active $Cdc42^{GTP}$ signals nucleation of polarized actin cables, upon which more Cdc42 is transported to the polarized site. However, several mechanistic details essential to the feasibility of the model remained unclear: Is Cdc42 concentrated onto exocytic vesicles to allow feedback of Cdc42 to the polar cap? How is the flux of membrane from exocytic vesicles, through the cortex and out through endocytosis prevented from having a dilutive effect on the Cdc42 concentration at the cap? These questions are the central focus of Chapter 2 of this dissertation, "Non-Uniform Membrane Diffusion Enables Steady-State Cell Polarization via Vesicular Trafficking."

Polarization via the actin-independent loop was thought to occur via a Bem1-dependent mechanism wherein $Cdc42^{GTP}$ recruited Bem1 in complex with the GEF Cdc24, allowing further Cdc42 to be activated in the region. This model was supported by the finding that Bem1 is required for actin-independent polarization and for proper localization of Cdc24. Mathematical modeling supported the feasibility of the mechanism when combined with Rdi1 recycling of

inactive but not active Cdc42. However, the model was based largely on genetic interactions of *BEM1* with Ras-like GTPase *RSR1*, which, though interpreted as to signify a requirement for Bem1 for polarization in the absence of spatial cues, could have alternate explanations. In Chapter 3, "Independence of symmetry breaking on Bem1-mediated autocatalytic activation of Cdc42," we critically test the proposed Bem1-mediated feedback loop in actin-independent conditions. We also examine the role of Rsr1 in polarization and the relationship of spatial cues with the Bem1 pathway. Finally, we use mathematical modeling to test the feasibility of polarization without localized activation of Cdc42 when Rdi1 recycling is targeted back to the cap.

Chapter 2.

Non-uniform membrane diffusion enables steady-state cell polarization via vesicular trafficking

Brian D. Slaughter[1*], Jay R. Unruh[1*], Arupratan Das[1], Sarah E. Smith, Boris Rubinstein[1], and Rong Li[1,2]

[1] Stowers Institute for Medical Research, 1000 East 50th Street, Kansas City, MO 64110

[2] Department of Molecular and Integrative Physiology, University of Kansas Medical Center, 3901 Rainbow Boulevard, Kansas City, KS 66160

* These authors contributed equally

Author contributions: Sarah E. Smith performed TIRF experiments. Arupratan Das performend experiments with Lact-C2-GFP probe. Brian D. Slaughter and Jay R. Unruh performed all other experiments. Brian D. Slaughter and Jay R. Unruh analyzed data with help from Sarah E. Smith and Arupratan Das. Jay R. Unruh wrote and performed the simulations. Boris Rubinstein developed the analytical model. Brian D. Slaughter, Jay R. Unruh, and Rong Li wrote the manuscript, with help from Sarah E. Smith. Rong Li conceived of and led the project.

Abstract

Actin-based vesicular trafficking of Cdc42, leading to a polarized concentration of the GTPase, has been implicated in cell polarization, but it was recently debated whether this mechanism allows stable maintenance of cell polarity. In this study, we show that endocytosis and exocytosis are spatially segregated in the polar plasma membrane, with sites of exocytosis correlating with microdomains of higher concentration and slower diffusion of Cdc42 compared to surrounding regions. Numerical simulations using experimentally obtained diffusion coefficients and trafficking geometry revealed that non-uniform membrane diffusion of Cdc42 in fact enables temporally sustained cell polarity. We show further that phosphatidylserine (PS), a phospholipid recently found to be crucial for cell polarity, is enriched in Cdc42 microdomains and weakening a potential interaction between PS and Cdc42 enhanced Cdc42 diffusion in the microdomains but impeded the strength of polarization. These findings demonstrate a critical role for membrane microdomains in vesicular trafficking mediated cell polarity.

Introduction

The actin cytoskeleton and vesicular trafficking play crucial roles in cell polarization in a variety of systems from mammalian epithelial cells and *Drosophila* oocytes to plant pollen tubes(Cheung and Wu, 2008; Mullins, 2010; Orlando and Guo, 2009). The Rho-family GTPase Cdc42 is a highly conserved regulator of cytoskeleton organization and cell polarity(Etienne-Manneville, 2004a). A mechanism of cell polarization identified in the budding yeast *Saccharomyces cerevisiae* entails a positive feedback loop between Cdc42-stimulated actin assembly and actomyosin-based vesicular trafficking of Cdc42(Slaughter et al., 2009d; Wedlich-Soldner et al., 2003b), which results in spontaneous symmetry breaking and concentration of Cdc42 to a small patch of the plasma membrane (PM) at one end of the cell, often referred to as the polar cap. The polar cap marks the site for cell surface growth that leads to bud or shmoo formation(Park and Bi, 2007b), and its maintenance is facilitated by active endocytic recycling to counter membrane diffusion of Cdc42(Marco et al., 2007a; Slaughter et al., 2009a).

An analytical model with the assumption of balanced Cdc42 flux and mass conservation demonstrated the existence of a steady-state solution for this system of cell polarity(Marco et al., 2007a; Slaughter et al., 2009a). However, a surprising finding was reported in a recent study with a discrete simulation of Cdc42 trafficking that considered not only the protein dynamics but also insertion and excision of membrane patches through exocytic and endocytic events, respectively(Layton et al., 2011b). The simulations showed that in order for vesicular trafficking to establish a polar cap of Cdc42, Cdc42 must be concentrated on exocytic vesicles relative to the internal source membrane. However, even under this condition, the model

predicted that continued vesicle trafficking would deplete the internal pool over time. At this stage polarized exocytosis would dilute Cdc42 in the PM due to continual membrane insertion with low Cdc42 concentration, eventually leading to a dissipated polar cap. This result implies the implausibility of a stable polarized state through the vesicle trafficking-based mechanism.

In considering the dramatic difference in theoretical predictions with or without the discrete account of membrane dynamics and conservation, we reasoned that it was possible that crucial details were unknown and thus unaccounted for in the discrete model depicting exocytic and endocytic events. To this end, we performed dual-color confocal imaging using a highly sensitive single photon detector to investigate the spatiotemporal relationship between the dynamic Cdc42 distribution and the sites of endocytosis and exocytosis. In order to restrict our investigation to the membrane-based mechanism for polarized localization of Cdc42, experiments were performed in *Δrdi1* cells, lacking the yeast guanine nucleotide dissociation inhibitor (GDI). In this mutant background Cdc42 does not exchange rapidly between the cytosol and membrane compartments and cell polarity is actin-dependent(Slaughter et al., 2009a). In other words, this work addresses solely the feasibility of cell polarization through actin-based membrane trafficking, but not a redundant, cytosolic Cdc42 targeting pathway (Irazoqui et al., 2003b; Slaughter et al., 2009d; Wedlich-Soldner et al., 2004b). Below we present evidence not only that endocytosis and exocytosis of Cdc42 occur in spatially separate regions of the PM but also that Cdc42 diffusion in these regions is considerably different, resulting in microdomains with locally concentrated Cdc42. Contributing to Cdc42's slow diffusion in specific areas is the phospholipid phosphatidylserine (PS), which has been shown to be trafficked with secretory vesicles in yeast and is required for robust cell polarity(Fairn et al.,

2011). Modeling and experimental analyses demonstrate that these features, especially non-uniform Cdc42 diffusion, play important roles in stable maintenance of cell polarity maintained through membrane-based recycling.

Results

Spatial organization of Cdc42 at the PM

To determine the spatial organization of Cdc42 recycling at the PM, we first imaged GFP-Cdc42 with mCherry-tagged Myo5, which marks the sites of endocytosis immediately before endocytic internalization(Jonsdottir and Li, 2004). As expected endocytic patches are in general concentrated in the polar cap region, as demonstrated by a time series projection (**Fig 1, Fig. S1**). By confocal imaging using a highly sensitive detector (APD), instantaneous localization of Cdc42 within the polar cap was found to be heterogeneous, and exhibited dynamic and discrete puncta within the polar cap. Imaging with total internal reflection fluorescence (TIRF) microscopy showed these

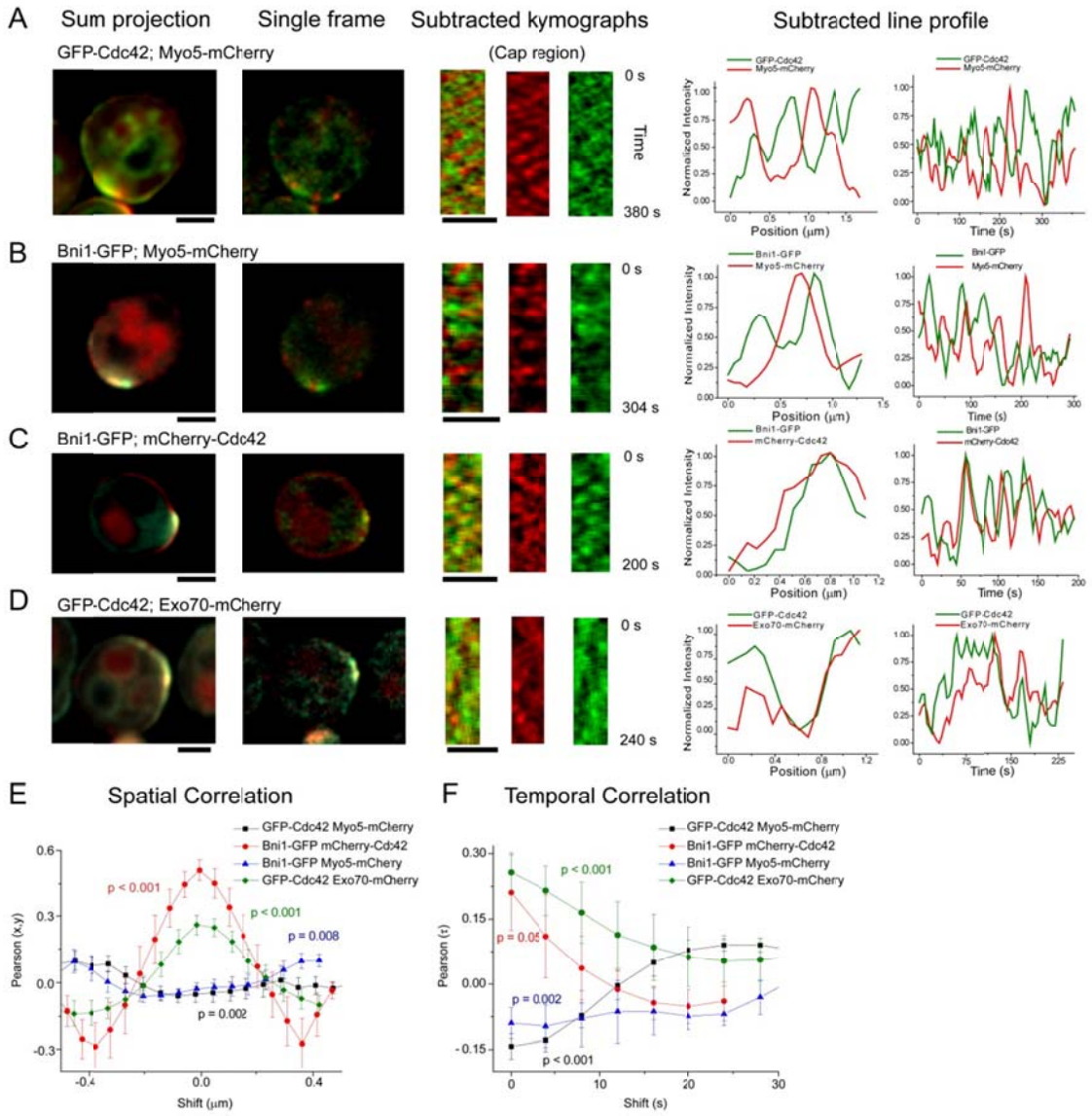

Figure 1. Spatial organization of endocytic and exocytic domains relative to Cdc42 distribution within the polar cap.

A-D. Left most column shows representative time-summed images of the localization of the indicated proteins. These images show the overall presence of the analyzed proteins in the polar cap. The column second from the left shows example single time point images showing punctate appearance of the proteins observed. The three columns that follow show sum-subtracted kymographs (merged followed by mCherry and GFP) of the polar cap region from image series showing anti-correlated (A,B) or correlated (C,D) fluctuations of the two proteins in each pair as indicated. Raw (non-average subtracted) kymographs are shown in Fig. S1. The second from right plot shows an example fluorescence profile at a single time point from the kymographs to the left, whereas the right most graph shows a time trace at a single cortical location. Scale bars: 2 μm. **E,F**. Average Pearson cross-correlation between red and green fluorescence spatially (along rows of the kymographs) (E) and temporally (columns of kymographs) (F). Negative correlation was observed for Bni1 with Myo5, and Cdc42 with Myo5, whereas positive correlation was observed between Bni1 and Cdc42 and Exo70 and Cdc42 at small space (E) or time shifts (F). Plots show mean and standard error of the mean (SEM) from

6 to 8 kymographs per pair. P-values are based on a one-component student's t-test, compared to zero, or a random distribution.

Cdc42 puncta to be associated with the PM rather than internal membrane structures close to the PM such as the cortical ER (**Fig. S2a**). Upon subtraction of the time-averaged membrane distribution, discrete fluctuations in protein levels along the PM became even more apparent (**Fig. 1a, Fig. S1a**). Interestingly, the Cdc42 puncta are spatially and temporally anti-correlated with the dynamic endocytic patches labeled with Myo5-mCherry (**Fig.1a, e, f**). The anti-correlated distribution of GFP-Cdc42 and Myo5-mCherry was also confirmed by using TIRF microscopy (**Fig. S2b**). Note that because Myo5 disappears from the endocytic patch just prior to vesicle internalization(Jonsdottir and Li, 2004), the observed low concentration of Cdc42 at Myo5 patches was not a consequence of endocytosis.

By using the same analysis as above, spatial and temporal anti-correlation were also observed between Myo5-mCherry and Bni1-GFP, which marks the ends of actin cables in the polar cap region and presumed sites of exocytosis(Evangelista et al., 2003) (**Fig. 1b,e,f**). By contrast, strong positive spatial and temporal correlation of mCherry-Cdc42 with Bni1-GFP was observed (**Fig. 1c,e,f**). Confirming the co-localization of Cdc42 puncta with sites of exocytosis, strong positive correlation was also observed in *RDI1* cells (**Fig.S3**) and between GFP-Cdc42 and Exo70-mCherry, a member of the exocyst complex(Boyd et al., 2004; Heider and Munson, 2012) (**Fig 1d,e,f**). These results reveal the existence of two types of regions within the polar cap: regions of high Cdc42 concentration (referred to as Cdc42 puncta) correlating with sites of exocytic vesicle

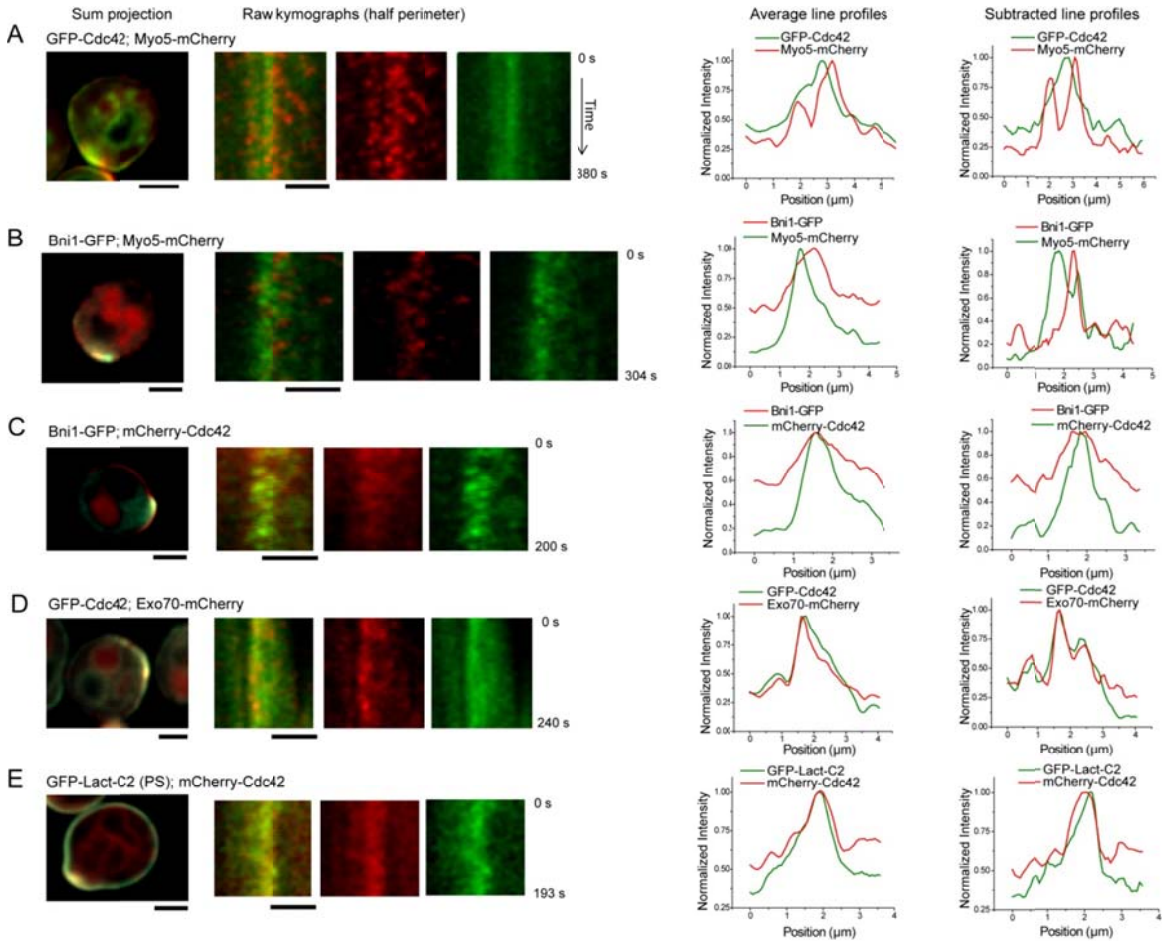

Figure S1. Non-average subtracted data corresponding to the data shown in Figure 1. A time series-sum projection (left), along with raw kymographs (merged followed by individual channels) of GFP-Cdc42 with Myo5-mCherry **A.** Bni1-GFP with Myo5-mCherry **B.** Bni1-GFP with mCherry-Cdc42 **C.** GFP-Cdc42 with Exo70-mCherry **D.** and mCherry-Cdc42 with GFP-Lact-C2 **E**. Scale bars: 2 □m. The plots on the right compare show normalized average line profiles (averaged over time for each kymograph) and a normalized average-subtracted single line profile for the green and red-labeled proteins. Note that on a cell perimeter-wide, average scale, there will be overlap of any pair of polarized proteins. However, line profiles generated from single images (without average subtraction (right column), or with average subtraction, show non-smooth distributions. (See also Figure 1 and Methods in Supplementary Information).

delivery, surrounded by regions in the polar cap with relatively low concentration of Cdc42 where sites of endocytosis are preferentially located. The Cdc42 puncta do not appear to distinguish between the active (GTP-bound) or inactive (GDP-bound) form of Cdc42, and show positive correlation with the distribution of the Cdc42 guanine nucleotide exchange factor (GEF) Cdc24, suggesting that Cdc42 can be locally activated within the puncta (**Fig. S3**).

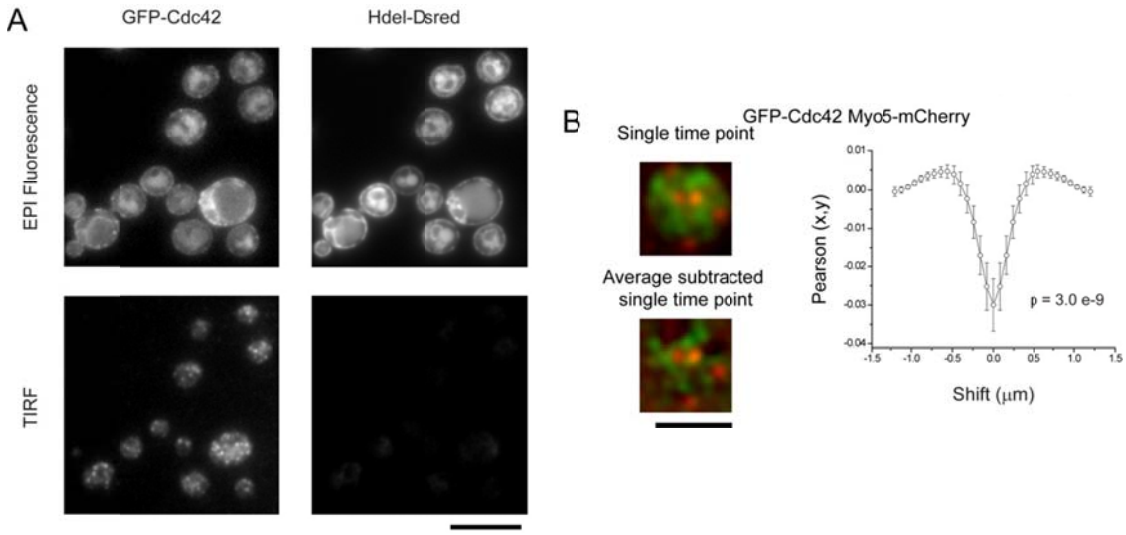

Figure S2. TIRF imaging of the Cdc42 microdomains. A. Epi-fluorescence images of GFP-Cdc42 and ER marker Hdel-Dsred, compared to TIRF images. Microdomains of GFP-Cdc42 were clearly visible at a TIRF plane that omitted the cortical ER, demonstrating that the microdomains of Cdc42 are associated with PM, not internal membrane localization. **B.** Two-color analysis of correlation of GFP-Cdc42 and Myo5-mCherry on the PM using TIRF microscopy. A single-time point and average-subtracted time point is shown (See Supplementary Methods). Spatial image cross-correlation was applied to each time point, and averaged for all time points to generate a Pearson correlation plot for each cell. The average for n= 13 cells is shown.

Heterogeneous Membrane diffusion of Cdc42

It was surprising to find that Cdc42 displays a punctate distribution and remains concentrated at the sites of exocytic delivery, given its reported, fairly rapid overall diffusion coefficient in the PM(Marco et al., 2007a). One possible explanation is that the regions with high or low Cdc42 concentrations have different Cdc42 diffusion coefficients, leading to a heterogeneous distribution. To test this, we performed inverse fluorescence recovery after photobleaching (iFRAP) experiments. In iFRAP, a region of the cell is photobleached, and loss of fluorescence is monitored in an adjacent

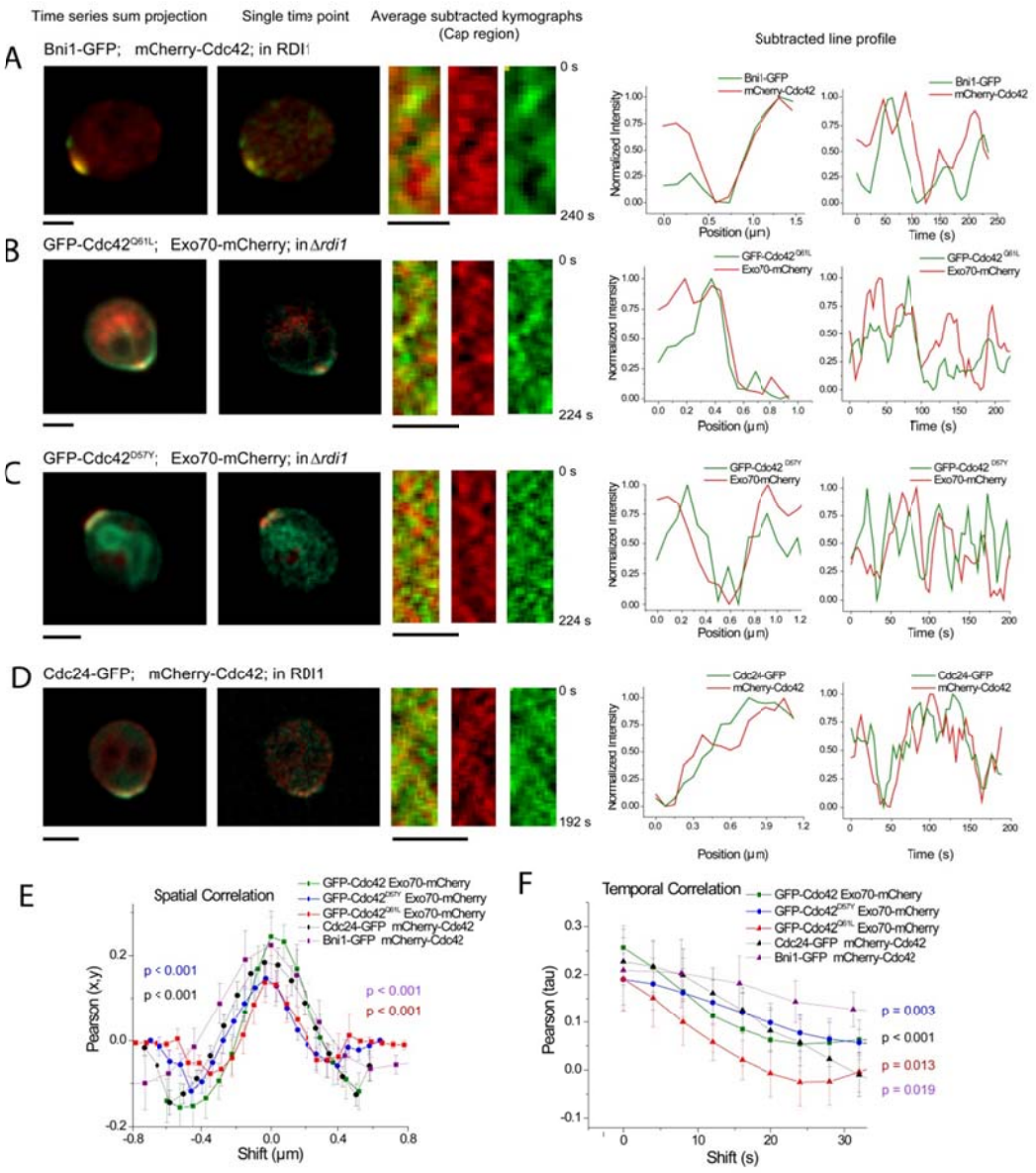

Figure S3. Both active and inactive Cdc42 and Cdc42 GEF are enriched in the same microdomains. A-C. Same analysis as shown in main text Figure 1 for Bni1-GFP with mCherry-Cdc42 in the wt background (RDI1) (**A**) Exo70-mChery with GFP-Cdc42^{Q61L} (**B**) and Exo70-mChery with GFP-Cdc42^{D57Y} in *rdi1* (**C**) and mCherry-cdc42 with Cdc24-GFP in the RDI1 background. **D**. The left most column shows representative time-summed images of the localization of the indicated proteins, while the second column from the left shows an example single time point image. The three columns that follow show sum-subtracted kymographs (merged followed by individual colors) of the polar cap. The second from right plot shows an example average subtracted spatial profile of the cap region, while the right most plots shows example fluorescence traces over time at a single cortical location. Bni1 and Cdc42 were positively correlated in the wt (RDI1) background, similar to the *rdi1* background. Like wild-type Cdc42, the GTP (Q61L) and GDP (D57Y) locked Cdc42 mutants were positively correlated with Exo70, suggesting the microdomains do not have a preference for the nucleotide bound state of Cdc42. Positive correlation of

Cdc42 and its GEF, Cdc24, was also observed. Scale bars: 2 m. e,f. Average spatial and temporal correlation.

(unbleached) region to reveal dynamics of removal of protein from the unbleached area. We used iFRAP to observe the dissipation of the polar cap through diffusion following bleaching of the cytosolic pool and the membrane outside the polar cap (**Fig.2a**). To avoid complication from Cdc42 endocytic recycling via actin-dependent exocytosis and endocytosis, this analysis was done immediately following treatment with Latrunculin A (LatA) to block Cdc42 recycling in the *Δrdi1* background. Little overall fluorescence was lost from the PM during the duration of the iFRAP measurement, confirming that loss of intensity from the unbleached region was due to membrane diffusion, not cytosolic recycling (data not shown, see Methods). Membrane kymographs from the iFRAP experiments revealed that the Cdc42 puncta no longer moved laterally in the membrane, consistent with stoppage of endocytic patch movement in the presence of LatA(Newpher et al., 2005).

Particularly noticeable was the fact that the Cdc42 puncta persisted for 60 to 90 seconds after photobleaching the cytosol and surrounding membrane (**Fig. 2b**). Numerical simulation of the iFRAP experiment using a single apparent diffusion coefficient of 0.013 $\mu m^2/s$, based on the average iFRAP decay rate and geometry (see Methods), matches the experimental decay time; however, with uniform diffusion, the simulation predicts that the heterogeneous initial distribution would rapidly equilibrate with surrounding regions (**Fig. 2c**). This was clearly contrary to what was observed experimentally (**Fig. 2b**). To quantitatively compare the experimental observation with

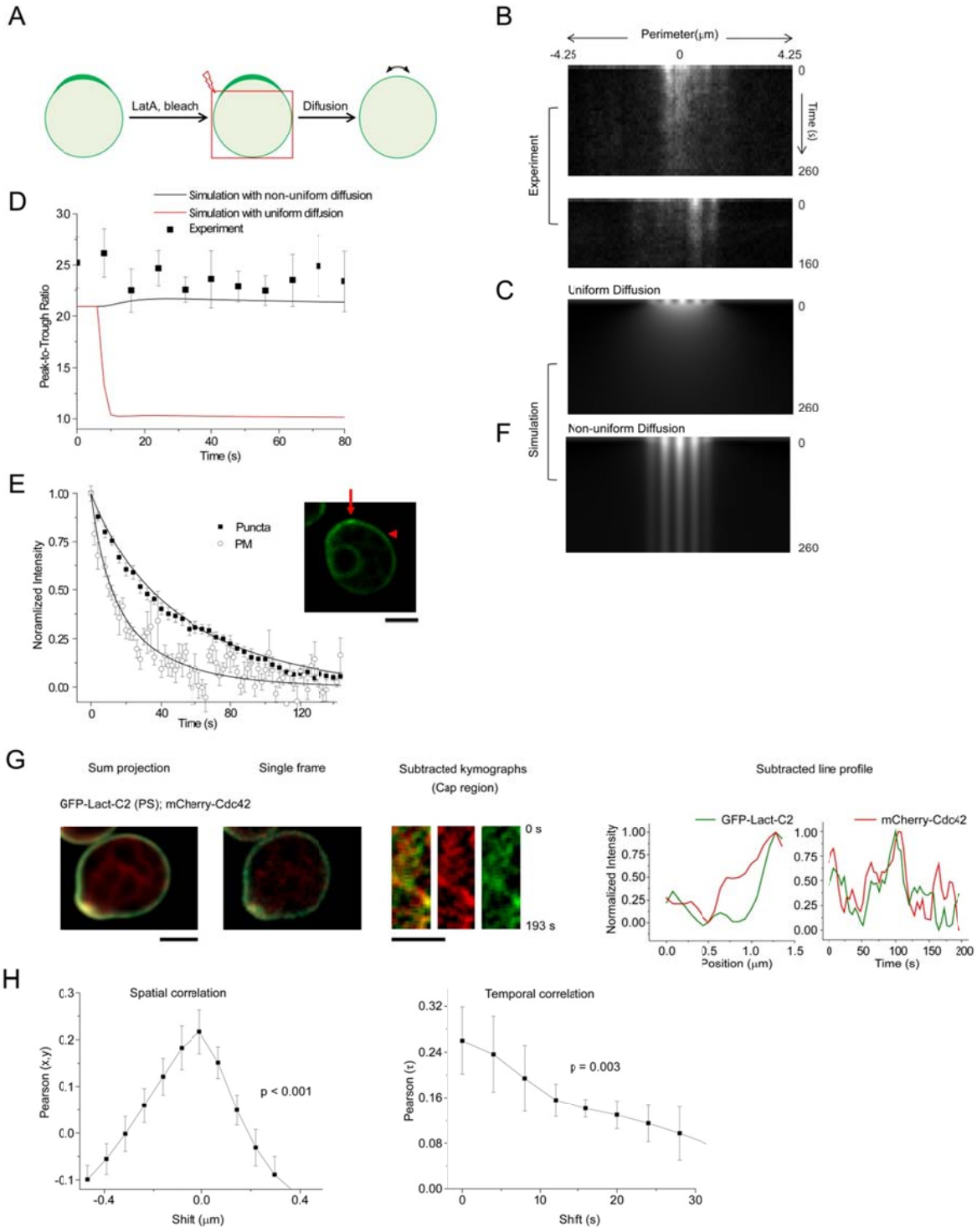

Figure 2. Cdc42 exhibits different diffusion properties in distinct regions of the plasma membrane.
A. Experimental scheme for observing Cdc42 diffusion in the PM by iFRAP (inverse FRAP) analysis. **B**. Two representative kymographs showing the decay of GFP-Cdc42 fluorescence in the polar cap following bleaching of the cytosol and surrounding membrane in *Δrdi1* cells treated with LatA. Cells

were examined shortly after LatA treatment while the polar cap was still intact. **C.** Simulation of the decay of the Cdc42 polar cap in the above iFRAP experiment with a uniform diffusion coefficient of 0.013 μm^2/sec. **D**. Comparison of the simulated evolution of peak-to-trough ratios (defined as the ratio of Cdc42 intensity in puncta to that in-between puncta) during an iFRAP experiment assuming uniform or non-uniform diffusion with that observed experimentally. **E.** Average fluorescence decay curves from iFRAP measurements at puncta (arrow in the inset image; n = 17) or a PM location close to but outside the polar cap (arrowhead in the inset image; n = 28). Smooth black lines represent the simulated decay profiles from which the slow and fast diffusion coefficients were obtained (see Methods**). F** Simulated iFRAP kymograph based on an initial heterogeneous distribution and two different diffusion coefficients as determined in (D).

model simulations, we calculated the evolution of the peak-to-trough ratio, or the ratio of Cdc42 intensity in puncta to that in-between puncta (see **Fig. S4**), as a function of time in the iFRAP experiment. With uniform diffusion, the peak-to-trough ratio was predicted to decay rapidly to a value of 1 within ~10 s (**Fig. 2d**). By contrast, the experimentally observed peak-to-trough ratio remained constant throughout the time frame of the experiment (over 80 s, **Fig. 2d**), suggesting that the observed Cdc42 diffusion was inconsistent with having a uniform diffusion coefficient throughout the PM. To directly assess the existence of non-uniform diffusion of Cdc42 in the PM, we compared the kinetics of fluorescence decay between Cdc42 puncta and non-puncta regions adjacent to the polar cap in iFRAP experiments. A dramatic difference in fluorescence decay profiles was indeed observed (**Fig 2e**). The decay profile outside the puncta is consistent with a diffusion coefficient of 0.053 μm^2/s, supporting the conclusion of heterogeneous diffusion. In order to model the iFRAP data more accurately, we fixed the diffusion coefficient away from the puncta and varied the size, shape, and diffusion coefficient of the patch region to match the experimental decay

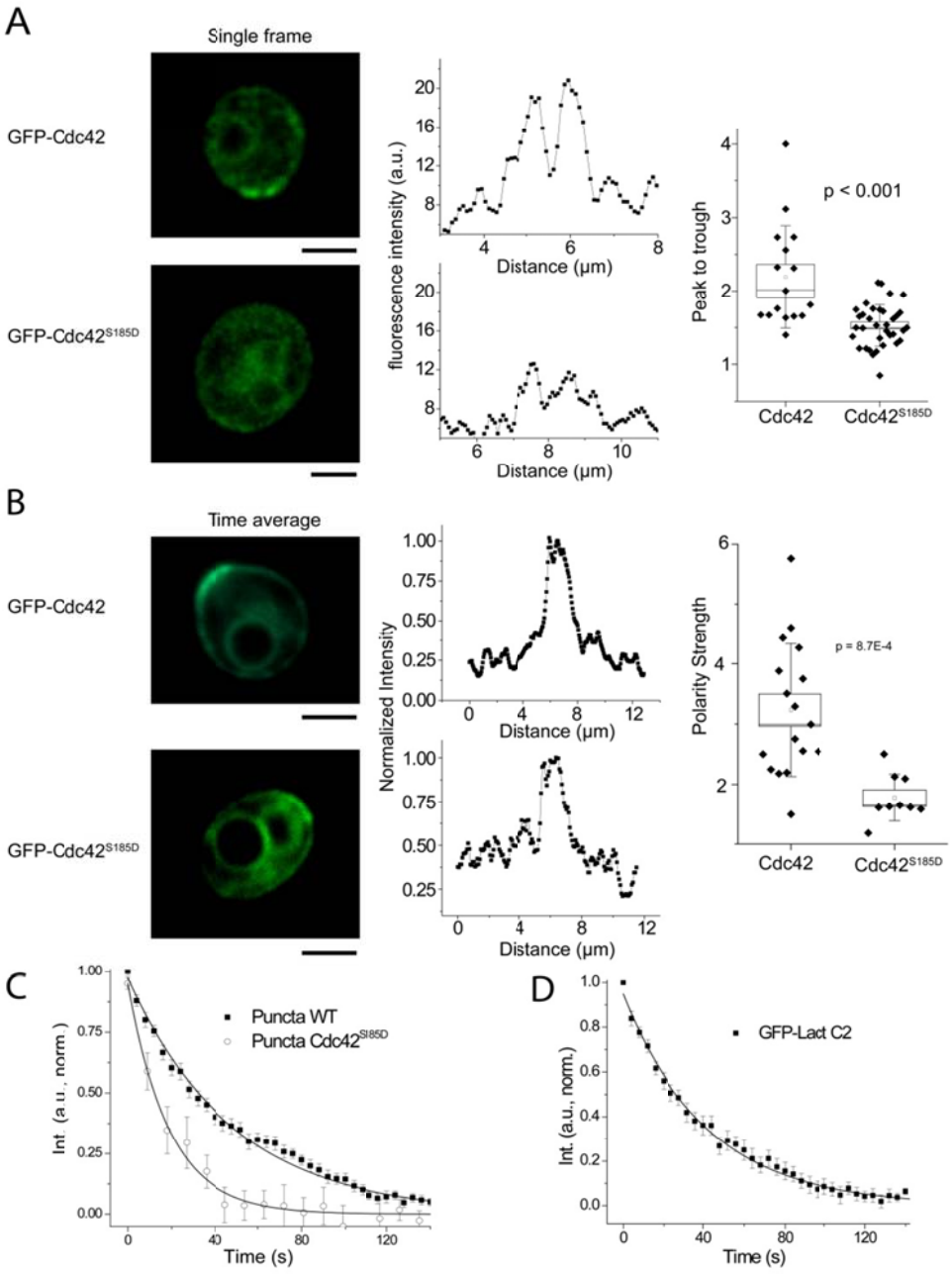

Figure S4. Effects of the S185D mutation on Cdc42 diffusion and polarity strength. A. Single frame analysis of peak to trough ratios for Cdc42 and Cdc42^{S185D}. All data came from the *Δrdi1* background. Cells were treated with 50 μM LatA to eliminate recycling and imaged prior to polar cap dissipation. The graphs in the middle show fluorescence traces along the PM of the cells to the left. **B.** Comparison of polarity strength between wild type and mutant (See Supplemental Methods). In each box plot the small box shows the mean, the line median, large box SEM and whiskers SD. **C.** iFRAP decay profiles of Cdc42 and Cdc42^{S185D} puncta in *Δrdi1* cells treated with 50 μM LatA. D. Average iFRAP decay profile of GFP-Lact-C2 in *Δrdi1* cells treated with 50 μM LatA. An exponential fit is shown. All scale bars are 2 μm.

time and peak-to-trough ratios. Modeling of the iFRAP data with the diffusion coefficient profile shown in **Fig. S6** led to an estimated membrane diffusion coefficient of 0.0061 $\mu m^2/s$ at the puncta (**Fig. 2e**) (see Methods for model details). Simulation of iFRAP experiments using these two different diffusion coefficients gave rise to peak-to-trough ratios that closely resembled the experimentally observed values (**Fig. S6**) and persisted throughout the experimental time frame, validating the assumption of two non-identical diffusion coefficients for Cdc42 at and away from the puncta (**Fig. 2d,f**).

Two well-characterized microdomains are known to exist in the yeast PM and include the membrane compartment of Pma1 (MCP) and the membrane compartment of Can1 (MCC)(Brach et al., 2011; Malinska et al., 2003). However, we found no overlap of Pma1-mCherry or Pil1-mCherry, a marker for the MCC (Brach et al., 2011), with sites of Cdc42 enrichment (**Fig. S5**). Pma1-mCherry, in particular, was completely absent from areas of polarized growth (where GFP-Cdc42 is preferentially localized); this was not due to relatively slow mCherry maturation as the same observation was made with Pma1-GFP alongside mCherry-Cdc42 (**Fig. S5**). Recent studies reported that phosphatidylserine (PS) is delivered to the polar cap via secretory vesicles and plays an important role in Cdc42 localization, possibly through interaction between the negatively charged head group of PS and a polycationic peptide near the COOH terminus of Cdc42(Das et al., 2012a; Fairn et al., 2011). It was conceivable that the regions of slow Cdc42 diffusion correlate with microdomains where PS is accumulated.

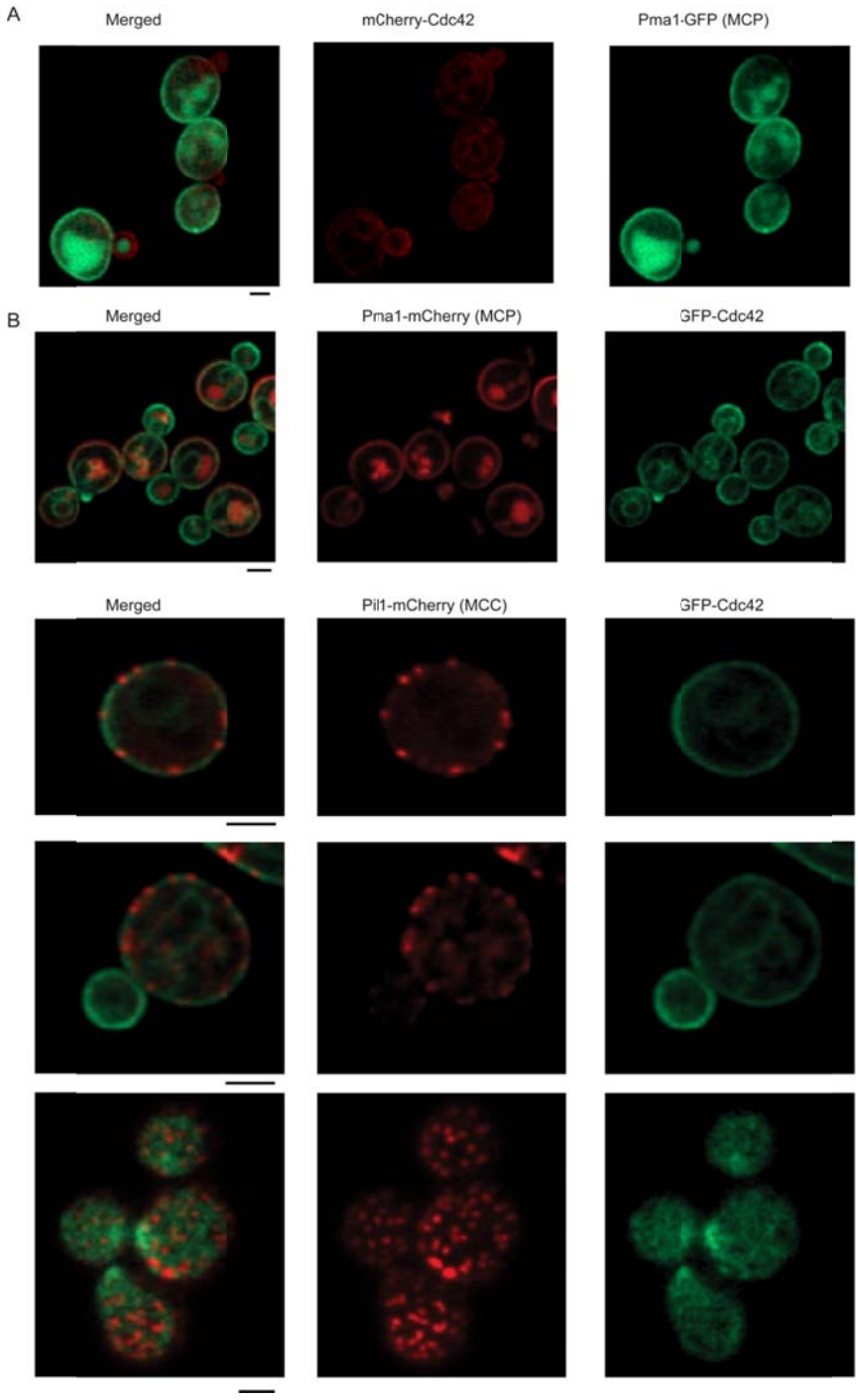

Figure S5. Cdc42 puncta do not colocalize with Pma1 or Pil1. Representative images of (**A**) Pma1-GFP with mCherry-Cdc42 (top), or GFP-Cdc42 with Pma1-mCherry (bottom) or (**B**) Pil1-mCherry with GFP-Cdc42. For the lowest panel in B, the focus was set to the bottom membrane of the cells. Scale bar is 2 μm.

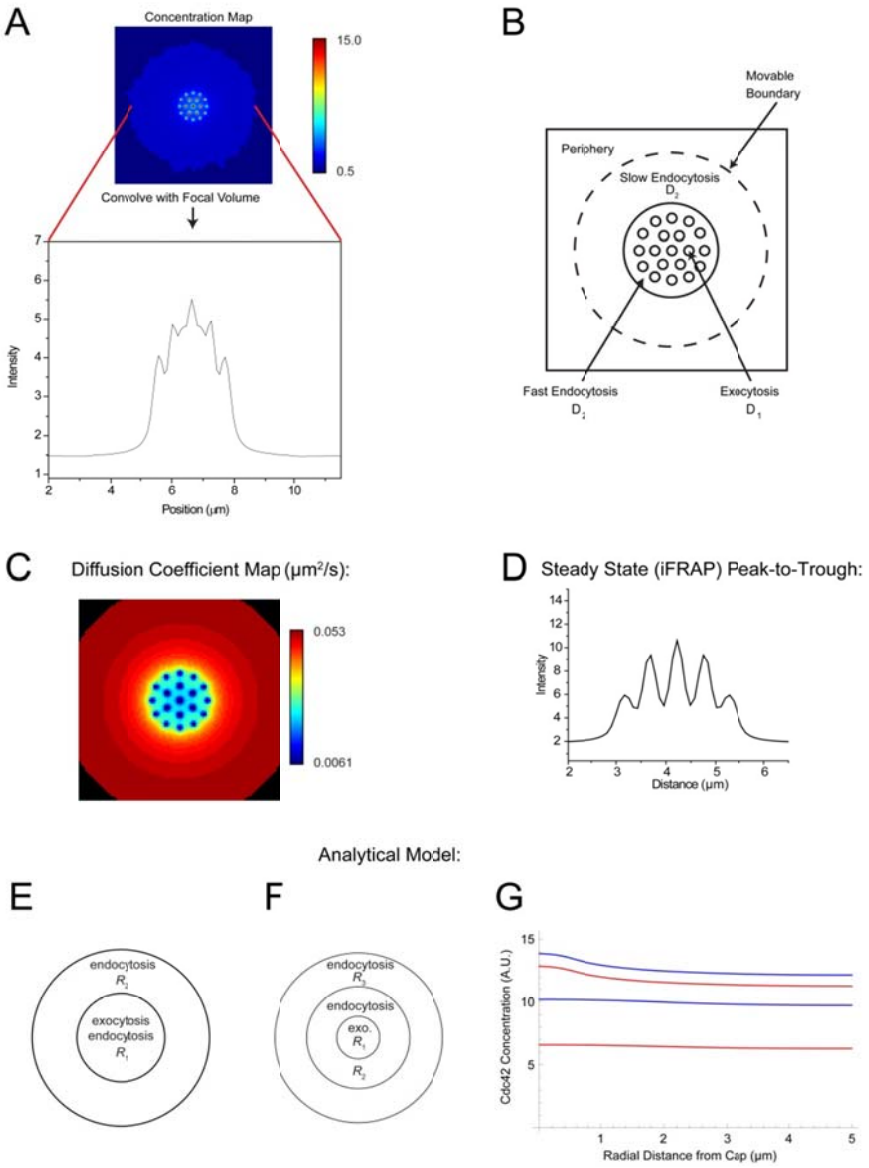

Fig. S6. Numerical simulation and analytical model of Cdc42 polarity. **A.** The simulation model 2D profile (top), 1D profile convolved with the microscope focal volume (bottom). **B.** An illustration of the compartments used in the simulation. **C.** A typical diffusion coefficient heat map used for the iFRAP and membrane traffic models. D. The steady-state iFRAP model profile prior to bleaching with diffusion coefficients of 0.053 and 0.0061 $\mu m^2/s$ showing a peak-to-trough ratio approximately matching experimental values. **E-F.** The analytical model geometry and solutions. Model geometry without spatial separation of endocytosis and exocytosis **E** and with spatial separation (**F**). **G**. Radial distribution of Cdc42 protein on the membrane. The blue solid curve corresponds to the case of spatial separation and non-uniform diffusion (as in **D**.) and an exocytic vesicle relative concentration (κ of 3.4. The red solid curve corresponds to the above diffusion but with (κ) of 1. The two lower dashed curves are for the case of geometry without the spatial separation of endocytosis and exocytosis with uniform diffusion coefficient D = 0.0013 $\mu m^2/s$ as described for the uniform **i**FRAP simulations with $\kappa = 3.4$, blue, and $\kappa = 1$, red, Cdc42 accumulation on exocytic vesicles.

Indeed, when membrane kymographs were compared between the PS biosensor GFP-Lact-C2(Das et al., 2012a; Fairn et al., 2011; Yeung et al., 2008) and mCherry-Cdc42, high spatial and temporal cross-correlation was observed (**Fig. 2h**, compared to **Fig. 1**). Reducing the potential charge interaction between Cdc42 and PS with the *cdc42*^{S185D} mutation(Das et al., 2012a) led to faster diffusion in the puncta (Fig. S4c) and reduced Cdc42 concentration in the microdomains, as indicated by a reduced peak-to-trough ratio in the polar cap (**Fig. S4a**). Modeling of this data gave a Cdc42^{S185D} diffusion coefficient at the puncta of 0.022 $\mu m^2/s$ (see Methods), more than 3 times faster than that for wild-type Cdc42. iFRAP of GFP-Lact-C2 following LatA treatment showed slow diffusion (**Fig. S4d**), consistent with reports of slow diffusion of other phospholipids in the yeast PM(Greenberg and Axelrod, 1993). These data suggest that the Cdc42 puncta may be explained by biased diffusion toward membrane microdomains that are enriched for PS.

Simulations of Cdc42 polarity establishment

With the above details in the spatial organization of Cdc42 trafficking and diffusion, we performed discrete numerical simulations of Cdc42 polar cap formation and maintenance. First we implemented the exact model in the recent work(Layton et al., 2011b). Discrete simulations were performed assuming a flat, circular membrane with a predefined membrane area to which Cdc42-containing exocytic vesicles are delivered (see Supplementary Methods and **Fig. S6** for description of simulations).

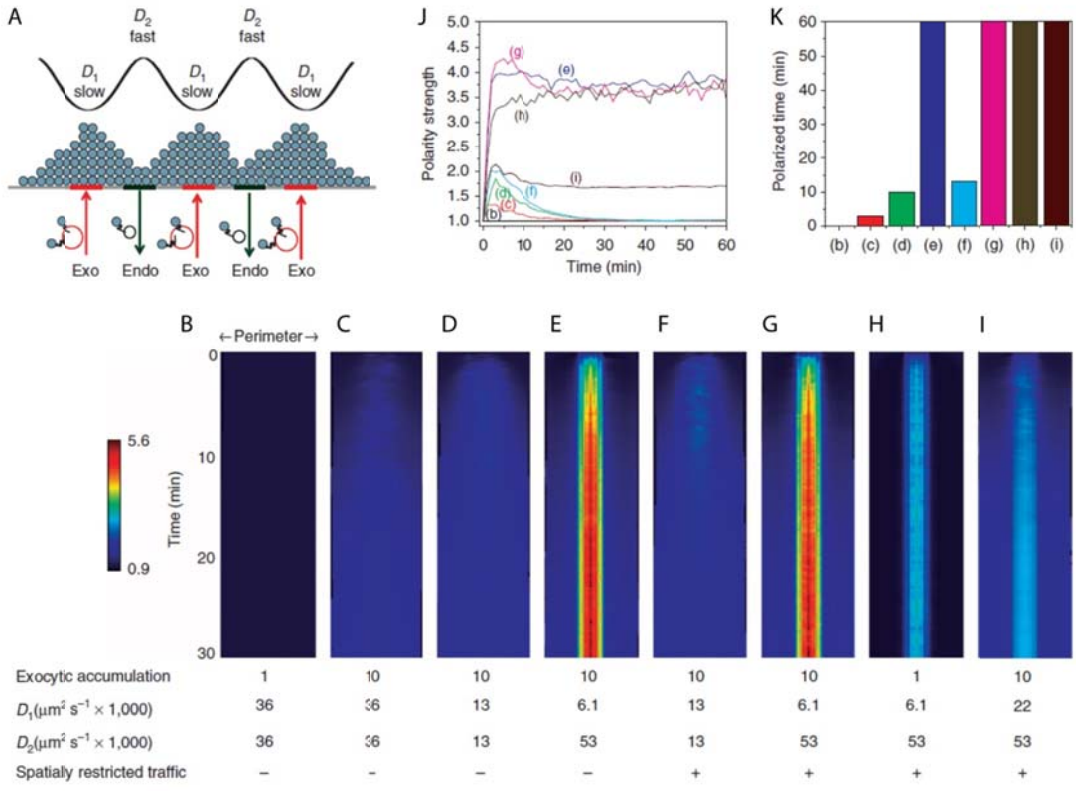

Figure 3. Numerical simulation of Cdc42 polarization under various conditions.
A. Cartoon representation of the relative spatial organization of endocytosis and exocytosis and non-uniform diffusion in the polar cap region. Blue balls represent Cdc42 molecules. Red and green circles depict exocytic (exo) and endocytic (endo) vesicles, respectively. The table to the right describes the parameters and conditions simulated in B-I, including the different diffusion coefficients, exocytic vesicle Cdc42 enrichment, and spatial relationship of endocytosis and exocytosis used in each simulation. Exocytic accumulation refers to the enrichment of Cdc42 on secretory vesicles compared to internal membrane. **B-I.** Simulations of Cdc42 polarization with assumptions similar to those used previously (**B-D**)(Layton et al., 2011b) (i.e. uniform diffusion and spatially merged endocytosis and exocytosis) and with geometric factors observed in this study (**E-I**) with conditions specified in the table at the upper right. **J-K.** Quantification of polarity strength as a function of time (**j**), defined as the ratio of maximum/minimum Cdc42 concentration over the entire cell periphery, color coded to match the quantification of polarity duration in (**K**), defined as the time during which polarity strength is above 1.3, for the simulations shown in B-I.

Upon vesicle docking, the exocytic membrane is inserted into the PM along with its cargo such as Cdc42. The PM is then expanded isotropically to accommodate the added area, and diffusion serves to redistribute Cdc42 along the PM. The material and membrane area-associated with the exocytic vesicle are removed from a well-mixed internal membrane

compartment. Endocytosis is accomplished by isotropically invaginating the membrane, leading to loss of Cdc42 and surface area from the PM. Simulations assuming uniform diffusion and spatially merged endocytosis and exocytosis confirmed the previous conclusion that without Cdc42 concentrating on vesicles, exocytosis does not lead to polarization (**Fig. 3b**), and that concentration of Cdc42 on secretory vesicles allowed initial formation of a weak polar cap that diminished rapidly (**Fig. 3c,j,k**). A slower but uniform diffusion coefficient at a value consistent with the average iFRAP decay rate enhanced the strength and duration of polarity but was still insufficient for achieving a stable polarized state (**Fig. 3d, j, k**).

Strikingly, the incorporation of two different Cdc42 diffusion coefficients as estimated following the geometry observed experimentally (**Fig. 3a**) was sufficient to produce a stable polar cap lasting > 60 min, well beyond the time span of the yeast polarized growth phase (**Fig. 3e, j, k**). Conceptually, the presence of microdomains with slower diffusion than the surrounding areas helps to concentrate Cdc42 even when the internal pool is being depleted. The incorporation of spatially separate endocytic and exocytic sites did not lead to sustainable polar cap in the absence of non-uniform diffusion (**Fig. 3f,j,k**), but resulted in slightly stronger initial polar cap formation when added to the model with non-uniform diffusion (**Fig. 3g,j,k**). As a test case, we modeled the polarization of the $Cdc42^{S185D}$ mutant assuming that D_2 (off-puncta diffusion) is the same as wild-type Cdc42 (see Methods). We found a D_1 (at-puncta diffusion) of 0.022 $\mu m^2/s$ matched the experimental decay time. Despite the reduced diffusion non-uniformity for this mutant, the model predicts that a polarized distribution could be obtained (**Fig. 3i**) but the resulting steady-state polarity strength, defined as the ratio of maximum/minimum Cdc42 concentration over the entire cell periphery, would be greatly

compromised (**Fig. 3j**), qualitatively consistent with the diminished polarity strength observed for Cdc42^{S185D} (**Fig. S4b**, see below for quantitative validation of this prediction).

Another prediction of the previous model(Layton et al., 2011b) was that in order for Cdc42 to polarize initially, Cdc42 must concentrate strongly on secretory vesicles compared to internal membrane and PM(Layton et al., 2011b). However, the concentration of Cdc42 on vesicles in yeast cells has been difficult to determine by conventional imaging due to the small size of the vesicles (80-100 nm), their mobility in the cytosol, and the presence of a considerable non-vesicle-bound pool. Thus, to estimate Cdc42 concentration on vesicles, we used fluorescence correlation spectroscopy (FCS), which is uniquely able to determine the stoichiometry of proteins in mobile fractions in live cells(Slaughter and Li, 2010). The average molecular brightness of GFP-Cdc42 was higher than that of the monomer control, suggesting that at least one diffusing pool of Cdc42 had a stoichiometry higher than 1 (**Fig. 4a**; (See Methods). As previously shown in wild-type cells(Das et al., 2012a), the autocorrelation profile of GFP-Cdc42 in the *Δrdi1* background did not fit to a single-component but instead fit well to a two-component diffusion model (**Fig. 4b**) ($p < 0.001$), with the fast and slow species having cytosolic diffusion coefficients of 3.4 ± 1.7 and 0.10 ± 0.1 $\mu m^2/s$, respectively. Whereas the fast diffusion coefficient was close to that expected for a small soluble

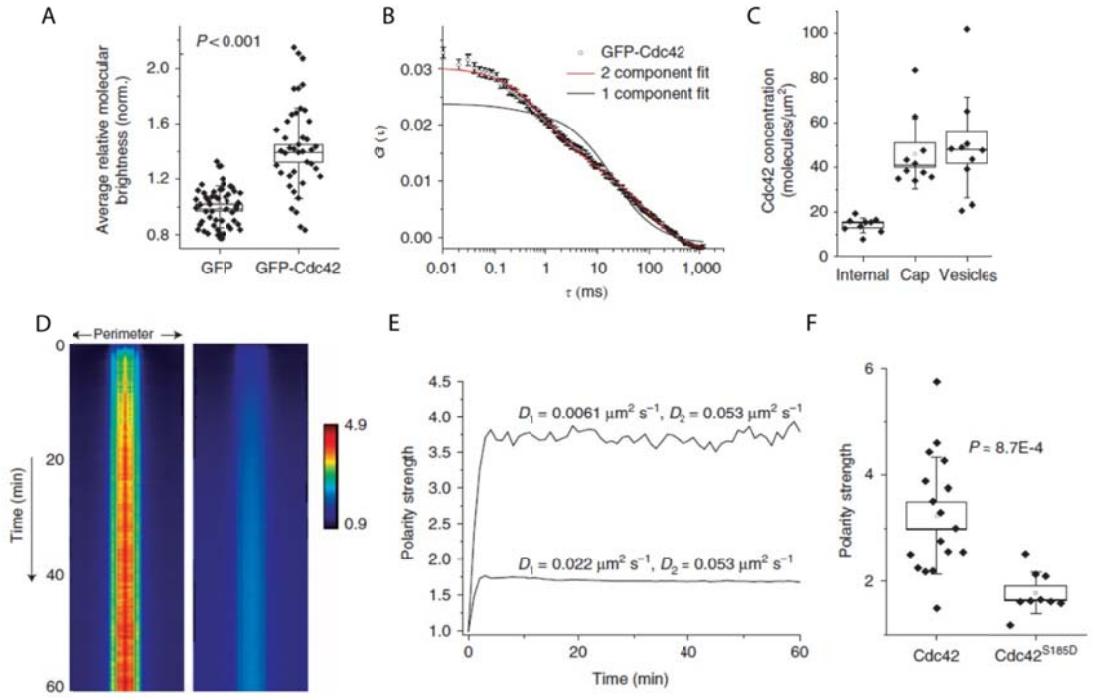

Figure 4. Determination of Cdc42 concentration on exocytic vesicles and numerical simulation of Cdc42 polarization using measured parameters.

A. Average molecular brightness of mobile GFP-Cdc42 in polarized, unbudded *Δrdi1* cells compared to a cytosolic GFP control. In each box plot the small box shows the mean, line shows median, large box the SEM, and whiskers show SD. **B.** Average autocorrelation decay of GFP-Cdc42 in *Δrdi1* fitted with 1-component or 2-component models for free 3D diffusion (note these are different from the models used to simulate 2D membrane diffusion of Cdc42 on the PM in Figure 2). **C**. Calibrated imaging was used to compare the concentration of GFP-Cdc42 on exocytic vesicles (from FCS analysis) to the GFP-Cdc42 concentration at formed polar caps. Internal membrane concentration was estimated as the concentration on PM in non-polarized cells (see text for explanation). Box plots presented as in (**A**). **D**. Simulated kymograph for polar cap formation that included non-uniform diffusion for Cdc42 (left panel, D_1= 0.0061 μm^2/s ; D_2=0.053 μm^2/s) and Cdc42^{S185D} (right panel, D_1= 0.022 μm^2/s; D_2=0.053 μm^2/s and 3.4 fold enrichment of Cdc42 onto exocytic vesicles as determined by FCS and calibrated imaging. **E.** Polarity strength (as explained in Figure 3j legend) as a function of time from the simulations in (d). **F**. Comparison of experimental polarity strength between wild type and mutant (see Supplemental Methods). Box plots are as described in (**A**).

Cdc42 species, perhaps unprenylated Cdc42, the slow one may be due to a vesicle-bound pool.

In support of this conclusion, the *cdc42^{C188S}* mutation, which eliminates the prenylation

site(Ziman et al., 1993), had a drastically diminished slow pool (**Fig. S7a**), whereas the *sec6-4*

mutant that accumulates secretory vesicles at the restrictive temperature(Govindan et al., 1995; Lamping et al., 2005) had an enhanced amplitude of the slowly diffusing species (**Fig. S7b**). By contrast, the relative amplitude of the slow pool was not diminished in an *arp3-2* mutant, which blocks endocytosis at the restrictive temperature (**Fig. S7c**). Furthermore, the diffusion coefficient of the slow pool was consistent with an average stokes radius of 50-100 nm based on free diffusion model (See Methods), consistent with the known size of exocytic vesicles but not the much smaller endocytic vesicles (Mulholland et al., 1994; Prescianotto-Baschong and Riezman, 1998).

FCS analysis of Cdc42 diffusion

To determine if the 'fast' pool represents monomeric Cdc42, we examined cross-correlation between GFP-Cdc42 and mCherry-Cdc42. Cross-correlation was observed between GFP-Cdc42 and mCherry-Cdc42 with a slow, not fast, transit time (Supplementary Information) (**Fig. S7d**), suggesting that the fast pool of Cdc42 was monomeric, whereas at least a fraction of the slow diffusing pool contained multiple Cdc42 molecules per mobile particle. We fixed the brightness of the fast pool to that of monomer GFP, and freely fit the brightness of the slow pool (see Methods), which yielded an average stoichiometry of Cdc42 in the slow pool of 1.5 $\pm$ 0.2 proteins/particle or a concentration of 49 $\pm$ 7 molecules/μm^2 on vesicles of 100 nm diameter (**Fig. 4c**, Supplementary Information)(Novick et al., 1980; Prescianotto-Baschong and Riezman, 1998). By using calibrated imaging (see Methods), we determined the average

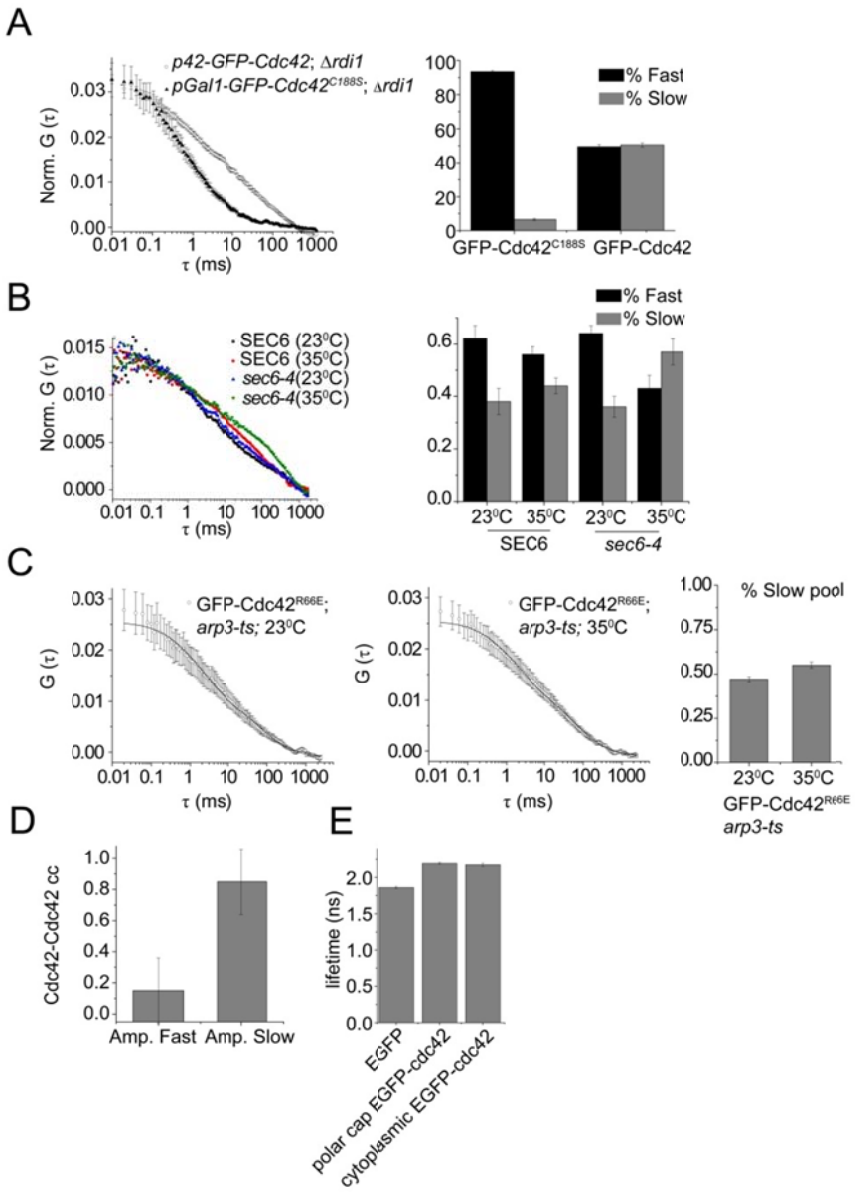

Fig. S7. **Live-cell fluorescence correlation spectroscopy analysis of the slow and fast diffusing pools of Cdc42 in the cytosol. A.** The presence of the slowly diffusing pool was dependent on Cdc42 prenylation, and was nearly eliminated for the Cdc42^{C188S} non-prenylated mutant[25]. **B.** The amplitude of the slowly diffusing pool was dramatically increased in the *sec6-4* mutant at the restrictive temperature. At this temperature, exocytic vesicles accumulate due to their inability to fuse with the plasma membrane[26,27]. **C.** The autocorrelation decay of GFP-Cdc42^{R66E} (defective in Rdi1 binding) in *arp3-2* at the permissive and restrictive temperature was fitted to a two-component model to determine the relative amplitude of the slow pool. The diffusion of the GFP-Cdc42^{R66E} mutant has been shown to recapitulate wild-type Cdc42 in the *Δrdi1* background[21]. The slow pool was not diminished by the reduction in endocytosis at the restrictive temperature in the ts arp3-2 mutant D. Cross-correlation of GFP-Cdc42 and mCherry-Cdc42 was fitted to a two-component model with coefficients of diffusion fixed to the fast and slow transit time for Cdc42. The vast majority of the cross-correlating species of Cdc42 were present in the

slowly diffusing pool. In all bar graphs, the error bars represent the SEM. **E**. Fluorescence lifetime of cytoplasmic EGFP, EGFP-Cdc42 in the polar cap, and cytoplasmic EGFP-Cdc42. Error bars represent the standard error in the mean.

concentration of Cdc42 at the polar cap to be 46 $\pm$ 5 molecules/μm^2 (**Fig. 4c**). Fluorescence lifetime imaging verified that GFP has a similar lifetime freely diffusing in the cytosol as it does bound to either cytosolic Cdc42 or membrane bound Cdc42 (Fig. S7e), therefore fluorescence intensity is an accurate measure of relative protein abundance. Prior to cell polarization, where Cdc42 concentration is likely in equilibrium between the external and internal membrane, the Cdc42 concentration at the PM was measured to be 14 $\pm$ 1 molecules/μm^2, ~3.4 times lower than that at the polar cap or the concentration on exocytic vesicles in polarized cells (**Fig. 4c**).

Simulation of the model with a 3.4x concentration of Cdc42 on secretory vesicles coupled with non-uniform diffusion and segregated endocytosis and exocytosis on the PM showed long lasting and stable polar caps (Fig. 4d,e, left panel, wild-type, right panel, $Cdc42^{S185D}$). The predicted polarity strength agreed well with that observed experimentally for both wild-type Cdc42 and $Cdc42^{S185D}$ (**Fig. 4e**). Interestingly, our model predicts the presence of non-uniform diffusion to be sufficient for prolonged polarity even in the absence of Cdc42 accumulation on secretory vesicles (assuming equal concentrations between secretory vesicles and internal membranes) (**Fig. 3h, j, k**), although in this case it takes slightly longer to reach the steady-state polarity strength (**Fig. 3j**). In addition, in the case of a reduction in biased diffusion (something that could

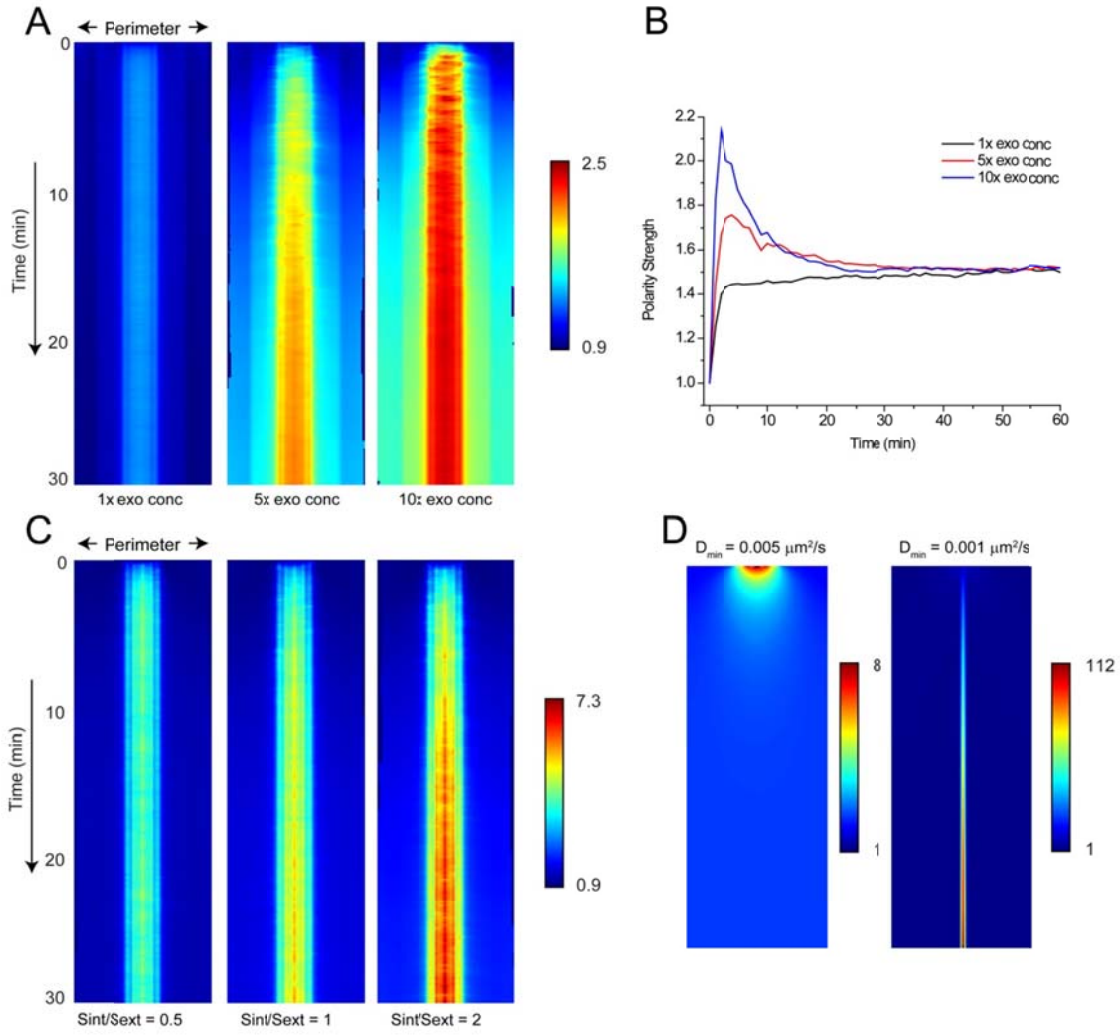

Figure S8. **Simulations with varying parameters. A.** Membrane trafficking simulation kymographs performed as in Figure 3G but with D1 = 0.02 $\mu m^2/s$ and D2 = 0.04 $\mu m^2/s$ and different exocytic Cdc42 accumulation ratios as indicated under the kymographs. **B.** Polarity strength plots for the simulations in (**A**). **C.** Effect of changing the relative internal membrane area with other parameters identical to Fig. 3G. D. Simulaion kymographs of models for linearly concentration-dependent diffusion with different limiting minimum D values.

happen in nascent caps or under environmental perturbation), concentration of Cdc42 onto exocytic vesicles allows for increased polarity strength (**Fig. S8a**).

Given the stability of the polar cap in the discrete simulations, we revisited the presence of a polarized steady state with an analytical model by incorporating non-uniform diffusion using a simple geometry that represents exocytosis in a central region with slower diffusion than the rest of the PM, and endocytosis outside this region (Supplementary Methods) (**Fig. S6b-d**). A polarized steady-state solution was indeed found. By contrast, no significant steady-state polarization was obtained given uniform Cdc42 diffusion (**Fig. S6d**).

Discussion

A role for actin and actin-based vesicular trafficking in driving cell polarization was first revealed in an experimental system where overexpression of constitutively active Cdc42 leads to spontaneous polarization of G1-arrested yeast cells(Wedlich-Soldner et al., 2003b). Subsequent studies demonstrated that during normal cell polarization at the start of bud formation, the actin-mediated mechanism functions in parallel with a pathway that relies on the adaptor protein Bem1(Irazoqui et al., 2003b) and that both pathways are required for achieving a signal-responsive and robust polarized state(Brandman et al., 2005; Slaughter et al., 2009a; Wedlich-Soldner et al., 2004b). Mechanistic details by which these pathways drive cell polarization remain elusive. Mathematical modeling provides a powerful tool for quantitative exploration of conceptual models derived from experimental evidence(Mogilner et al., 2012). Failure of a model to predict the expected outcome is indicative of crucial gaps in our understanding based on which model assumptions are made. The results described in this study demonstrate that for the actin/membrane trafficking-based mechanism to achieve a stable polarized state with simultaneous balance of protein and membrane flux, Cdc42

diffusion in the PM must be non-uniform with the presence of microdomains toward which Cdc42 diffusion is biased. Previous work demonstrated that membrane proteins in yeast diffuse more slowly than their counterparts in mammalian cells and that if the diffusion is slow enough, recycling through endocytosis would be sufficient to polarize the proteins(Valdez-Taubas and Pelham, 2003). We found in this study that although overall slow diffusion enhances temporary polarization, it is the non-uniformity of Cdc42 diffusion that allows sustained polarization. Our findings may be of particular importance to the polarization of mammalian cells where overall membrane diffusion is more rapid.

Lateral segregation into distinct, co-existing microdomains has recently been reported as a widely occurring phenomenon for plasma membrane-associated proteins in yeast(Spira et al., 2012). It is proposed that self-assembly of these microdomains is an emergent outcome of multiple weak interactions between proteins and lipids. The possible role for Cdc42-PS interaction in determining Cdc42 localization and mobility is reminiscent of early work on electrostatic interactions of PS with the myristylated protein, MARCKS. A polycationic region near the N-terminal myristate lipid anchor was postulated to be surrounded by negatively charged PS, causing a 'lipid shell' that may also recruit additional lipids (Anderson and Jacobson, 2002). Interestingly, this contributes to a punctate appearance of MARCKS, in which MARCKS colocalizes with proteins such as F-actin and talin (Allen and Aderem, 1995; Rosen et al., 1990). We speculate that a similar mechanism may contribute to the formation of Cdc42 microdomains, which are also rich for the formin-family actin nucleator Bni1. A role for PS in Cdc42 microdomain formation and the crucial requirement for these microdomains in Cdc42

polarization are consistent with the recent finding that Cdc42 polarizes extremely poorly in the *cho1* mutant deficient in PS synthesis(Fairn et al., 2011).

Aside from PS, the Cdc42 microdomains, which can harbor either GTP- or GDP-bound Cdc42, are also enriched for proteins such as Bni1, Exo70, and Cdc24. All three proteins are capable of direct interaction with Cdc42,(Evangelista et al., 1997a; Wu et al., 2010; Zhang et al., 2008; Zheng et al., 1995b) and Exo70 and Cdc24 also contain lipid-binding motifs (Harlan et al., 1994; Toenjes et al., 1999; Zhang et al., 2008). Our observation of two apparent diffusion coefficients for Cdc42 does not conflict with the possibility that the slow apparent diffusion is due to Cdc42 binding and dissociating from other components of the microdomains. Whereas Cdc24 governs Cdc42 activation, Bni1 and Exo70 are key effectors mediating downstream actin nucleation and exocytosis. Thus, the Cdc42 microdomains may not only result from multiple protein-protein and protein-lipid interactions but also represent centers of Cdc42 signaling in the establishment of cell polarity. In Supplementary Information, we also entertained a model of concentration-dependent diffusion with Cdc42 concentration inversely related to its own diffusion coefficient but found this model unable to recapitulate the microdomain dynamics (**Fig. S8c**).

Based on the evidence presented, we favor a model where targeted delivery of Cdc42 through vesicle trafficking is accompanied by the deposition of lipid components such as PS, which help to provide an initial Cdc42 diffusion trap. Interaction of Cdc42 with Cdc24 leads to Cdc42 activation, accompanied by additional recruitment of Cdc24 through Cdc42 effectors such as Cla4 and Bem1 as previously proposed(Kozubowski et al., 2008). Further recruitment of

the Cdc42 effectors such as Bni1 and Exo70 (or Sec3)(Zhang et al., 2008) not only mediates localized actin cable assembly and vesicle exocytosis but also re-enforces the microdomains that slow Cdc42 diffusion through additional protein and lipid interactions.

Although the presence of non-uniform diffusion remedies the issue of unstable polarity predicted by a model based on a set of simple assumptions,(Layton et al., 2011b) our findings do not rule out other potential mechanisms that can contribute to polarity maintenance. For example, a ring of septins appears around the polar cap just minutes after initial Cdc42 polarization(Iwase et al., 2006). The septin ring serves as a diffusion barrier to restrict lateral diffusion of Cdc42(Orlando et al., 2011; Takizawa et al., 2000) and could prevent the potential decline of polarity strength. In addition, whereas the simplest assumption posits Cdc42 protein flux balance to be accompanied by membrane conservation, this coupling may not be obligatory due to the presence of multiple pathways for membrane trafficking and recycling(Orlando and Guo, 2009). In conclusion, membrane microdomains have been studied extensively in many cellular systems(Anderson and Jacobson, 2002; Lingwood and Simons, 2010; Spira et al., 2012) and have been implicated in GTPase signaling(Norambuena and Schwartz, 2011; Parton and Hancock, 2004). The results presented in this study not only demonstrate the theoretical feasibility of vesicular trafficking to achieve a stable polarized state but also predict a critical role for membrane microdomains in this process by modulating the diffusion properties of a master polarity regulator. As such, the macroscopic organization of the cell may originate in part from microscopic self-organization of protein-membrane complexes.

Methods

Yeast culture and drug treatment

Yeast strains used in this study are listed in Supplemental Table 1. Yeast cells were grown in synthetic complete media to mid-log phase prior to analysis. For the iFRAP experiments with LatA (BioMol), 50 µM LatA was added for immediately prior to data acquisition. In most experiments, GFP-Cdc42 was controlled under the *CDC42* promoter(Slaughter et al., 2009a); however, for GFP-Cdc42^{S185D}, GFP-Cdc42^{C188S}, and GFP-Cdc42^{R66E} in the *arp3-2* mutant, and GFP-Cdc42 in the *sec6-4* mutants, the inducible *GAL1* promoter was used to drive GFP-Cdc42 expression. In these experiments, the *GAL1* promoter was turned on with galactose for 90 to 120 min. At this induction time, the induced expression of Cdc42 proteins was at a level similar to the expression level using the *CDC42* promoter(Slaughter et al., 2009a). The functionality of the tagged proteins was previously validated in the strain background of S288c(Boyd et al., 2004; Buttery et al., 2007; Jonsdottir and Li, 2004; Slaughter et al., 2009a).

Generation of membrane kymographs.

Two-color timelapse movies were acquired using the avalanche photodiode (APD) imaging module of a Zeiss Confocor 3. The 488 nm and 561 nm laser lines were used to excite GFP and mCherry, respectively, and emission was collected through BP 505-540 and LP 580 filters. Prior to kymograph generation, images were spatially binned 2x2 to result in a pixel size

of approximately 80 nm, and kymographs were generated in ImageJ. Using custom built plugins in ImageJ, the average profiles in space and time were subtracted prior to correlation to eliminate photobleaching and retain only fluctuations in membrane concentrations (and not the overall cap profile). A pinhole of 1.5 to 1.8 airy units was used, and images were acquired with either 2 or 4 second time resolution. Average spatial and temporal Pearson product-moment correlations functions were generated using the following equations(van Steensel et al., 1996):

$$Corr(\xi) = \frac{\mathrm{cov}_x[I_g(x), I_r(x+\xi)]}{\sqrt{\mathrm{var}_x[I_g]\mathrm{var}_x[I_r]}}; Corr(\tau) = \frac{\mathrm{cov}_t[I_g(t), I_r(t+\tau)]}{\sqrt{\mathrm{var}_t[I_g]\mathrm{var}_t[I_r]}}.$$

Here $\mathrm{cov}_a[x,y]$ is the covariance of x and y variables over either the spatial coordinate ($a = x$) or the temporal coordinate ($a = t$) and $\mathrm{var}_a[x]$ is the similarly defined variance.
Average correlation curves were generated from between 5 and 7 kymographs, and the p-value compared to zero listed was computed by the one-sample Student's t-test using OriginPro software.

Determination of membrane diffusion of GFP-Cdc42 in Δrdi1 cells from iFRAP experiments.

To eliminate complications from Cdc42 recycling, *Δrdi1* cells were treated with 50 µM LatA, followed immediately by photobleaching of the cytosol and majority of cell membrane (70 to 90%), and the decay of fluorescence in the unbleached PM region due to membrane diffusion was monitored by time-lapse acquisition using APD. The average decay of the unbleached region was fit to an exponential to determine the characteristic half-time. To ensure that the majority of the loss of localized fluorescence in the iFRAP measurement was

due to membrane diffusion, and not internalization, the recovery of the bleached cytosolic protein was monitored, and compared to the whole cell intensity following the bleach step. The cytosolic increase during the measurement was corrected for geometry, as previously described(Slaughter et al., 2009a). Less than 15% of the total membrane fluorescence was lost during the measurement to internalization, while the loss of the unbleached region to the surrounding membrane reached 80 to 90% during the time course of the measurement. These measurements indicate that the decrease in localized membrane intensity in the iFRAP measurement was largely due to membrane diffusion, and not internalization.

For determination of the fast diffusion coefficient outside the cap area, iFRAP data was generated outside of the region containing puncta, and fit to get the representative tau value. Simulations were used to determine the diffusion coefficient that matches this tau, given an average unbleached membrane area consisting of 71 μm^2 and a bleach region of circumference 2.6 μm.

Given the complex relationship between non-uniform diffusion coefficients with unknown experimental spatial distribution and the fluorescence decay, we chose to use a semi-quantitative parameter matching approach to the iFRAP data analysis to determine the diffusion coefficient of molecules inside the puncta regions. This approach consisted of simulation of a 2D iFRAP experiment with polar cap geometry similar to that observed experimentally and 19 regions of reduced diffusion centered on the cap region to emulate the regions of enhanced fluorescence and reduced diffusion observed experimentally (**Fig.2E, Fig. S6**). The diffusion coefficient in the patch regions is described as a sum of damped Lorentzians (Lorentzians to the 0.8 power) subtracted from the fast diffusion value. Since this function at

times exceeds the minimum diffusion coefficient, it is truncated at that value, giving the central patches a somewhat larger size (**Fig. S6**). The slow diffusion patches were placed at distances of 0.62 and 1.2 μm from the center of the simulation plane. The simulation was carried out with a Gaussian convolution method as described for the more complex trafficking simulation described below, but with a square membrane employing periodic boundary conditions. To expedite the simulations, the diffusion coefficient profile was digitized to 32 values and diffusion probability lookup tables were created for these values prior to the simulation. The fast diffusion coefficient was estimated with uniform diffusion. The slow diffusion coefficient and the size of the slow diffusion patches in the simulation were varied to match the experimental peak-to-trough ratio in the prebleached steady-state as well as the experimental half-time of the puncta. This process was repeated iteratively to make sure that scaling the diffusion coefficients did not affect the peak to trough ratio significantly.

For $Cdc42^{S185D}$, membrane localization was reduced to the point where iFRAP data away from the cap could not be obtained reliably. To estimate the diffusion coefficient inside the puncta, we analyzed the puncta iFRAP data as described above, with the simplification that D_2 was held the same as for wild-type Cdc42. This resulted in values of 0.022 and 0.053 μm2/sec for D_1 and D_2, respectively, for a ratio of 2.4.

Cytosolic Diffusion of GFP-Cdc42 in Δrdi1 cells

The diffusion profile of GFP-Cdc42 in *Δrdi1* was measured in live yeast cells using fluorescence correlation spectroscopy (FCS) as previously described (Slaughter et al., 2011). GFP was excited using the 488 nm laser line of a Zeiss Confocor 3. Emission was sent through a 565

nm dichroic and a BP 505-540 nm filter. Avalanche photodiodes (APDs) were used to collect photons. The autocorrelation decay was calculated using standard methods (*4*) and fit using a 1-component and 2-component model, with a triplet time of 250 µs. The two-component fit was justified using a standard t-test ($p < 0.001$). The two-component fit yielded transit times of 2.1 ± 1.1 and 72 ± 9 ms for the fast and slow pool, respectively.

FCS determination of concentration of Cdc42 on vesicular structures.

The amplitude of an FCS curve can be written as a function of the relative number of molecules and molecular brightness:

$$G(0) = \frac{\gamma \sum_i \varepsilon_i^2 N_i}{I^2}.$$

The average intensity obeys the simple relationship:

$$I = \sum_i \varepsilon_i N_i$$

Here ε_i and N_i are the molecular brightness and average number in the focal volume respectively for species *i*. In this study, two diffusion components for Cdc42 are observed, one that is a monomer and diffuses freely in the cytosol with a short diffusion time, and a second that is composed of vesicles with a Poisson distribution of Cdc42 molecules on them and a slow diffusion time. Given that the above equation is additive, we can write separate equations for the amplitudes of the slow and fast components:

$$G(0)_{fast} = \frac{\gamma \varepsilon_{GFP}^2 N_{fast}}{I^2},\ G(0)_{slow} = \frac{\gamma \varepsilon_{GFP}^2 N_{slow} \sum_n n^2 Poi(n,\overline{n})}{I^2} = \frac{\gamma \varepsilon_{GFP}^2 N_{slow} \left(\overline{n}^2 + \overline{n}\right)}{I^2}.$$

Here ε_{GFP} is the molecular brightness of monomeric GFP, *n* is the vesicle occupancy, $\bar{n}$ is the average vesicle occupancy, and η is a shape factor used in microscopy (Thompson, 1991). We can also write an expression for the average intensity:

$$I = \varepsilon_{GFP} N_{fast} + \varepsilon_{GFP} \bar{n} N_{slow}$$

Given the experimentally measureable variables of $G(0)_{fast}$, $G(0)_{slow}$, the average intensity, and the molecular brightness of ε_{GFP} from observation of a control sample, it is possible to calculate the three unknowns: N_{fast}, N_{slow}, and $\bar{n}$.

In the case of free diffusion, the Stokes-Einstein equation predicts an inverse relationship between diffusion coefficient and the hydrodynamic radius cubed. Hence, comparison of diffusion time of something of unknown size to cytosolic GFP, of known size, allows for an estimate of molecular radius of the unknown particle, if a spherical shape is assumed.

Calibrated imaging to determine the Cdc42 level in the polar cap

FCS and calibrated imaging were used to measure Cdc42 concentration at the cap for comparison to that in exocytic vesicles. For unbiased estimation of cortical intensity, it is necessary to remove cytosolic fluorescence. The intensity profile of the cytosol perpendicular to the cortex is the convolution of a step function with the microscope point spread function (PSF). If the PSF is considered to be a Gaussian in the xy plane, this profile is given by an error function. The intensity profile of the cortex, on the other hand, is simply the 1D projection of the PSF. Therefore, the perpendicular intensity profile is given as follows:

$$I(r) = b + I_{edge} \exp\left[\frac{-2(r - r_{edge})^2}{\omega_0^2}\right] + \frac{I_{cyto}}{2}\left(1 + \operatorname{erf}\left[\frac{\sqrt{2}(r - r_{edge})}{\omega_0}\right]\right).$$

Here b is the background intensity outside of the cell, I_{edge} is the amplitude of the edge intensity, I_{cyto} is the amplitude of the cytosolic intensity, r_{edge} is the position of the edge, and ω_0 is the PSF "waist" or two times the standard deviation of the PSF.

For experimental determination of the above parameters, photon counting images were acquired with a pixel size of 0.126 µm and an average profile perpendicular to the cortex was obtained over a width of 4 pixels using a custom ImageJ plugin. This profile was then fit to the above function using non-linear least squares also with a custom ImageJ plugin to obtain the parameters of interest, namely I_{edge}. The concentration on the membrane is related to its intensity amplitude (I_{edge}) as follows:

$$I_{edge} = \varepsilon_{GFP} C A_{PSF}$$

Here ε_{GFP} is the molecular brightness of GFP at the center of the PSF in units of counts per pixel dwell time as defined above. C is the membrane concentration and A is the area of the PSF on the membrane. The GFP molecular brightness can be determined from an equivalent image of yeast expressing 1x GFP as well as FCS measurements on that same cell as follows:

$$\varepsilon_{GFP} = \frac{I \cdot G(0)}{\gamma}.$$

Here I is the average image intensity, not the intensity from the FCS measurement and both FCS and imaging are done with the same pinhole settings. The area of the PSF on the membrane was calculated as 0.6 µm^2 from an xz cross section of a 3D image of a 100 nm fluorescent bead taken with the same pinhole settings as the confocal imaging. The gamma factor was calculated from the same measurement using the following formula (*3*):

$$\gamma = \frac{\int PSF^2(\vec{r})d\vec{r}}{\int PSF(\vec{r})d\vec{r}}.$$

Calculation of polarity strength

To calculate polarity strength, a time average of GFP-Cdc42 fluorescence was obtained and the perimeter profile was fitted to a Gaussian distribution. The polarity strength (Fig. 4F, Fig. S4b) was defined as the peak value compared to the baseline

Total Internal Reflection Fluorescence microscopy

TIRF imaging was carried out using a Nikon TE2000 inverted microscope (Nikon Instruments , Melville, NY) equipped with a T-Fl-TIRF 2 Illuminator, a CFI APO 60X Oil TIRF NA 1.49 objective, a Chroma dichroic filter Z488/561x (Bellows Falls, VT), and a Photometrics CoolSnap HQ^2 camera (Tucson, AZ). Laser excitation sources for TIRF were Coherent Sapphire 488-50 and Sapphire 561-50 (Santa Clara, CA) and the Epi-fluorescence excitation source was an XCite Series 120 lamp (Lumen Dynamics Group, Mississaugua, Ontario). For GFP-Cdc42 and Myo5-mCherry TIRF experiments, time series were acquired at 3s/timepoint for 100 to 200 timepoints per movie. The GFP-Cdc42 was imaged with Chroma emission filter ET525/50m and exposure time of 200ms. DsRed was imaged with a Chroma emission filter ET600/50m and exposure time 1s.

For GFP-Cdc42, Hdel-DsRed images, GFP exposure was set to 700ms and DsRed was imaged with Chroma emission filter ZET488/561m and exposure 200ms. Image drift was corrected using a custom image alignment plugin in ImageJ, and averages were generated of six

sequential time points (over a 50 second period) in the series, with 2 x 2 pixel spatially binning. Epi-fluorescence images are single images binned 2 x 2 and were taken with Chroma filter sets FITC HYQ (460-500, 505, 510-560) for GFP and TRITC HYQ (530-560, 570, 590-650) for mCherry, respectively, with exposure 700ms. Images were corrected for differences in exposure times.

For two-color TIRF movies of GFP-Cdc42 and Myo5-mCherry, the same filter sets were used as described above. Images for red and green were taken at 3 second intervals. Prior to spatial cross-correlation, the average green and red images were subtracted from each time point. Spatial image cross-correlation[55] was applied to each image (a simple two dimensional extension of our earlier 1D analysis), and the average for all frames was generated.

Fluorescence lifetime imaging

Fluorescence lifetime imaging was performed essentially as described in Shivaraju et al. 2012 [56]. Briefly, excitation was accomplished with two photon excitation at 920 nm and emission was collected with the Carl Zeiss Confocor3 module with a Becker and Hickl SPC-830 FLIM acquisition board (Berlin, Germany). Fluorescence decay profiles were created from cytosolic and polar cap regions. These were then fit to single exponential decays with iterative reconvolution using an instrument response function generated from SHG of urea crystals. This was repeated for many cells to obtain average lifetimes and SEM values. The lifetime of GFP was 1.86 ns (SEM = 0.02). The lifetimes of cap and cytosolic GFP-cdc42 were 2.19 (SEM = 0.01) and 2.17 (SEM = 0.02) ns, respectively.

Simulations of polarity establishment

Simulations were written with custom Java code and kymographs were generated using ImageJ. The simulation was performed in a similar way to Layton et al.[10] with a few changes to simplify the coding of the model and allow for non-uniform diffusion. Briefly, the model consists of a two-dimensional array of intensities larger than the size of the circular membrane as well as a matching two-dimensional Boolean mask denoting the membrane shape and a central circular window of exocytosis that also contains enhanced endocytosis. The model also included an internal membrane that is considered well mixed. Addition of more internal membrane area did not affect simulations that include non-uniform diffusion, as these already achieve prolonged polarity (not shown), but did prolong initial cap formation in simulations in the case of uniform diffusion, where depletion of the internal pool eventually leads to cap dissipation (Fig. S8c). As a variation on the Layton et al. method, we chose to physically expand the membrane in response to exocytosis and contract it in response to endocytosis rather than re-interpolating the membrane to maintain the grid size. The expansion and contraction was made isotropic by randomly rotating the entire membrane before a horizontal insertion or removal and randomly rotating back after insertion or removal. Membrane external to the insertion or removal site was shifted outward or inward to accommodate new material so as to avoid shifting of the cortical cap material. The region outside of the boundary was filled with the average of the boundary at each time step to ensure that interpolation associated with rotations did not lead to loss of protein. Despite these precautions, large diffusion coefficients outside the cap combined with the Gaussian convolution simulation method described below inevitably lead to a small amount of protein loss. Therefore, we added protein uniformly to the cap at each time stamp to maintain the total protein at a constant level. As with the Layton et

al. paper, the pixel size was set to 0.088 μm with a surface area equivalent to the surface area of a 50 □m diameter endocytic sphere. In this way, a single pixel is removed during endocytosis and four pixels are added during exocytosis.

Diffusion in our simulation was accomplished with a Gaussian convolution mechanism reminiscent of single particle tracking simulations[57]. We cannot use the standard finite differences approaches as they do not allow for non-uniform diffusion coefficients. For Brownian motion, the probability of a particle moving distance *d* in two dimensions with a shift in time □*t* is given as follows:

$$P(d,\Delta t) = \exp\left[-d^2 \Big/ 4D(\vec{r})\Delta t\right] \Big/ 2\pi\sigma^2 .$$

Simply stated, this is a Gaussian distribution with standard deviation $\sqrt{2D(\vec{r})\Delta t}$. Note that *D* is written as a spatially dependent variable. Given this simple model, the update rule for each pixel in our simulation at each frame is the sum of the neighboring probability distributions multiplied by their center intensities as follows:

$$I(\vec{r},t+T) = \sum_{\vec{\rho}} I(\vec{\rho},t)P(\left|\vec{\rho}-\vec{r}\right|,T) .$$

As is shown by Fig. 3B and 3C, these modifications do not significantly affect the results.

With these modifications, we extended the Layton et al. model to include a diffusion trap by spatially restricting exocytosis to 19 3x3 pixel regions coinciding with the valleys of the diffusion coefficient map (Fig. S6B and iFRAP simulation methods). Endocytosis was eliminated from these regions (Fig. S6B). Kymographs were generated by convolving the distribution with an asymmetric Gaussian simulating a vertical membrane intersecting a confocal image. The

radial waist of the Gaussian was set to 0.2 μm and the axial waist was set to 0.8 μm as expected for a 1.2 NA water objective such as the one used for the experiments in this article. Polarity strengths were determined by the max/min ratio of the kymograph. Polarity durations were measured as the amount of time that the polarity strength was above 1.3, the maximum polarity strength achieved under uniform diffusion and 10x exocytic concentration (see Fig.3c and j).

Concentration Dependent Diffusion

One possible model for generating nonuniform diffusion is one in which diffusion is concentration dependent. We modeled this scenario in the following way: The simulation was started with an initial protein distribution equivalent to the steady state distribution observed before bleaching in the iFRAP simulations. Protein densities were mapped to diffusion coefficients in an inverse linear fashion with lowest densities corresponding to a maximum diffusion coefficient of 0.05 $\mu m^2/s$ and highest densities corresponding to 80% of the chosen limiting minimum diffusion coefficient. The diffusion coefficients were mapped to 40 linearly distributed values to allow for lookup tables as described in the iFRAP simulation methods. Diffusion simulations were performed as for the iFRAP simulation, but at each time step, the diffusion coefficient profile was remapped to the current protein densities. In regions where densities mapped to diffusion coefficients below the minimum and above the maximum value the diffusion coefficients were set to the minimum and maximum values, respectively. Minimum D values reported are 0.005 and 0.001 $\mu m^2/s$ (Fig. S8d).

Analytical model

Continuous model: no spatial separation

Consider a model of Cdc42 protein dynamics on the surface of a polarized yeast cell. The standard model considers the case of a single transport window on the cell membrane surface. The dynamics of the protein concentration is described by the following equations

$$\frac{\partial f_1}{\partial t} = D_1 \Delta f_1 - m f_1 + h F_{int}, \quad 0 \le r \le d, \tag{1}$$

$$\frac{\partial f_2}{\partial t} = D_2 \Delta f_2 - n f_2, \; d \le r \le L, \tag{2}$$

where in the cap area represented by a circle R_1 with the radius d both endocytosis and exocytosis take place, while in the remaining part of the external membrane R_2 with the outer radius L slower endocytosis is observed (the geometry of this model is shown in Figure S6e). Here the diffusion coefficients $D_i, i = 1,2,$ correspond to the regions R_i. A quantity F_{int} denotes total protein amount on the internal membrane, it can be found from the total protein conservation condition

$$F_{tot} = F_{int} + \int_{R_1} f_1 dr + \int_{R_2} f_2 dr = const. \tag{3}$$

In (1-2) h denotes the exocytosis rate, while m and n are the rates of endocytosis. The model assumes unifom diffusion over the external membrane, so that $D_1 = D_2 = D$.

The model geometry implies axial symmetry of the solution, so that the Laplacian operator Δ in the polar coordinates $\{r, \phi\}$ reduces to

$$\Delta f = \frac{1}{r} \frac{\partial}{\partial r} \left(r \frac{\partial f}{\partial r} \right)$$

The equations (9-12) are subject to no-flux boundary conditions at $r = 0, L$:

$$f_1'(0) = 0, \quad f_2'(L) = 0. \tag{4}$$

The solutions also should be matched at the inner boundary at $r = d$

$$f_1(d) = f_2(d),\ f_1'(d) = f_2'(d), \tag{5}$$

with the additional condition $f_1(0) = G$ where the value G at the origin is undetermined yet.

In steady state the problem (1-2) reduces to

$$D\Delta f_1 = mf_1 - hF_{int}, \tag{6}$$

$$D\Delta f_2 = nf_2. \tag{7}$$

The general solution of this system reads

$$f_1 = \frac{hF_{int}}{m} + C_1 I_0(Mr),\ f_2 = C_2 I_0(Nr) + C_3 K_0(Nr), \tag{8}$$

where I_0 and K_0 denotes modified Bessel function of first and second kind respectively. The parameters M and N are defined through

$$M^2 = m/D, \quad N^2 = n/D.$$

The three coefficients $C_i, i = 1,2,3,$ are determined from the boundary conditions (4,5); the explicit expressions are cumbersome and are not presented here. Using the solutions (8) in (3) we obtain the steady state value of the internal membrane protein amount F_{int}.

Continuous model: spatial separation

The experimental data hints that the spatial structure of the external membrane is more complex. Below we introduce a model in which the cap area consists of a central circular area (region R_1) of the radius r_0 where exocytosis only takes place and the ring around it (region R_2 with external radius d) that contains the actin patches responsible for endocytosis. The

external circular area (region R_3 with external radius L) outside the cap is characterized by endocytosis with slower internalization rate than that of in the cap region (see Figure S6f).

The external membrane equations are written in the form

$$\frac{\partial f_1}{\partial t} = D_1 \Delta f_1 + hF_{int}, \quad 0 \le r \le r_0, \tag{9}$$

$$\frac{\partial f_2}{\partial t} = D_2 \Delta f_2 - mf_2, \, r_0 \le r \le d, \tag{10}$$

$$\frac{\partial f_3}{\partial t} = D_3 \Delta f_3 - nf_3, \; d \le r \le L, \tag{11}$$

where the diffusion coefficients $D_i, i = 1,2,3,$ correspond to the regions R_i. The total protein amount F_{int} on the internal membrane, is found from the total protein conservation condition

$$F_{tot} = F_{int} + \int_{R_1} f_1 dr + \int_{R_2} f_2 dr + \int_{R_3} f_3 dr = const. \tag{12}$$

The equations (9-12) are subject to no-flux boundary conditions at $r = 0, L$:

$$f_1'(0) = 0, \quad f_3'(L) = 0. \tag{13}$$

The solutions also should be matched at both inner boundaries at $r = r_0$ and $r = d$

$$f_1(r_0) = f_2(r_0), \; f_1'(r_0) = f_2'(r_0), \; f_2(d) = f_3(d), \; f_2'(d) = f_3'(d), \tag{14}$$

with the additional condition $f_1(0) = G$ where the value G at the origin is undetermined yet.

The measurements show that the diffusion is slower inside the exocytic central region R_1 as shown in Figure S6f, so that we approximate the diffusion coefficients as follows

$$D_1 = D(1 - A), \; D_2 = D_3 = D.$$

In steady state the problem (9-11) reduces to

$$D_1 \Delta f_1 = -hF_{int}, \tag{15}$$

$$D\Delta f_2 = mf_2, \tag{16}$$

$$D\Delta f_3 = nf_3. \tag{17}$$

The general solution of this system reads

$$f_1 = \frac{G - hF_{int}r^2}{4D_1},\ f_2 = C_1 I_0(Mr) + C_2 K_0(Mr),\ \ f_3 = C_3 I_0(Nr) + C_4 K_0(Nr). \tag{18}$$

The four coefficients C_i and the value of G are determined from the boundary conditions (13,14); the explicit expressions are very cumbersome and are not presented here. Using these expressions in condition (12) leads to determination of F_{int} which explicit expression is omitted too.

Quasidiscrete model

The model (9-11) can be adopted to describe vesicle-based mechanism of protein transport. We start consideration of the discrete vesicle based model by introducing the notation. The size of the internal cytosolic membrane is S_{int}, while the external cellular membrane has area $S_{ext} = \pi L^2$. We assume that the exchange of the vesicles between the membranes does not change their areas. The external membrane is made of three regions with the areas $S_1 = \pi r_0^2$, $S_2 = \pi(d^2 - r_0^2)$ and $S_3 = \pi(L^2 - d^2)$. The exocytosis rate (the off rate of the internal membrane) is k_{int}, and the surface area of exocytic and endocytic vesicles is A_{ex} and A_{en}, respectively. The endocytosis rates (the off rates of the external membrane) k_2 and k_3 are considered below. The conservation of the membranes surface area leads to the condition

$$(k_2 + k_3)A_{en} = k_{ext}A_{en} = k_{int}A_{ex} = K. \tag{19}$$

In the region R_1 the dynamics of the external membrane Cdc42 density f_1 is governed by the protein diffusion and exocytosis from the internal membrane, so that it is described by the equation

$$\frac{\partial f_1}{\partial t} = D_1 \Delta f_1 + \frac{k_{int}A_{ex}\kappa\rho_{int}}{S_1}, \quad 0 \le r \le r_0, \tag{20}$$

where D_1 is the local diffusion coefficient, ρ_{int} denotes the uniform internal membrane Cdc42 concentration and κ is the accumulation coefficient, i.e., we assume that the exocytic vesicle protein concentration is κ times larger than of internal membrane. The source term is proportional to the number of exocytic vesicles per unit of time k_{int}, their surface area A_{ex} and the concentration of the protein on each vesicle $\kappa\rho_{int}$. The vesicles are uniformly spread inside the region R_1, so that the source term is inversely proportional to the region surface area S_1.

In the regions R_2, R_3 the protein is removed from the external membrane, so that we have

$$\frac{\partial f_2}{\partial t} = D\Delta f_2 - \frac{k_2 A_{en} f_2}{S_2}, \quad r_0 \le r \le d, \tag{21}$$

$$\frac{\partial f_3}{\partial t} = D\Delta f_3 - \frac{k_3 A_{en} f_3}{S_3}, \quad d \le r \le L, \tag{22}$$

where $D = D_2$ is the local diffusion coefficient.

Parameters Estimate

Comparing the equations (20-22) with (9-11) we find for the protein endocytic rates m and n

$$m = \frac{k_2 A_{en}}{S_2}, \; n = \frac{k_3 A_{en}}{S_3}, \tag{23}$$

so that their ratio is computed as

$$R = \frac{m}{n} = \frac{S_3 k_2}{S_2 k_3}.$$

The protein exocytic rate reads

$$h = \frac{k_{int} \kappa A_{ex}}{S_{int} S_1}. \tag{24}$$

From (23) using the ratio R definition we find

$$k_2 = \frac{k_{ext}}{1 + S_3/(RS_2)}, \quad k_3 = \frac{k_{ext}}{1 + RS_2/S_3}.$$

Using the relation $D_1 = D(1 - A),$ denote the value of the diffusion averaged over whole membrane as D_{av}, which can be computed as

$$D_{av} = \frac{2}{L^2}\left(\int_0^{r_0} D_1 r dr + \int_{r_0}^{L} D r dr \right) = \frac{D}{L^2}(L^2 - A r_0^2).$$

This relation can be used to compute the value of parameter D. The region sizes were estimated as

$$r_0 = 0.55 \; \mu m, d = 2.0 \; \mu m, L = 5 \; \mu m.$$

The area of the internal membrane S_{int} was made equal to total area of the external membrane πL^2. The parameters values were selected as

$$R = 3, \; D_{av} = 0.013 \; \mu m^2/s, \; A = 0.6, \; k_{ext} = 1.67 \; 1/s, \; \kappa = 3.4, \; A_{en} = 0.0077 \; \mu m^2, \; F_{tot} = 1000.$$

The distribution of protein concentration on the external membrane computed with the above parameters is presented in Figure S6g.

Chapter 3.

Independence of symmetry breaking on Bem1-mediated autocatalytic activation of Cdc42

Sarah E. Smith[1,2], Boris Rubinstein[1], Ines Mendes Pinto[1], Brian D. Slaughter[1], Jay R. Unruh[1], and Rong Li[1,2,*]

[1]Stowers Institute for Medical Research, [2]Department of Molecular and Integrative Physiology, University of Kansas Medical Center

* Correspondence: rli@stowers.org

Author contributions: Sarah E. Smith performed all experiments. Sarah E. Smith analyzed data with help from Ines Mendes Pinto. Mathematical modeling was performed by Boris Rubinstein. ImageJ plugins and macros for image analysis were written by Jay R. Unruh and Sarah E. Smith. Yeast strains and plasmids were generated by Sarah E. Smith and Ines Mendes Pinto. Rong Li and Sarah E. Smith planned experiments with assistance from Boris Rubinstein, Brian D. Slaughter, and Jay R. Unruh. Sarah E. Smith and Rong Li wrote the manuscript. Rong Li conceived of and led the project.

Abstract

The ability to break symmetry and polarize through self-organization is a fundamental feature of cellular systems. A prevailing theory in yeast posits that symmetry breaking occurs via a positive feedback loop, wherein the adaptor protein Bem1 promotes local activation and accumulation of Cdc42 by directly tethering $Cdc42^{GTP}$ with its guanine nucleotide exchange factor (GEF) Cdc24. Here we find that neither Cdc24 localization nor the ability of Bem1 to bind $Cdc42^{GTP}$ is required for cell polarization. Instead, Bem1 functions primarily by boosting GEF activity. In the absence of actin-based transport, polarization of Cdc42 is accomplished through Rdi1, the Cdc42 guanine nucleotide dissociation inhibitor. A mathematical model is constructed describing cell polarization as a product of distinct pathways controlling Cdc42 activation and protein localization. The model predicts a non-monotonic dependence of cell polarization on the concentration of Rdi1 relative to that of Cdc42. This prediction was validated experimentally with modulated expression of Rdi1.

Introduction

Actin and microtubule cytoskeletons are key players driving cellular symmetry breaking in diverse morphogenetic systems (Li and Gundersen, 2008). Cytoskeletal polymers, through their inherent structural and biochemical polarity, orchestrate movement and localization of regulatory molecules, which in turn govern cytoskeleton assembly and organization. Such positive feedback loops between structural and regulatory components are features in most models of cell polarization (Goehring et al., 2011; Jose et al., 2013; Ku et al., 2012; Marco et al., 2007b; Seetapun and Odde, 2010; Slaughter et al., 2013; Wedlich-Soldner et al., 2003a). The budding yeast, however, presents a rather unique case where cellular symmetry breaking can be accomplished with or without contributions from the cytoskeleton (Ayscough et al., 1997; Irazoqui et al., 2003a; Wedlich-Soldner et al., 2004a). Yeast cells naturally bud in a defined pattern, termed bud site selection, guided by sites of previous cell division - bud scars (Casamayor and Snyder, 2002). However, cells are also known to polarize with equal efficiency, albeit in random orientations, when bud scar cues are eliminated or cells lose the ability to recognize them, reflecting a self-organizational mechanism at work.

A highly conserved regulator of cellular symmetry breaking and polarized morphogenesis is the small GTPase Cdc42 (Etienne-Manneville, 2004b). Localization of Cdc42 from an isotropic distribution around the cortex to a focused cap on one side of the cell is thought to be the key step in symmetry breaking, orchestrating, through Cdc42 effectors, a massive polarized reorganization of cellular components such as the actin cytoskeleton and the

secretory machinery, leading to the initiation of polarized growth to generate the bud. The Cdc42 polar cap is dynamically maintained: diffusion of Cdc42 within the membrane and exchange with the fast-diffusing cytosolic pool must be balanced by continuous recycling and retargeting of Cdc42 to the cap region (Marco et al., 2007b; Slaughter et al., 2009b; Wedlich-Soldner et al., 2004a).

Two distinct models have been proposed to explain symmetry breaking in yeast. One model relies on a positive feedback loop between Cdc42-regulated assembly of the actin cytoskeleton and actin cable-mediated transport of exocytic vesicles carrying Cdc42 to the nascent cap (Marco et al., 2007b; Wedlich-Soldner et al., 2003a). Crucial to this model, recent studies found that membrane microdomains and endocytic corralling serve to maintain Cdc42 concentration in the polar cap (Jose et al., 2013; Slaughter et al., 2013). This model was originally proposed to explain the finding that expression of constitutively active $Cdc42^{Q61L}$ in unpolarized G1-arrested cells results in spontaneous symmetry breaking via a mechanism dependent on actomyosin-based transport. In normally growing cell populations, however, disruption of actin only renders polarization less efficient (Wedlich-Soldner et al., 2004a).

An actin-independent model for cell polarization is centered on Cdc24, the lone Cdc42 GEF in yeast required for converting Cdc42 into the active, GTP-bound form. Cdc24 has been proposed to form a complex with Bem1 (Ito et al., 2001; Peterson et al., 1994; Zheng et al., 1995a), an adaptor-like protein sharing several protein interaction motifs (PB1, SH3, and PX) with animal cell polarity protein PAR6 and the p67Phox adaptor protein in the NADPH oxidase complex. Bem1 also has the ability to bind $Cdc42^{GTP}$ (Bose et al., 2001b; Yamaguchi et al., 2007), like PAR6 (McCaffrey and Macara, 2009), as well as effectors of Cdc42 such as the p21-

activated kinase (PAK) Cla4 (Bose et al., 2001b). The model posits that positive feedback occurs when the adaptor-GEF complex is recruited to an initial small accumulation of $Cdc42^{GTP}$ through the interaction with Bem1, leading to GEF localization and thus autocatalytic Cdc42 activation at the nascent cap (Butty et al., 2002a; Kozubowski et al., 2008). Supporting this idea, Bem1 is required for polarization in the presence of the actin inhibitor latrunculin A (LatA) and Bem1 can be recruited to ectopic caps formed by $Cdc42^{Q61L}$ (Wedlich-Soldner et al., 2004a). Several more recent studies further proposed the Bem1-mediated positive feedback loop to be the sole mechanism for symmetry breaking in yeast on the basis of synthetic lethality between *BEM1* and *RSR1*, encoding a Ras-like GTPase required for bud site selection (Howell et al., 2009; Kozubowski et al., 2008). This synthetic lethality was interpreted as to show that Bem1 is required for cell polarization in the absence of bud site selection, but Rsr1's function may not be limited to interpreting the bud scar cue (Park and Bi, 2007a).

Another unresolved question is how an autocatalytic activation of Cdc42 might lead to polarized localization of Cdc42. Soluble Cdc42 in the cytosol is chaperoned by Rdi1 (Das et al., 2012b; Koch et al., 1997; Slaughter et al., 2009b). Rdi1, like other Rho GDI proteins, has the ability to extract Cdc42 from the cortex (DerMardirossian and Bokoch, 2005) and this activity is facilitated by modulation of electrostatic interactions of Cdc42 with lipids by the lipid flippase Lem3 (Das et al., 2012b). The Rdi1-mediated Cdc42 recycling is required for maintaining the polar cap when actin is inhibited with LatA (Das et al., 2012b; Slaughter et al., 2009b). Rdi1 may passively facilitate polarization if it is prevented from extracting Cdc42 at the cap through a GEF-dependent mechanism (Kozubowski et al., 2008; Savage et al., 2012), but the rapid, Rdi1-

dependent exchange of Cdc42 at the polar cap (Slaughter et al., 2009b; Wedlich-Soldner et al., 2004a) argues against this idea.

In this work, we observe that *rsr1Δ bem1Δ* double mutant cells can in fact polarize without local accumulation of the GEF and that Rsr1 has a function in symmetry breaking beyond its role in bud site selection. We then tested the effects of *bem1* mutations that specifically disrupt each of its interactions on cell polarization. The results show that Bem1's function does not rely on its interaction with Cdc42 or Cla4, but rather, Bem1-Cdc24 binding boosts the overall level of the GEF activity. Based on experimental findings we constructed an alternative model to explain cytoskeleton-independent symmetry breaking centered on Rdi1-mediated Cdc42 recycling. Parameter requirements predicted for symmetry breaking were validated experimentally.

Results

Bem1 is not required for cell polarization in the absence of the bud scar cue

Investigation of how cells spontaneously break symmetry requires development of a physiological and yet spatial cue-independent system. Axial and bipolar budding patterns rely on the transmembrane markers Axl2 and Rax1/Rax2 complex, respectively, whose extensive N-glycosylation is thought to allow these proteins to interact with the cell wall, limiting diffusion of the bud scar signal (Fujita et al., 2004; Gao et al., 2007; Kozminski et al., 2003; Roemer et al., 1996; Sanders et al., 1999). Transmission of the bud scar signal to Cdc42 requires Rsr1 (Kozminski et al., 2003; Park and Bi, 2007a), forming the basis of using *rsr1Δ* as the genetic background for studying spontaneous symmetry breaking. However, evidence suggests that

Rsr1 may have a more general role in polarization: Rsr1 physically interacts with both Cdc42 (Kozminski et al., 2003) and Cdc24 (Park et al., 1997a; Zheng et al., 1995a), as well as Bem1 (Park et al., 1997a), and deletion of *RSR1* was reported to result in spatially unstable Cdc42 caps (Howell et al., 2012; Ozbudak et al., 2005), particularly in the presence of LatA. Thus, *rsr1Δ* could compromise both bud site selection and the core mechanism of cellular symmetry breaking.

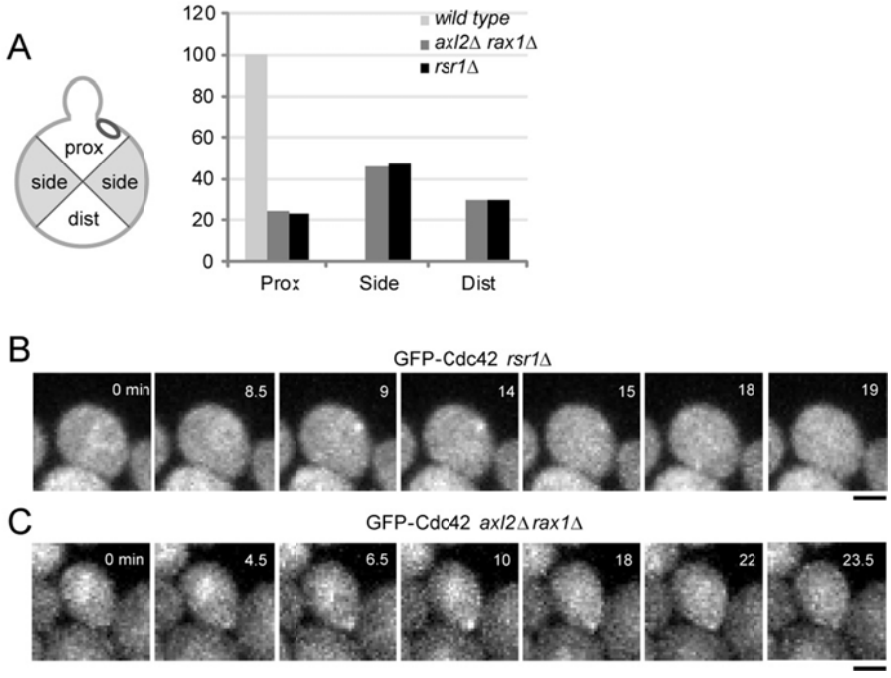

Figure S1. Characterization of spatial cue-independent polarization backgrounds. A. *axl2Δ rax1Δ* cells bud in random orientations, Related to Figure 1. Log phase, cycling cells were stained with calcofluar white and imaged as confocal z-stacks. Cells with buds and a single bud scar were scored for the position of the scar as in the proximal or distal quadrant of the cell relative to the bud, or to the side. n > 75 cells for each genotype. B-C. Dynamics of GFP-Cdc42 polar caps in *rsr1Δ* and *axl2Δ rax1Δ* cells in LatA. Cells of indicated genotypes were arrested in G1 via pheromone for 1.5hr, and released into LatA- containing SC media for 30 minutes prior to slide preparation on a 1% agarose pad containing 100μM LatA. Z-stack images were acquired at 30s intervals on a spinning disk confocal microsope equipped with an EM-CCD. Inset numbers indicate time in minutes relative to an arbitrary start point, the same start point as kymographs in Figure 1D-E. Images are maximum Z-projections.

To create a better genetic background for studying cellular symmetry breaking, we instead deleted the bud scar markers Axl2 and Rax1 to remove the structural cues for both axial and bipolar budding, as this leaves the Rsr1 GTPase module intact. We confirmed that *axl2Δ rax1Δ* cells bud in random orientations (**Fig. S1A**). Like *rsr1Δ* cells, *axl2Δ rax1Δ* cells grew similarly to the wild type under the standard experimental condition (**Fig. 1A**). We next measured the rate of polarization on the population level in the presence or absence of LatA after release from a pheromone-induced G1 arrest. *axl2Δ rax1Δ* cells polarized at rates similar to wild-type cells in both DMSO and LatA. By contrast, *rsr1Δ* cells showed slower polarization in the presence of LatA (**Fig. 1B-C**). Time-lapse imaging was then performed to examine polarization of GFP-Cdc42 in single polarizing *rsr1Δ* or *axl2Δ rax1Δ* cells in LatA. The single-cell analysis revealed a notable difference in polar cap stability between the different mutants: polar caps in *rsr1Δ* lasted for 400 ± 40s and then sometimes reappeared at a different location (**Fig. 1D,F; Fig. S1B**), whereas *axl2Δ rax1Δ* cells maintained stable polar caps for much longer periods, averaging 1000 ± 130s (**Fig. 1D-E; Fig. S1C**). This result is consistent with the polarization behavior reported previously for *rsr1Δ* cells (Howell et al., 2012; Ozbudak et al., 2005) and suggests that Rsr1 is important for decisive symmetry breaking in addition to its role in bud site selection.

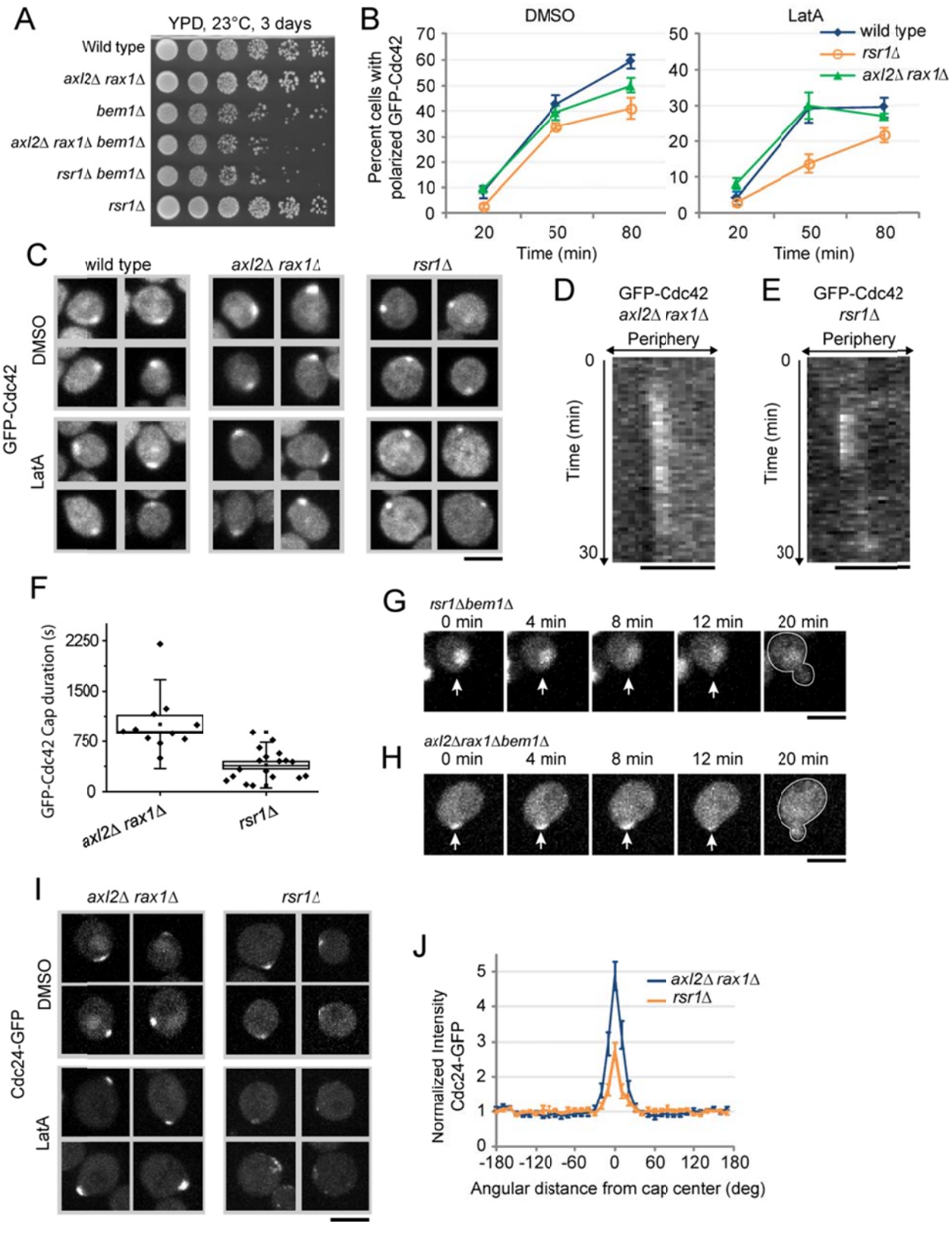
A
YPD, 23°C, 3 days
Wild type
axl2Δ rax1Δ
bem1Δ
axl2Δ rax1Δ bem1Δ
rsr1Δ bem1Δ
rsr1Δ
B
DMSO
LatA
wild type
rsr1Δ
axl2Δ rax1Δ
Percent cells with polarized GFP-Cdc42
Time (min)
C
wild type
axl2Δ rax1Δ
rsr1Δ
GFP-Cdc42
DMSO
LatA
D
GFP-Cdc42
axl2Δ rax1Δ
Periphery
Time (min)
E
GFP-Cdc42
rsr1Δ
Periphery
Time (min)
F
GFP-Cdc42 Cap duration (s)
axl2Δ rax1Δ
rsr1Δ
G
rsr1Δbem1Δ
0 min
4 min
8 min
12 min
20 min
H
axl2Δrax1Δbem1Δ
0 min
4 min
8 min
12 min
20 min
I
axl2Δ rax1Δ
rsr1Δ
Cdc24-GFP
DMSO
LatA
J
axl2Δ rax1Δ
rsr1Δ
Normalized Intensity Cdc24-GFP
Angular distance from cap center (deg)

Figure 1

Figure 1. Bem1 and GEF localization are not required for symmetry breaking. **A**. Cells with indicated genotypes were plated on YPD media and grown at 23°C for 3 days. Cells were grown overnight in liquid culture and then diluted to an OD of 1. This and a series of tenfold dilution were spotted left to right. **B**. Polarization of GFP-Cdc42 wild type, *axl2Δ rax1Δ*, and *rsr1Δ* cells after release from G1 arrest into media containing DMSO or LatA. The percentage of cells with polarized GFP-Cdc42 was determined at different time points (given in min) after release. The plots show mean from averaging 2 experiments and error bars correspond to standard error of the mean (SEM). >100 cells were counted per time point per experiment. **C**. Maximum projections of representative polarized cells from (A). Scale bar: 5 µm. **D-E**. Representative kymographs of polarizing GFP-Cdc42 in *axl2Δ rax1Δ* (D) and *rsr1Δ* (E) cells in LatA. Note the unstable polar cap in (E) relative to that in (D). Scale bar: 5 µm. See also Figure S1. **F**. Quantification of cap duration in LatA of polarized GFP-Cdc42 in *axl2Δ rax1Δ* (n = 11) and *rsr1Δ* (n = 18) cells from movies such as the ones shown in D-E. The intensity of the polar caps were measured and plotted over time and were fitted to Gaussian curves in OriginPro. The duration of the cap is reported as the full width half maximum of the Gaussian fit. Box: SEM, whiskers: standard deviation (SD). $P < 0.001$. **G-H**. Time-lapse imaging of Cdc24-GFP in *rsr1Δbem1Δ* (G) and *axl2Δrax1Δbem1Δ* (H) cells. Notice the lack of Cdc24 polarization in (G) despite successful cell polarization and budding, compared to strong Cdc24 polarization in H. Arrows point to incipient bud site. White outlines indicate the perimeter of the budded cell. Scale bar 5 µm. **I**. Maximum projections of representative cells with polarized Cdc24-GFP in *axl2Δ rax1Δ* and *rsr1Δ* cells in LatA or DMSO. Scale bar: 5 µm. **J**. Quantification of polarization of Cdc24-GFP in *axl2Δ rax1Δ* and *rsr1Δ* cells in LatA 50 min following pheromone arrest release from maximum projections of Z-stack images. Cells with polarized GFP-Cdc24 were identified and cortex masks were generated from a separate fluorescent channel (mCherry-Cdc42, see methods). Average intensity of the cortex within the mask was determined in 10° increments centered on the polar cap. The resultant intensity profiles were normalized against the average intensity of the cortex in the "back half" of the cell (-180° to -90° and 90° to 180°); these normalized profiles were averaged over n > 18 cells. Error bars correspond to SEM. For comparison of values at 0°, $P< 0.001$.

Although extensive data was interpreted based on the assumption that Bem1 is required for viability in the *rsr1Δ* background (Howell et al., 2012; Howell et al., 2009; Kozubowski et al., 2008), both *bem1Δ rsr1Δ* double mutant cells and *bem1Δ axl2Δ rax1Δ* triple mutant cells grew similarly to *bem1Δ* alone in the S288c genetic background (**Fig. 1A**), suggesting that Bem1 is nonessential for symmetry breaking. Strikingly, time-lapse imaging revealed that, although cells polarized and budded normally in *bem1Δ rsr1Δ* cells, there was no apparent Cdc24 localization to the incipient bud site. (**Fig. 1G**). In contrast, *bem1Δ axl2Δ rax1Δ* cells showed prominent polarization of Cdc24-GFP before bud emergence (**Fig. 1H**), similar to *bem1Δ* cells as previously reported (Butty et al., 2002a; Gulli et al., 2000a). Polar localization of

Cdc24-GFP in LatA was also significantly reduced in *rsr1Δ* cells compared with *axl2Δ rax1Δ* cells (**Fig. 1I-J**). Taken together, these results show that, although Rsr1 and Bem1 together control Cdc24 localization in the polar cap, this function (and hence local activation of Cdc42) is not crucial to cell polarization and bud formation.

Symmetry breaking does not rely on Bem1-mediated Cdc42-to-Cdc24 feedback loop

All existing models assume that Bem1 functions in symmetry breaking by mediating a positive feedback loop connecting Cdc42 and Cdc24 as outlined in **Figure 2A**. Whereas this assumption was supported by gain of function experiments where, for example, Cdc24 covalently linked to Cla4 could bypass the requirement for Bem1 for viability in *rsr1Δ* background (Kozubowski et al., 2008), the assumption has not been rigorously tested using loss-of-function approaches under more physiological settings. To this end, we pursued an unbiased investigation into how Bem1 participates in symmetry breaking by systematically disrupting each of the known physical interactions of Bem1 (**Fig. 2B**) using specific point mutations validated in previous studies (Butty et al., 2002a; van Drogen-Petit et al., 2004; Yamaguchi et al., 2007) (**Fig. 2C**). We note that all *bem1* mutants analyzed below were in the *axl2Δ rax1Δ* background for observing symmetry breaking in the absence of the bud scar cue.

We began by disrupting the binding of Bem1 to $Cdc42^{GTP}$, which was thought to recruit Bem1 (and thus the associated GEF Cdc24) to the polar cortex, a critical step in the proposed Bem1-dependent feedback loop. This was achieved by replacing *BEM1* with a centromeric plasmid expressing *bem1* (under the *BEM1* promoter) bearing the N253D mutation, which lies in the Cdc42 interaction (CI) domain and was previously shown to abolish Bem1 binding to

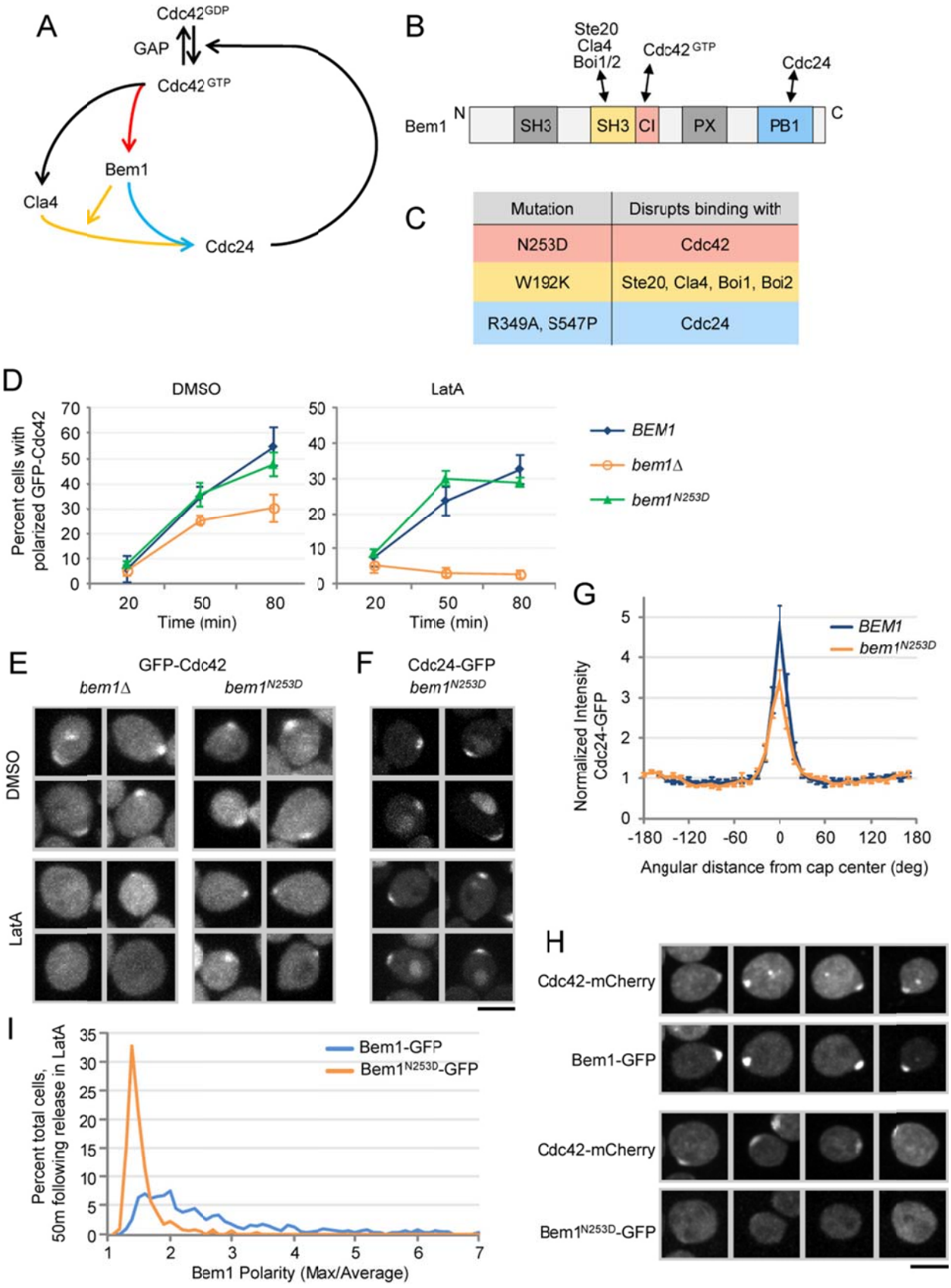
A
Cdc42GDP
GAP
Cdc42 GTP
Bem1
Cla4
Cdc24
B
Ste20
Cla4
Boi1/2
Cdc42 GTP
Cdc24
Bem1
N
SH3
SH3
CI
PX
PB1
C
C
Mutation
Disrupts binding with
N253D
Cdc42
W192K
Ste20, Cla4, Boi1, Boi2
R349A, S547P
Cdc24
D
DMSO
LatA
Percent cells with polarized GFP-Cdc42
Time (min)
BEM1
bem1Δ
bem1N253D
E
GFP-Cdc42
bem1Δ
bem1N253D
DMSO
LatA
F
Cdc24-GFP
bem1N253D
G
Normalized Intensity Cdc24-GFP
Angular distance from cap center (deg)
BEM1
bem1N253D
H
Cdc42-mCherry
Bem1-GFP
Cdc42-mCherry
Bem1N253D-GFP
I
Percent total cells, 50m following release in LatA
Bem1 Polarity (Max/Average)
Bem1-GFP
Bem1N253D-GFP

Figure 2

Figure 2. Direct Bem1-Cdc42^{GTP} interaction is not required for GEF localization or cell polarization. A. Schematic drawing of the proposed Bem1 feedback loop. **B**. Bem1 domains and known interacting partners. **C**. Bem1 mutations used in this study and their projected effects on Bem1 interactions. **D**. Polarization of GFP-Cdc42 in *axl2Δ rax1Δ BEM1*, *axl2Δ rax1Δ bem1Δ*, and *axl2Δ rax1Δ bem1^{N253D}* cells, as in Fig 1B. The plots show mean and SEM from 2 experiments with >100 cells counted per time point per experiment. **E**. Maximum projections of representative polarized cells from (D). Scale bar: 5 µm. **F**. Maximum projections of representative cells with polarized Cdc24-GFP in *axl2Δ rax1Δ bem1^{N253D}* cells, following pheromone arrest release in LatA or DMSO. Scale bar: 5 µm. **G**. Polarization of Cdc24-GFP in *axl2Δ rax1Δ* cells and in in *axl2Δ rax1Δ bem1^{N253D}* cells, as in Fig 1J. For the comparison of peak values at 0°, $P < 0.01$. **H**. Localization of Bem1-GFP or bem1^{N253D}-GFP in cells with polarized mCherry-Cdc42 following pheromone arrest release in LatA. Z-stack images of representative cells were subjected to a 1x1 Gaussian filter prior to maximum projection. Scale bar: 5 µm. **I**. Histogram of Bem1-GFP polarity (maximum pixel intensity/average pixel intensity per cell) for Bem1-GFP and bem1^{N253D}-GFP at 50 minutes following pheromone arrest release in LatA. n= 520 cells were quantified for each genotype.

active Cdc42 (Yamaguchi et al., 2007). Surprisingly, polarization of GFP-Cdc42 was unaffected in *bem1^{N253D}* cells in the *axl2Δ rax1Δ bem1Δ* background compared to *BEM1* cells in the same background in the absence or presence of LatA (**Fig. 2D,E**). Cdc24-GFP localization was reduced in *bem1^{N253D}* cells in the *axl2Δ rax1Δ bem1Δ* background in LatA (**Fig. 2F-G, P<0.01**) but remained higher than in *rsr1Δ* cells (compare Fig. 2G with Fig. 1J). If the N253D mutation indeed disrupted Bem1-Cdc42 interaction, Bem1^{N253D}-GFP should be unable to polarize to the Cdc42 cap. Indeed Bem1^{N253D}-GFP polarized poorly (Fig.2H), and we quantified the polarization strength of Bem1^{N253D}-GFP compared to Bem1-GFP, which indicated a significant ($P<10^{-64}$) reduction of polarization of Bem1^{N253D}-GFP compared to Bem1-GFP (**Fig. 2I**). This supports the *in vivo* disruption of Cdc42-Bem1 interaction and shows that symmetry breaking does not require localization of Bem1 to the site of Cdc42 accumulation.

Bem1-Cdc24 interaction contributes to polarization by boosting GEF activity

We next disrupted the interaction between Bem1 and Cdc24, thought to be required for recruitment of Cdc24 to the site of active Cdc42 accumulation. Cdc24 and Bem1 interact

through hetero-dimerization between PB1 domains located at the COOH termini of these proteins (Butty et al., 2002a; Ito et al., 2001). Supporting a crucial role for this interaction in symmetry breaking, mutations in Bem1 abolishing PB1 domain binding (*bem1*^{R349A,S547P}) resulted in failure of cells to polarize in the presence of LatA, whereas polarization in these mutants was only reduced without LatA, similar to that in *bem1Δ* (**Fig. 3A,B**).

Because Cdc24 was able to polarize even in the absence of polarized Bem1 (**Fig. 2F**), it was unlikely that the failed polarization of PB1 domain mutant cells was due to a lack of Cdc24 localization. A previous study hypothesized that Cdc24 exists in an auto-inhibited form and that binding by Bem1 might help to relieve this inhibition (Shimada et al., 2004b). To investigate this possibility, we developed a FRET-based biosensor (Hodgson et al., 2008; Itoh et al., 2002) for Cdc42 activation that consists of a linked construct of yeast Cdc42 with the CRIB domain from Cla4 (**Fig. 3C**), which interacts only with the active, GTP-bound form of Cdc42. These are flanked by GFP and mCherry, such that when the CRIB and Cdc42^{GTP} within the sensor are bound, the GFP and mCherry are brought in close proximity for energy transfer to occur, as illustrated in **Figure 3C**. The polybasic-CAAX box region of *CDC42* was moved C-terminally to mCherry to allow proper prenylation and membrane anchorage. Higher FRET efficiency indicates higher net GEF activity toward Cdc42. FRET was measured in the 30° arc over the cap region using the acceptor photobleaching approach as described in Experimental Procedures (**Fig. 3C-E**). Mutations were introduced into the Cdc42 portion of the biosensor, resulting in either a constitutively GTP-bound (Q61L) or GDP-bound (D57Y) state to serve as positive or negative controls, respectively. The positive and the negative controls showed well-separated

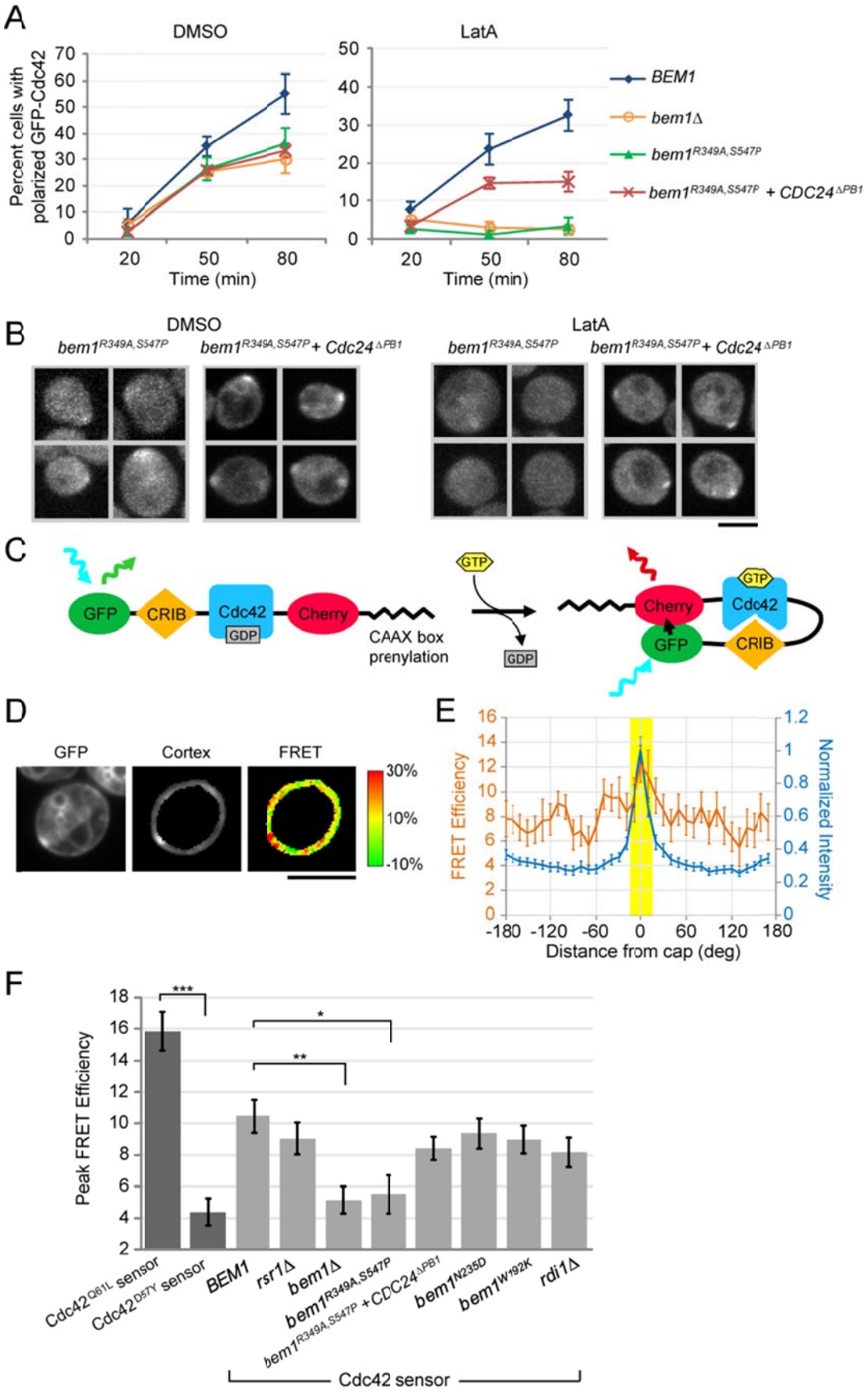
A
DMSO
LatA
Percent cells with polarized GFP-Cdc42
Time (min)
BEM1
bem1Δ
bem1R349A,S547P
bem1R349A,S547P + CDC24ΔPB1
B
DMSO
LatA
bem1R349A,S547P
bem1R349A,S547P+ Cdc24ΔPB1
C
GFP
CRIB
Cdc42
GDP
Cherry
CAAX box prenylation
GTP
GDP
D
GFP
Cortex
FRET
30%
10%
-10%
E
FRET Efficiency
Normalized Intensity
Distance from cap (deg)
F
Peak FRET Efficiency
Cdc42Q61L sensor
Cdc42D57Y sensor
BEM1
rsr1Δ
bem1Δ
bem1R349A,S547P
bem1R349A,S547P +CDC24ΔPB1
bem1N235D
bem1W192K
rdi1Δ
Cdc42 sensor

Figure 3. Bem1 contributes to symmetry breaking by boosting the GEF activity of Cdc24.
A. Polarization of GFP-Cdc42 in *axl2Δ rax1Δ BEM1* cells, *axl2Δ rax1Δ bem1Δ* cells, *axl2Δ rax1Δ* $bem1^{R349A,S547P}$ cells, and *axl2Δ rax1Δ* $bem1^{R349A,S547P}$ cells expressing $cdc24^{\Delta PB1}$ from the *CDC24* promoter. Experimental procedure was as described in Fig 1B. The plots show mean from averaging 2 experiments and error bars correspond to standard error of the mean (SEM). >100 cells were counted per time point per experiment. **B**. Maximum projections of representative cells from (A). Scale bar: 5 µm. **C**. Schematic representation of the FRET-based biosensor for Cdc42 activation. Active $Cdc42^{GTP}$ binds the CRIB domain, bringing the flanking GFP and mCherry into proximity and allowing FRET. **D**. A representative wild-type cell expressing the biosensor containing wild-type Cdc42. Leftmost panel shows the sum of the time series for GFP. The center panel shows the same image with cortex mask applied (see Experimental Procedures). The right panel shows the FRET efficiency at each pixel within the cell as indicated by the heat bar. Scale bar: 5 µm. **E**. Average FRET Efficiency (Orange curve) was measured and plotted in 10° increments along the cortex in the masked image (see B, center image). Average normalized GFP intensity at the cortex (Blue curve) was also measured and plotted. Each plot shows mean from >25 cells and error bars show SEM. **F**. FRET efficiency in the cap region in indicated strains. The left two bars were from wild-type cells expressing positive and negative control sensors. FRET efficiency was measured as the average FRET within the 30° region surrounding the cap region (yellow region highlighted in panel C). Each histogram show mean from >25 cells and error bars show SEM. Significance: * $P < 0.005$, ** $P < 0.0005$, *** $P < 10^{-10}$

FRET efficiencies ($n > 25$ cells for each strain, $p < 10^{-8}$), whereas the wild-type biosensor showed a FRET level intermediate between the controls as expected (**Fig. 3F**).

We introduced the above Cdc42 activation biosensor into various mutant strains. Deletion of *RSR1* resulted in FRET measurements similar to that in wild-type cells ($p = 0.3$), whereas deletion of *BEM1* resulted in a significant lower FRET efficiency ($p < 10^{-3}$) (**Fig. 3F**). Interestingly, disruption of the Bem1-Cdc24 interaction through the $bem1^{R349A,S547P}$ mutation reduced the biosensor FRET by an extent similar to that by *bem1Δ* (**Fig. 3F**, $P = 0.8$ compared with *bem1Δ,* $P < 0.01$ compared with *BEM1*). By contrast, GEF activity in $bem1^{N253D}$ cells was not significantly different from the wild type (**Fig. 3F**, $P = 0.4$). These results show that the Bem1 interaction with Cdc24 is primarily responsible for enhancement of the latter's GEF activity. Since it was proposed that the PB1 domain of Cdc24 acts as an auto-inhibitory domain, and that binding by Bem1 may help relieve the auto-inhibition (Shimada et al., 2004a), deletion of the

PB1 domain should result in a constitutively active version of Cdc24. Indeed, Cdc24$^{\Delta PB1}$ expressed under the *CDC24* promoter from a centromeric plasmid boosted biosensor FRET in *CDC24 bem1*^{R349A,S547P} cells (**Fig. 3F**, P = 0.1 compared with *BEM1*, P < 0.01 compared with *bem1*^{R349A,S547P}). Importantly, the de-regulated GEF (Cdc24-*Δ*PB1) partially rescued cell polarization in *bem1*^{R349A,S547P} cells in the presence of LatA (**Fig. 3A-B**), supporting the notion that Bem1's role in cell polarization without actin is mainly mediated through its interaction with Cdc24, which stimulates Cdc24 GEF activity.

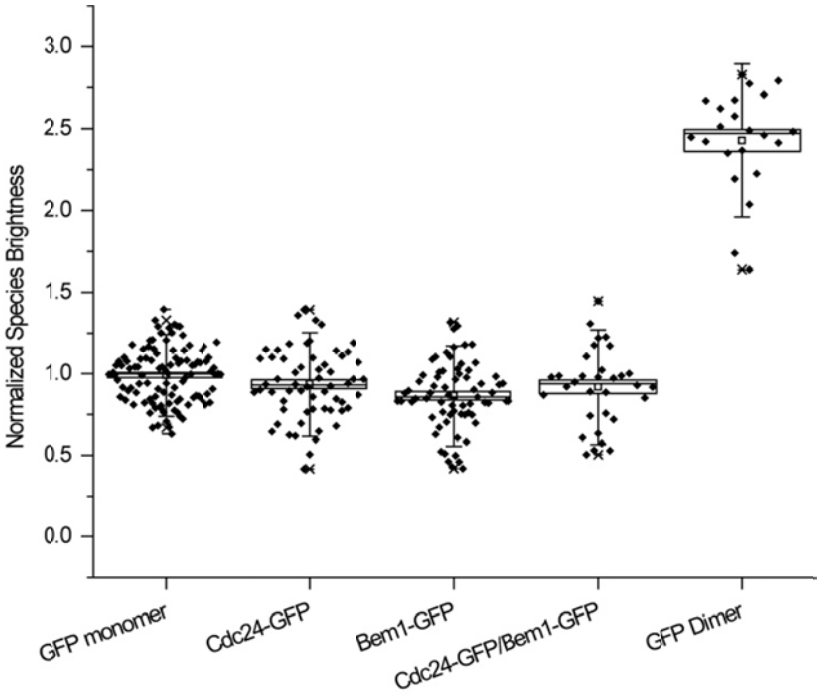

Figure S2. Bem1 and Cdc24 do not form mobile complexes, either homotypically or with each other.

Fluoresence Correlation Spectroscopy (FCS) was performed on cells expressing either monomeric GFP, Cdc24-GFP, Bem1-GFP, both Bem1-GFP and Cdc24-GFP, or GFP-GFP linked dimer. Brightness of mobile species was calculated from the amplitude *G(0)* of the FCS autocorrelation curve as $I \cdot G(0)/\gamma$, where *I* is the average intensity of the measurement and γ is a measurement of the point spread function. Meaurements were normalized to the monomer. Box, SE, Whiskers, SD. n > 25 measurements for each strain.

Wondering if Bem1 and Cdc24 travel as a complex in the cytosol, we used FCS to measure the species brightness of Bem-GFP, Cdc24-GFP, or both compared with monomeric GFP. We found that both Bem1-GFP and Cdc24-GFP were of monomeric brightness, and that when both Bem1-GFP and Cdc24-GFP were expressed, the brightness of the species were not increased (**Figure S2**). This suggests that Cdc24 and Bem1 neither homotypic nor heterotypic mobile complexes.

A second mechanism by which Bem1 has been suggested to modulate Cdc24 activity is mediation of complex formation between Cdc24 and the Cdc42 effector Cla4. Cdc24 is hyperphosphorylated by Cla4 in this complex, which requires direct binding of both Cla4 and Cdc24 by Bem1 (Bose et al., 2001b; Gulli et al., 2000a; Wai et al., 2009). Expression of a fusion construct of $Cdc24^{\Delta PB1}$ linked with Cla4 was shown to rescue the synthetic lethality of *Δrsr1 Δbem1* in the yeast strain background used in a previous study (Kozubowski et al., 2008), which was interpreted as supporting a sufficiency of complex formation between Cdc24 and Cla4 for symmetry breaking. However, we found that the rescued cells failed to polarize in the presence of LatA (**Fig. 4A-B**), suggesting that the fusion construct relies on an actin-dependent mechanism to accomplish the rescue. Because Bem1 and Cla4 interact through the Bem1 SH3 domain and a proline-rich motif in Cla4 (Bender et al., 1996), we tested the disruption of the projected Bem1-Cla4-Cdc24 complex by mutating the invariant tryptophan ($bem1^{W192K}$) in the SH3 domain required for binding to proline-rich motifs (Larson and Davidson, 2000). $bem1^{W192K}$ resulted in a slight but significant ($P < 0.01$ at 50 min) reduction in the percentage of polarized cells in the presence of LatA compared to the control (**Fig. 4C-D**), but biosensor measurements

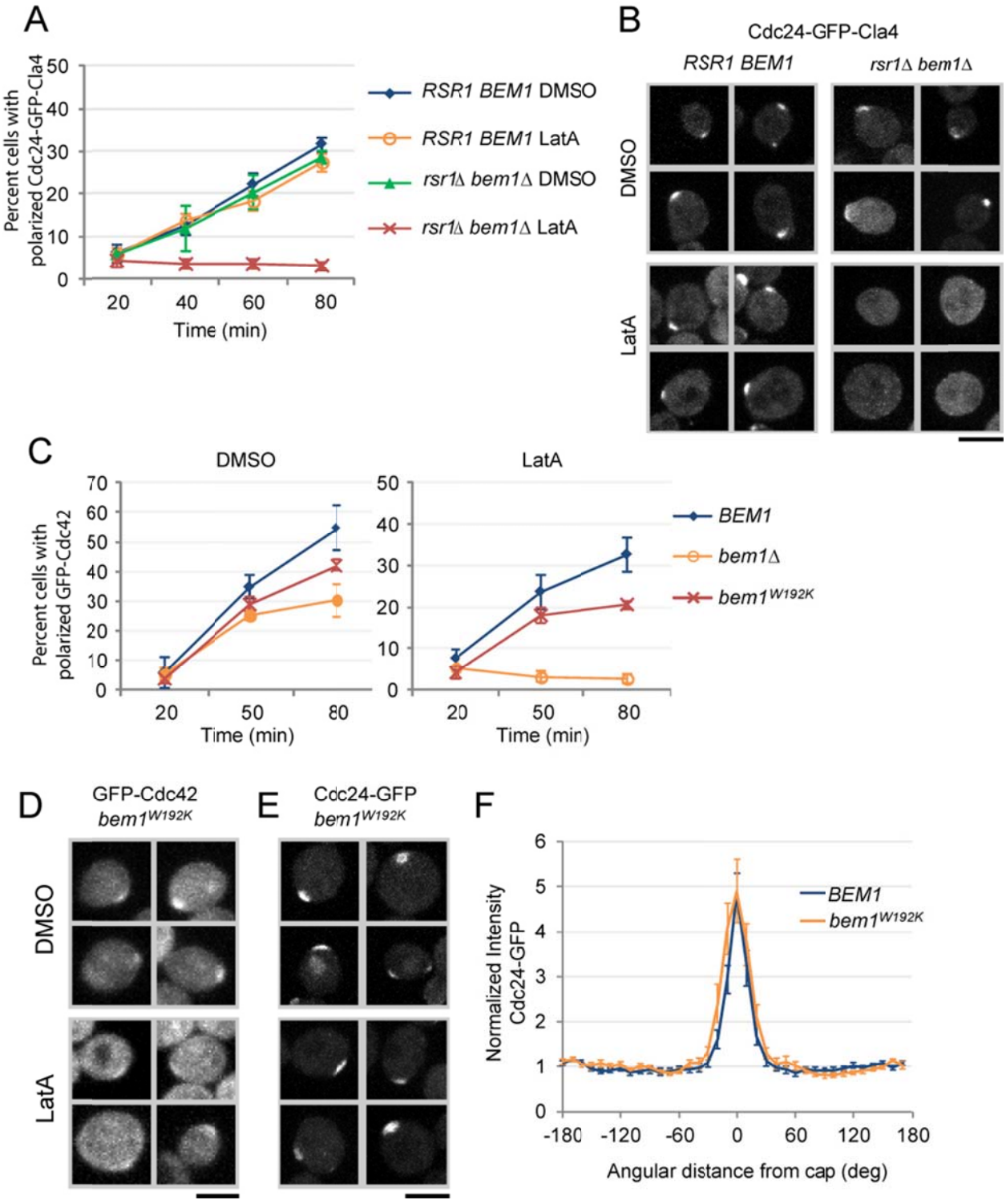

Figure 4. The Bem1-Cla4 interaction is not required for Cdc24 localization or symmetry breaking. A. Polarization of Cdc24$^{\Delta PB1}$-GFP-Cla4 in *RSR1 BEM1* cells and in *rsr1Δ bem1Δ* cells in DMSO or LatA upon release from G1 pheromone arrest. Experimental procedure was as described in Fig 1B. The plots show mean from averaging 3 experiments and error bars correspond to standard error of the mean (SEM). >100 cells were counted per time point per experiment. **B**. Maximum projections of representative

cells from (A). Scale bar: 5 µm. **C**. Polarization of GFP-Cdc42 in *axl2Δ rax1Δ BEM1* cells, *axl2Δ rax1Δ bem1Δ*, and *axl2Δ rax1Δ bem1*^{W192K} cells, as in Fig 1B. **D**. Maximum projections of representative polarized cells from (C). Scale bar: 5 µm. **E**. Maximum projections of representative cells with polarized Cdc24-GFP in *axl2Δ rax1Δ bem1*^{W192K} cells, following pheromone arrest release in LatA or DMSO. Scale bar 5 µm. **F**. Quantification of Cdc24-GFP polarization in *axl2Δ rax1Δ* cells and in *axl2Δ rax1Δ bem1*^{W192K} cells, as in Fig 1I. For the comparison of peak values at 0°, P=0.5. Plots show normalized profiles averaged over n > 17 cells. Error bars correspond to SEM.

showed GEF activity similar to that in the wild type polar cap (P = 0.3) (**Fig. 3F**). Importantly, the localization of Cdc24 was also normal in the *bem1*^{W192K} background(**Fig. 4E-F**). These results suggest that GEF localization and activity at the polar cap is largely independent of the interaction of Bem1 with its SH3 domain ligands.

Symmetry breaking without actin requires Rdi1-mediated cytosolic targeting of Cdc42

The above results indicate that, although each of the interactions in the proposed Bem1 feedback loop has some role in the polarization of different polarity regulators, Bem1's function in symmetry breaking is mainly to boost Cdc42 activation, which does not have to be locally restricted. How then does Cdc42 polarize without actin? In addition to the membrane-bound pool, which is targeted by actin, Cdc42 exists in the cytosol in a soluble pool as the Rdi1-bound complex (Koch et al., 1997; Slaughter et al., 2009b; Tiedje et al., 2008). *rdi1Δ* cells fail to polarize Cdc42 in the presence of LatA following release from pheromone G1 arrest (**Fig. 5A-B**), suggesting that targeting from the Rdi1-bound cytosolic pool is not only required for maintaining but also for establishing Cdc42 protein polarization when actin is disrupted. The polarization defect in *rdi1Δ* cells in the presence of LatA was not due to insufficient GEF activity: biosensor measurements indicated the GEF activity in *rdi1Δ* cells to be similar to that in the wild type (**Fig.3F**, P = 0.89), and expression of Cdc24$^{\Delta PB1}$ did not rescue the polarization defect of

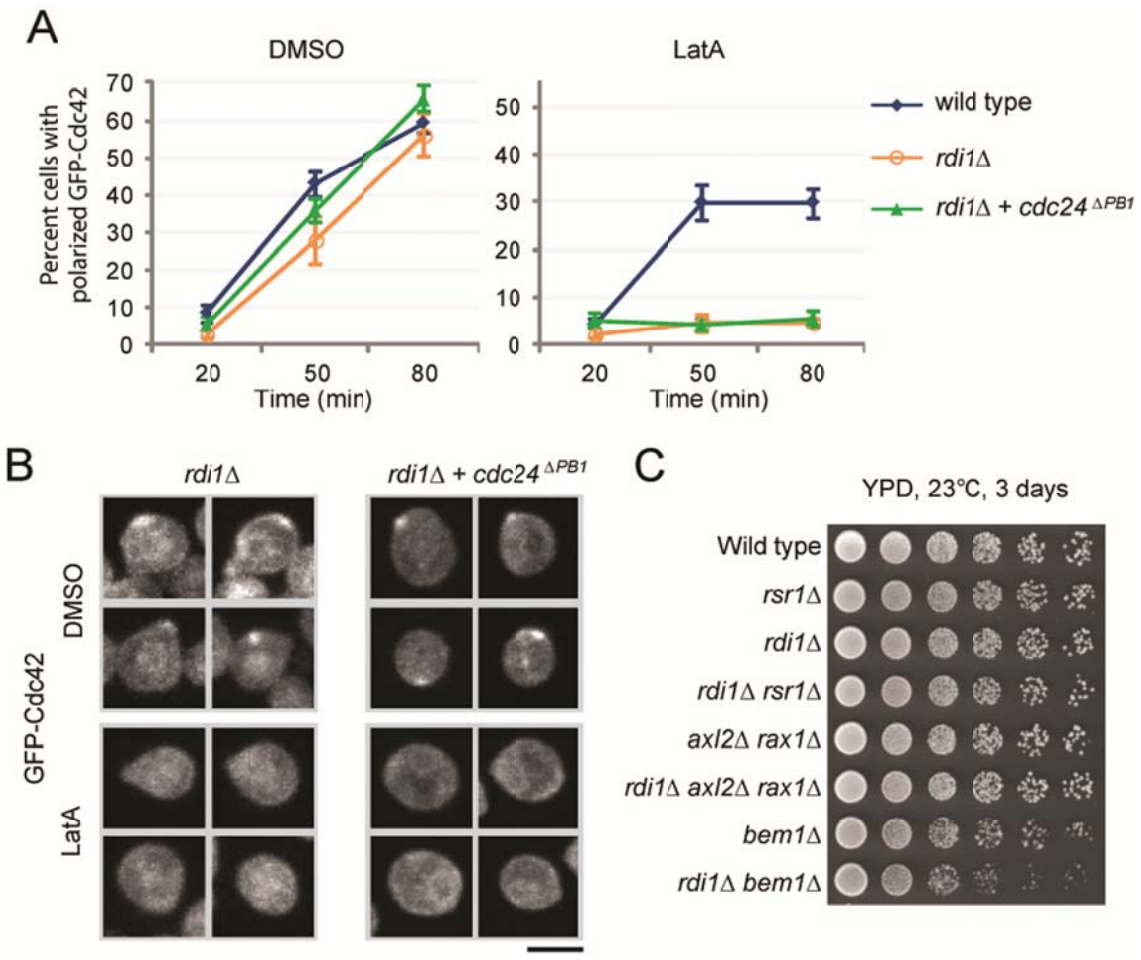

Figure 5. Rdi-mediated cytosolic targeting of Cdc42 is essential for symmetry breaking without actin. **A**. Polarization of GFP-Cdc42 in wild type cells, *rdi1Δ* cells, and *rdiΔ* cells expressing *cdc24*$^{\Delta PB1}$ from the *CDC24* promoter in DMSO or LatA after release from G1 pheromone arrest. Experimental procedure was as described in Fig 1B. The plots show mean from averaging 3 experiments and error bars correspond to SEM. >100 cells were counted per time point per experiment. **B**. Maximum projections of representative cells from (A). Scale bar: 5 µm. **C**. Serial dilution of cells with indicated genotypes from an overnight culture with an OD of 1 were plated on YPD media and grown at 23°C for 3 days.

rdi1Δ cells (**Fig.5A,B**). Furthermore, deletion of *RDI1* did not affect growth of *rsr1Δ* or *axl2Δ rax1Δ* cells, suggesting that Rdi1 is not required for cellular symmetry breaking when actin is intact, but deletion of *RDI1* moderately exacerbated the slow growth phenotype of *bem1Δ* cells (**Fig. 5C**). Taken together the above results show that targeting of Cdc42 from the cytosolic Rdi1-bound pool is central to Cdc42 polarization in the absence of actin-based vesicular

trafficking, and that this process is distinct from GEF activation, which does not have to be spatially confined.

Analytical model of actin-independent asymmetry breaking without localized GEF activation

As a theoretical exploration of the polarization mechanism based on findings of this study, we used a minimalistic approach, similar to several previous studies (Altschuler et al., 2008; Goryachev and Pokhilko, 2006; Mori et al., 2011; Otsuji et al., 2007), to discover the conditions that could allow asymmetry breaking through Rdi1-mediated Cdc42 targeting from the cytosol but not local activation of the GEF. Main components of the one-dimensional model include: Cdc42 on the membrane (local concentration $u(x,t)$), a fraction ($a_1 < 1$) of which is in the active GTP-bound form, Cdc42 in cytosol $v(x,t)$, free (cytosolic) Rdi1 $R_f(x,t)$, and the cytosolic Rdi1-Cdc42 complex $R_c(x,t)$. Considering a simplest case where the activity G that dissociates the Rdi-Cdc42 complex is proportional to squared density of active Cdc42 , $G(u) = a_2(a_1 u)^2$, i.e., $G(u) = Au^2$, where $A = a_2 a_1^2$; the membrane targeting term for Cdc42 then reads $Au^2 R_c$ (**Fig.6A**). Cdc42 internalization is given by the term $\beta u R_f$, where β is the extraction rate of membrane-bound Cdc42 by free Rdi1. Because cytosolic Cdc42 exists in Rdi1- and vesicle-bound states (Das et al., 2012b; Slaughter et al., 2013), we assume $R_c = \gamma v$, where $0 < \gamma < 1$. Based on recently published data on the mobile pools of Cdc42 by using fluorescence correlation spectroscopy (Das et al., 2012b),□□ was estimated to be 0.4. Using the conservation condition for mean concentration of Rdi1 (R) in the cell, we have $R_f = R - R_c = R - \gamma v$.

The cell is represented as a line segment with a size L. Dynamics of the Cdc42 concentrations are described in the region $0 \le x \le L$:

$$\begin{aligned} \frac{\partial u}{\partial t} &= \gamma A(u-u_b)^2 v - \beta(u-u_b)(R-\gamma v) + D_u \frac{\partial^2 u}{\partial x^2}, \\ \frac{\partial v}{\partial t} &= -\gamma A(u-u_b)^2 v + \beta(u-u_b)(R-\gamma v) + D_v \frac{\partial^2 v}{\partial x^2}, \end{aligned}$$

where u_b denotes a non-zero but small basal uniform concentration of Cdc42 in the membrane (see Supplementary Information). The diffusion of Cdc42 in the cytosol is much faster than that in the membrane: $D_v >> D_u$. The equations are subject to no-flux boundary conditions, and the total amount CL of Cdc42 in the cell is conserved. A linear stability analysis showed that the growth rate of small perturbations to an initial uniform distribution is proportional to the activation level of Cdc42 (see Supplementary Information); Simulations of the model showed the perturbations lead to growth of a single peak of Cdc42 to a steady level (Fig.6B).

We explored the parameter space for R (cellular Rdi1 level) and A (essentially a parameter describing the activation level of Cdc42 that also impacts Cdc42 targeting) required for symmetry breaking. For a fixed value of A, simulations showed that formation of stable polarity responds non-monotonically to *R*, such that polarization occurs when R is in the range of 0.5-0.8 (note R values are normalized to the global concentration of Cdc42, *C* = 1, and the upper but not lower boundary depends on the value of A, see Discussion). When R is above this range, no polarization occurs due to a lack of Cdc42 targeting to membrane, whereas when R is below the range, a high level of Cdc42 uniformly distributes on the membrane (Fig.6C). To perform a qualitative experimental test of this prediction, we induced expression of Rdi1 under the *GAL1* promoter for varying time periods prior to release from pheromone arrest into LatA-

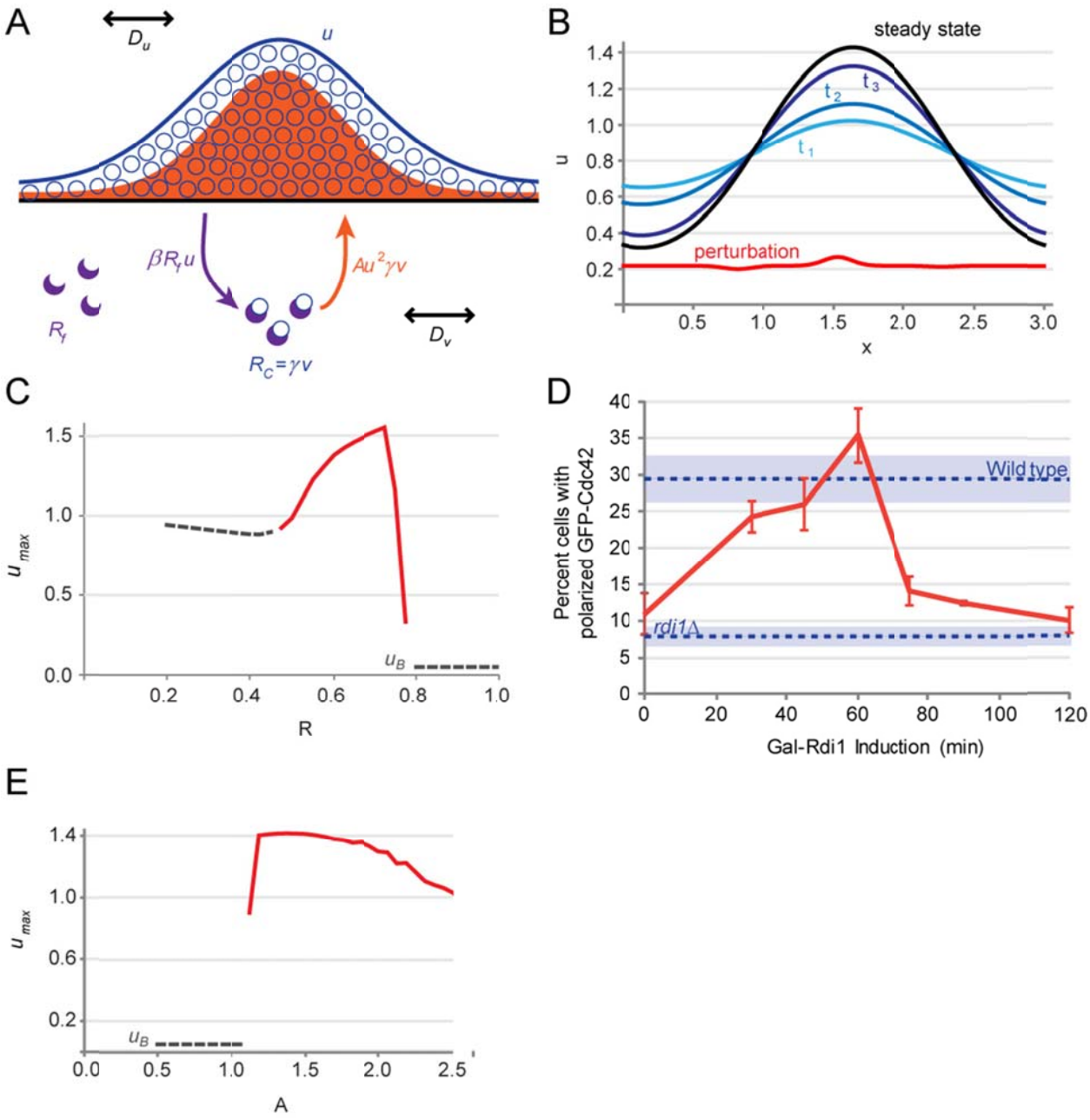

Figure 6. Mathematical model of Rdi1-dependent symmetry breaking and parameter validation. A. Schematic of analytical model for Rdi1-dependent polarization. Distribution of Cdc42 across the cortex is given by $u(x,t)$ (blue curve), of which a constant fraction a_1 is activated. Cdc42 extraction is proportional to free Rdi1, R_f (purple crescents) and $u(x,t)$ by a constant β. Targeting of Cdc42 to the cortex is assumed to be proportional to the squared distribution of active Cdc42^{GTP}, $(a_1u)^2$, the profile of which is represented by the filled orange curve. Cytosolic diffusion D_v and cortical diffusion D_u are shown in black. **B**. Simulation of cell polarization via the Rdi1-dependent mechanism. Initial distribution of cortical Cdc42 at the time of perturbation is shown in red, with steady state shown in black and intermediate time points in blue. The parameter values used in the simulation shown are: $C=1, \gamma=0.4, \beta=0.2, D_v=0.1, D_u=0.01, u_b=0.05, L=3,$ $A=1.75,$ and $R=0.6.$ **C**.

Simulated data for Rdi1 dependent polarization, showing dependence of polarization strength u_{max} on *R*, Rdi1 concentration relative to Cdc42. Grey dashed lines indicate cortical Cdc42 concentration in unpolarized states, while the red curve indicates average u_{max} over 25 simulations for parameter values where polarization is allowed. The parameter values are as in B, and changing value of *R*. **D**. Experimental assessment of the impact of Rdi1 expression level on polarization without actin. Expression of Rdi1 was induced under the *GAL1* promoter for indicated amounts of time (x axis) concurrent with a 1h G1 pheromone arrest, followed by a 0.5h pheromone arrest in glucose media prior to release into LatA containing media (see diagram in Figure S2). The percentages of polarized cells were counted at 50 minutes following release. P = 0.35, wild type compared with 60min Gal induction. The plots show mean from 1 experiment and error bars correspond to SEM. >200 cells were counted per time point. **E**. Simulated data for Rdi1-dependent polarization, showing dependence of polarization strength u_{max} on *A*. Grey dashed lines indicate cortical Cdc42 concentration in unpolarized states, while the red curve indicates average u_{max} over 25 simulations for parameter values where polarization is allowed. The parameter values are as in B, with *R*=0.6 and changing value of *A.*

containing media (see **Fig. S3A**). Quantifying the percentage of polarized cells at 50 minutes after the release, it was apparent that cell polarization occurs optimally at the concentration of Rdi1 induced for 60 min with galactose and declines sharply above and more gradually below this expression level (**Fig.6D**). Measurement of average fluorescence intensities of Rdi1-GFP and GFP-Cdc42, each expressed under its endogenous promoter, confirmed that Rdi1 concentration is ~0.6 fold of that of Cdc42, within the allowable range for symmetry breaking (**Fig. S3B**). We also fixed the value of R and varied A and found that symmetry breaking requires a threshold level of Cdc42 activation (**Fig. 6E**), which is qualitatively consistent with the experimental findings in Figure 3 (discussed further below).

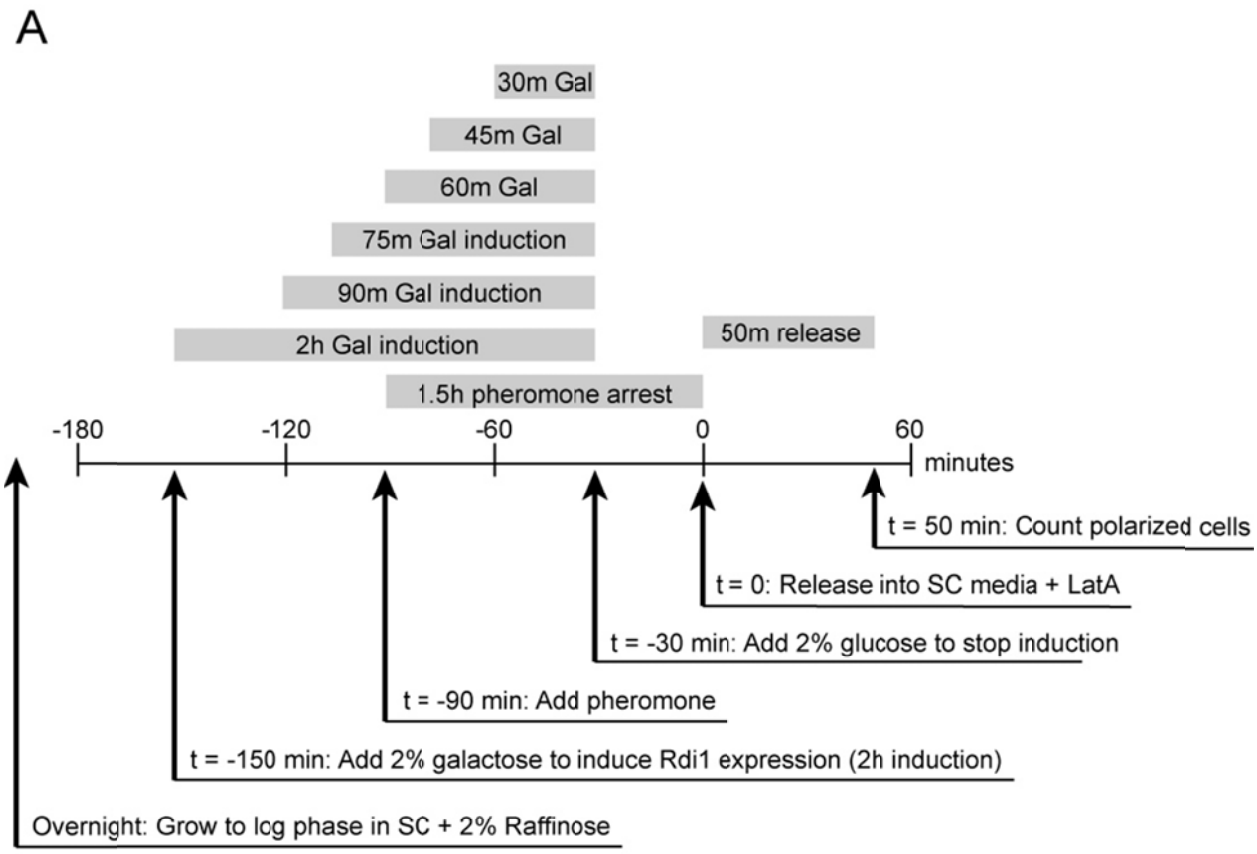

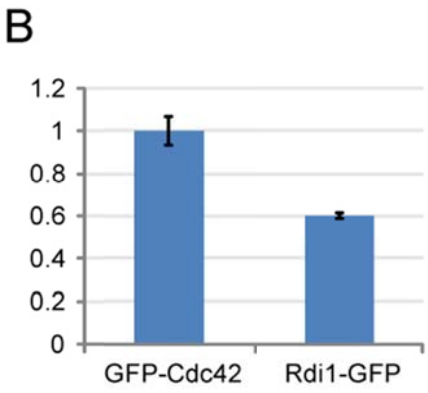

Figure S3. Impact of Rdi1 level on polarization. A. Schematic drawing of experimental procedure for Figure 6D. Expression of Rdi1 was induced under the *GAL1* promoter concurrent with pheromone-induced G1 arrest. Timelines for various induction times are shown as grey boxes, with a detailed timeline for the 2h induction procedure as an example below. **B**. Comparison of Rdi1 and Cdc42 levels in wild type strains. Average fluorescence of cells expressing Rdi1-GFP or GFP-Cdc42, each under the endogenous promoter, normalized against GFP-Cdc42 fluorescence. Histograms show mean and SEM, n > 500 for each strain.

Discussion

Distinct pathways of Cdc42 activation and localization contribute to symmetry breaking

For successful mitotic division, yeast cells must polarize toward a unique site once and only once each cell cycle, a feat requiring precise spatial and temporal control of Cdc42 protein localization and activity. The results described above, especially the observation that symmetry breaking and cell polarization can still occur when the GEF Cdc24 is diffuse, indicate that mechanisms of Cdc42 localization and activation may be decoupled. In any single location on the cortex, induction of downstream events or feedback circuits that rely on Cdc42 effectors depends on the concentration of $Cdc42^{GTP}$, a product of two factors: 1) total Cdc42 protein concentration (controlled by localization on the cortex), and 2) relative abundance of the GTP-bound state of Cdc42 (controlled by GEF/GAP balance) in that location. Modulation of either factor can be envisioned to affect the local $Cdc42^{GTP}$ level and therefore the capacity for initiating the downstream reactions required for symmetry breaking (**Fig. 7**). This concept is sufficient to interpret all the experimental observations made in this study.

Specifically, our results show that when both the actin-based vesicular trafficking and Rdi1-dependent cytosolic targeting mechanisms are intact, symmetry breaking occurs even without strong GEF localization or the benefit of Bem1's GEF boosting ability (**Fig.7b**). Thus, given robust protein localization, even suboptimal activation could achieve a threshold level of $Cdc42^{GTP}$ required for inducing downstream effector pathways and positive feedbacks for symmetry breaking. Alternatively, optimal GEF activation may compensate for suboptimal protein localization such as in the case of actin disruption with LatA (**Fig 7c**). However, when

both activation and protein targeting are inhibited to a certain degree, such as the combination of *bem1Δ* and actin inhibition, the threshold of $Cdc42^{GTP}$ concentration could not be achieved to engage the downstream reactions and positive feedback loops for symmetry breaking (**Fig 7d**).

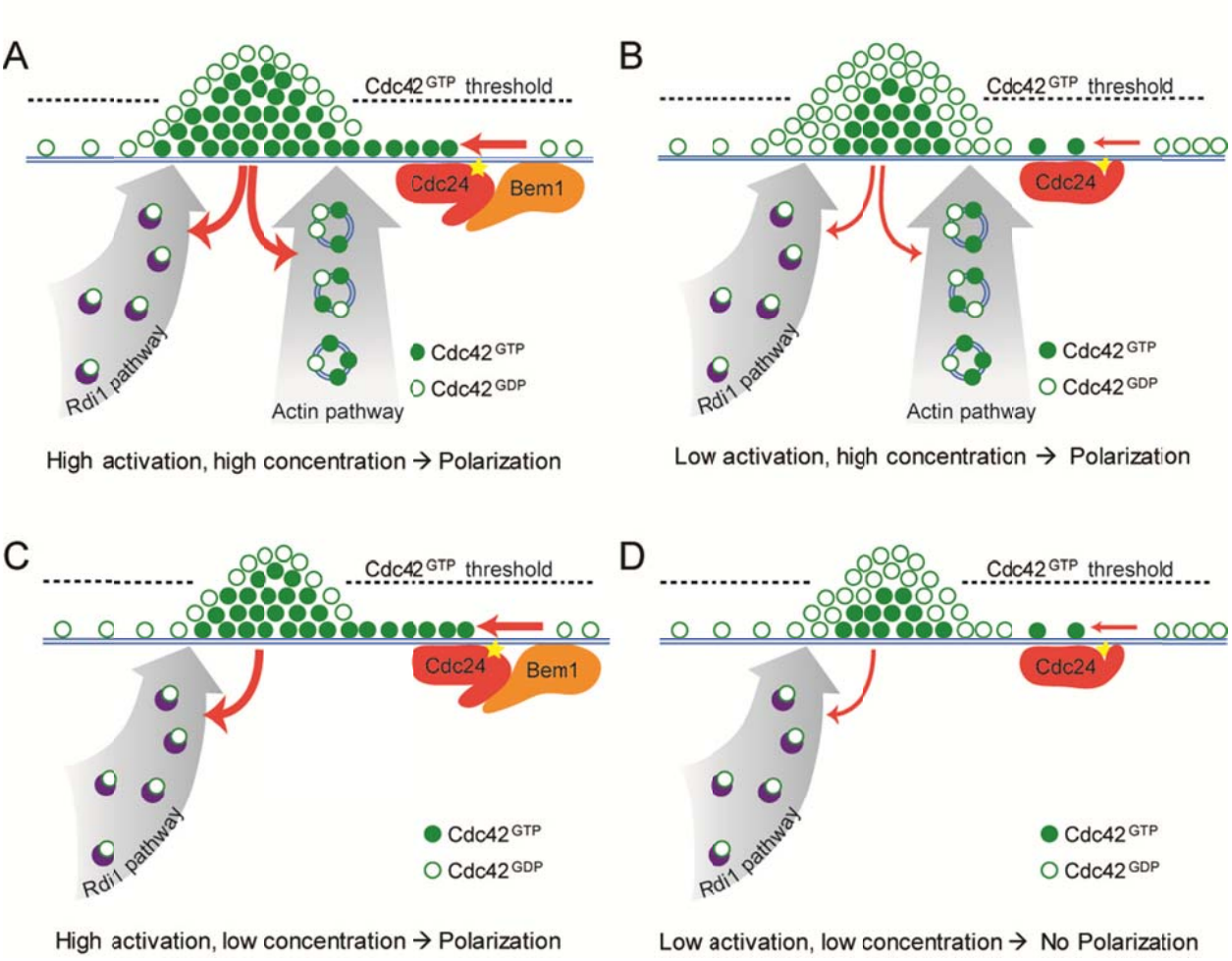

Figure 7. A schematic explanation of the phenotypic observations based on the cooperation between Cdc42 targeting and activation. The concentration of active $Cdc42^{GTP}$ (filled green circles) on the cortex is a fraction of total Cdc42 (filled and open green circles) determined by the GEF activity of Cdc24 boosted by Bem1. Cdc42 localization is controlled by both actin-dependent vesicle (blue circles) trafficking and Rdi1-dependent (purple crescents) pathways. Local concentration of active $Cdc42^{GTP}$ must reach a threshold level (dotted line) before imposing sufficient feedback for symmetry breaking. **A**. Wild-type cells - both Cdc42 activity and localization are maximized. The level of $Cdc42^{GTP}$ is well above the threshold. **B**. *bem1Δ* cells - GEF activity is reduced, but with the localization of total Cdc42 remaining high, the threshold level of $Cdc42^{GTP}$ is still attained. **C**. LatA-treated wild-type cells - Elimination of the actin-based target pathway reduces localization of Cdc42, but with high activation, the $Cdc42^{GTP}$ threshold can still be reached. **D**. LatA-treated *bem1Δ* cells - Decreasing both the activation

level and the localization of total Cdc42 prevents attainment of the threshold level of $Cdc42^{GTP}$ for symmetry breaking.

The function of Bem1 in cellular symmetry breaking

The previous conclusion that Bem1 is essential for symmetry breaking was built on the synthetic lethal interaction between *bem1Δ* and *rsr1Δ* and the implicit assumption that *rsr1Δ* affects only bud site selection but not the core symmetry-breaking mechanism. The results presented here and in previous studies have shown that Rsr1's function is clearly beyond bud site selection but that *bem1Δ* or *bem1Δ rsr1Δ* double mutant cells are capable of polarization as long as actin is intact. Our approach of interaction-specific perturbation by using point mutations has revealed different, as opposed to concerted, functions for the various Bem1-mediated interactions in cell polarization. The mutant analysis shows that the Bem1-Cdc42 interaction is important for localization of Bem1 to the polar cap, but this is neither crucial for Cdc24 localization nor required for symmetry breaking with or without actin. This result also implies that Bem1 can fulfill its main function in symmetry breaking without itself being localized. In contrast to the mutant with disrupted Bem1-Cdc42 interaction, disruption of Bem1-Cdc24 interaction prevented symmetry breaking only when actin was inhibited. This defect correlates with significantly reduced GEF activity and can be rescued by a Cdc24 construct that enhanced GEF activity but was unable to bind Bem1. These results strongly suggest that the main function of Bem1 is to boost the overall GEF activity of Cdc24.

Previous work suggested that Cdc24 exists in an auto-inhibited state, with the central catalytic domain shielded by the C-terminal, Bem1-binding PB1 domain (Shimada et al., 2004a). Our finding that deletion of the PB1 domain partially rescues symmetry breaking in Bem1-

Cdc24 binding mutants in the presence of LatA supports this idea, as do our biosensor measurements. Bem1 binding may also enhance GEF activity through a second mechanism: bridging a complex between Cdc24 with the PAK kinase Cla4, thus facilitating Cdc24 hyperphosphorylation. Although mutagenesis of as many as 38 phosphorylated sites on Cdc24 did not result in any observable phenotype (Wai et al., 2009), disruption of Bem1 SH3 domain binding to polyproline motifs via the *bem1*^{W192K} mutation resulted in a partial decrease in polarization efficiency in the presence of LatA (**Fig 5C**). However, as the *bem1*^{W192K} mutation would also disrupt the interaction with Boi1 and Boi2, which are together required for viability (Bender et al., 1996), the effect of this mutation does not permit simple interpretation. Nevertheless, we speculate that, in addition to GEF activation, Bem1 functions as a *bona fide* adaptor with multiple weak ligand interactions to enhance the affinity of protein complexes required for robust cell polarization.

The emerging role of Rdi1 and Rsr1 in cellular symmetry breaking

Our results show that Rdi1 plays a critical role in actin-independent polarization of Cdc42. As a Rho GDI, Rdi1 is the cytosolic chaperone of prenylated Cdc42 and thus governs the targeting of this pool of Cdc42 to the site of polarization. Our previous work showed that Rdi1 is required for rapid recycling of Cdc42 that helps maintain a dynamic polarized Cdc42 concentration in the presence of significant membrane diffusion (Das et al., 2012b; Slaughter et al., 2009b). In order to recycle Cdc42 back to the polar cap, however, the Rdi1-Cdc42 complex must be broken apart, and what catalyzes this reaction remains a key missing link in the cytosolic Cdc42 targeting pathway. We envision that to enable symmetry breaking via this

cytosolic targeting pathway, active Cdc42 on the plasma membrane controls the dissociation of the Rdi1-Cdc42 complex in some manner, restricting Cdc42 anchoring to sites of prior Cdc42 accumulation. Modeling of experimentally observed Cdc42 dynamics during steady-state polarity predicted that the window of targeting Cdc42 from the cytosolic complex must overlap with that of actin-based delivery (Slaughter et al., 2009b), but the biochemical mechanism underlying this spatial restriction remains unknown.

The Ras-like GTPase Rsr1 has long been known to be essential for bud site selection, but our results, as well as the finding presented in several previous studies (Kang et al., 2010; Kozminski et al., 2003; Park et al., 2002) , indicate that its role in polarization is more extensive and nuanced than previously thought: Rsr1 is not merely a translator of the bud scar mark for the choice of the next polarization site, but it is also participates in the cell-intrinsic symmetry breaking mechanism. The finding that Bem1 and Rsr1 share a role in Cdc24 localization provides an alternative explanation for the previously reported synthetic lethality of *bem1Δ* and *rsr1Δ*: perhaps in some yeast strain backgrounds, without GEF localization, *bem1Δ rsr1Δ* cells are unable to achieve a sufficient level of cortical $Cdc42^{GTP}$ to initiate the feedback that brings about symmetry breaking.

The idea that spatial landmarks direct polarization by harnessing the core symmetry breaking machinery implies that linkage molecules may have a significant role in the core machinery itself. Indeed, although Rsr1 is not strictly required for polarization, especially when actin is intact, in its absence the established polar cap exhibits drastically reduced spatial and temporal stability, as shown in this and previous studies (Howell et al., 2012; Ozbudak et al., 2005). Previous studies attributed this instability to GAP-mediated negative feedback, and if so,

Rsr1 may play role in locally regulating this negative feedback, thus enhancing the stability of the polar cap. How the Rsr1 GTPase module fulfills such a role and how this role may also enable precise choice of the bud site adjacent to, but not on top of, the bud scar remains to be a question of considerable interest.

A new model of cytoskeleton-independent symmetry breaking

Models of yeast cell polarity have focused on achieving a stable, non-uniform distribution of Cdc42 on the membrane (Onsum and Rao, 2009). Existing models are mass-conserved reaction-diffusion models (Altschuler et al., 2008; Goryachev and Pokhilko, 2006; Mori et al., 2011; Otsuji et al., 2007). Analysis of these models showed that the polarization is due to Turing-type instability (Rubinstein et al., 2012), the physical reason for which lies in the significant difference in the Cdc42 diffusion constants in the cytosol and in the membrane, in addition to specific nonlinear dependence of protein recruitment on the local concentration of Cdc42 in the membrane. Cdc42 concentrations in the cytosol and on the membrane are considered as "master" variables, while concentrations of other proteins are consequences of the master variable dynamics.

One model introduced by Goryachev and Pokhilko (2008), which formed the basis for subsequent studies (Howell et al., 2012; Savage et al., 2012), assumes polarization occurs via a mechanism of autocatalytic activation of Cdc42 through recruitment of Bem1-Cdc24 complex. Rdi1 was incorporated into the model as a passive aide in Cdc42 recycling, prevented through a GEF-dependent mechanism from extracting Cdc42 at the cap. The authors considered a

complex model consisting of eight reaction-diffusion equations for dynamics of membrane bound and cytoplasmic proteins diffusing in two (2D) and three dimensions (3D) respectively (Goryachev and Pokhilko, 2008). Using several simplifying assumptions they reduced the original model to a 1D version for the "master" variables only. Both the full and the reduced models produced qualitatively the same results showing the existence of robust clustering of Cdc42 on the membrane. In our approach we focused on the development of the minimalistic 1D model designed to grasp major features of the actin-independent polarization process.

Our model differs mechanistically from that of Goryachev and Pokhilko in the lack of reliance on autocatalytic activation of Cdc42 via a proposed Bem1-Cdc42-Cdc24 complex. Rather, symmetry breaking is achieved through autocatalytic Cdc42 protein recruitment from the cytosolic Rdi1-Cdc42 complex. We demonstrate through both model simulation and experimental measurements that symmetry breaking depends on a window of Rdi1 concentration relative to that of Cdc42. In contrast, cells have more permissive requirements on the level of GEF activity, such that although a threshold level is required, higher levels are well tolerated. This explains the main experimental findings that cell polarization can occur with varying degree of GEF concentration in the polar cap and that *bem1* mutations that impair GEF activation are more detrimental to polarization when cells are reliant on the Rdi1-based targeting pathway (i.e. when actin-based transport pathway is disabled).

In summary, a key insight resulting from the analyses carried out in this work is that activation and localization of Cdc42 are achieved via distinct mechanisms that contribute quantitatively and productively to symmetry breaking. Although both aspects of Cdc42

regulation are required, partial deficiency in either may be compensated due to the presence of multiple mechanisms achieving the other. This cooperation underscores both the complexity and robustness of the yeast cell polarity system.

Materials and Methods

Detailed model description

Consider a one-dimensional model describing Cdc42 protein dynamics in a yeast cell undergoing symmetry breaking transition from a uniform state to a polarized state.

For the actin-independent pathway, we introduce the following components of the model: Cdc42 on the membrane (local concentration $u(x,t)$) with active fraction $a_1 < 1$, Cdc42 in cytosol $v(x,t)$, free (cytosolic) Rdi1 $R_f(x,t)$, protein complex Rdi1-Cdc42 $R_c(x,t)$, and a certain activity $G(u)$ leading to breaking-up of the complex into free Rdi1 and membrane-anchored Cdc42. Consider a simplest case when this activity is proportional to squared density of active membrane Cdc42, i.e., $G(u) = a_2 a_1^2 u^2 = Au^2$, where $A = a_2 a_1^2$.

The membrane targeting term reads $G(u)R_c$ and internalization term is $\beta u R_f$, where β is the extraction rate. Assuming that the Rdi1-Cdc42 complex exists as a fraction of total cytosolic Cdc42, we find $R_c = \gamma v$, where $0 < \gamma < 1$. Given conservation of total amount of Rdi1 (R) in the cell, we also have $R_f = R - R_c = R - \gamma v$.

Spatio-temporal dynamics of Cdc42 is described by the equations in the region $0 \le x \le L$:

$$\begin{aligned} \frac{\partial u}{\partial t} &= \gamma A u^2 v - \beta u(R - \gamma v) + D_u \frac{\partial^2 u}{\partial x^2}, \\ \frac{\partial v}{\partial t} &= -\gamma A u^2 v + \beta u(R - \gamma v) + D_v \frac{\partial^2 v}{\partial x^2}, \end{aligned} \tag{1}$$

where the diffusion of the Cdc42 cytosolic form is much faster than the membrane one: $D_v >> D_u$. The cubic nonlinearity is shown to be critical for the Turing-type instability in polarization models (Goryachev and Pokhilko, 2008). The system of equations (1) is subject to no-flux boundary conditions. Summing up the equations and integrating over the spatial interval we obtain the Cdc42 mass conservation condition

$$\int_0^L (u + v) dx = CL = const, \tag{2}$$

where the constant C is the model parameter representing the mean Cdc42 concentration. The reaction terms used in (1) lead to a basic uniform solution $u = 0$ corresponding to absence of Cdc42 on the membrane. In order to have some non-zero basal level u_b on the membrane we modify the reaction term in (1) to arrive at:

$$\begin{aligned} \frac{\partial u}{\partial t} &= f(u,v) + D_u \frac{\partial^2 u}{\partial x^2}, \\ \frac{\partial v}{\partial t} &= -f(u,v) + D_v \frac{\partial^2 v}{\partial x^2}, \\ f(u,v) &= \gamma A (u - u_b)^2 v - \beta (u - u_b)(R - \gamma v). \end{aligned} \tag{3}$$

Being stationary and spatially uniform, the solution $\{u_0, v_0\}$ is independent of time and spatial variables, so that all derivatives vanish and this solution should satisfy the equation $f(u_0, v_0) = 0$. From (2) it follows that the basic solution satisfies the condition $u_0 + v_0 = C$, and we find from (3)

$$u_0 = \frac{AC - \beta + Au_b - s}{2A}, \quad v_0 = \frac{AC + \beta - Au_b + s}{2A},$$
$$s = \sqrt{(AC + \beta - Au_b)^2 - 4\beta AR/\gamma}. \tag{4}$$

As the uniform steady state concentrations should be non-negative we find a necessary condition on the model parameters: $R > \gamma C$, which was shown to be satisfied with experimental measurements and the estimated value of 0.4 for ?.

A previous study (Rubinstein et al., 2012) showed that the maximal linear growth rate σ_m of the perturbation can be approximated by the partial derivative of f with respect to the variable u

$$\sigma_m \approx \partial f/\partial u = 2\gamma A(u_0 - u_b)v_0 - \beta(R - \gamma v_0),$$

computed at the basic solution (4). Meanwhile, the basic solution satisfies the relation $\gamma A(u_0 - u_b)v_0 = \beta(R - \gamma v_0)$, which produces an estimate for the growth rate for membrane Cdc42 in the form

$$\sigma_m \approx \beta(R - \gamma v_0) = \gamma A(u_0 - u_b)v_0.$$

The last relation shows that the growth rate of membrane Cdc42, which determines the kinetics of polarization establishment, is proportional to the concentration of Rdi1 (R). It also depends on the activation level A, and more precisely it is determined by the balance between the activation level A and the Rdi1 expression R.

For a fixed value of activation, with increase in R the internalization term wins over the membrane targeting term, eventually blocking polarization. On the other hand for small $R < \gamma C$, polarization is also not possible. This means that there exists a range of the Rdi1 expression level R for which the polarization is possible, and the upper boundary of this range

varies with A. This behavior is illustrated in the Figure 6C where the maximal value u_{max} of the membrane-bound Cdc42 concentration obtained by simulation of equations (3) is shown for a fixed value of A and increasing R. The nonpolarized state (with the ratio $u_{max}/u_{min} < 1.2$) is shown by the dashed curve. The parameter values used in this simulation are: $C = 1$, $\gamma = 0.4$, $\beta = 0.2$, $D_v = 0.1, D_u = 0.01, u_b = 0.05$, $L = 3$. The simulations for each set of the parameters was performed 25 times and the mean values of u_{max} were computed.

Genetic manipulations

Site-directed mutagenesis was performed using the QuikChange II XL Site-Directed Mutagenesis Kit (Stratagene), and the final product was sequenced to ensure that there were no secondary mutations introduced. All yeast strains used in this study are described in Table S2. Techniques for yeast cell culture and genetics were essentially as described(Burke et al., 2000). Transformation of plasmid DNA into yeast was performed based on the lithium acetate method (Ito et al., 1983). Transformation of DNA fragments was performed by the same method, but after transformation, cells were recovered in non-selective media for at least two-cell cycle time before plating on selective media, and genomic integration was confirmed by PCR.

Alpha factor release assays

Cells were arrested for 1.5 h using 20 µg/ml α-factor, and released into the cell cycle by washing three times in sterile water before resuspending in fresh media with either 50µM LatA or equivalent DMSO. Samples containing Bem1-GFP, Cdc24-GFP, or Cdc24-GFP-Cla4 were imaged as live cells 50 min after release. For quantification, samples containing Cdc24-GFP-Cla4 were

visualized as live cells at 20, 40, 60 and 80 minutes following release. Samples containing GFP-Cdc42 were taken at 20, 50 and 80 minutes after release and fixed in 4% paraformaldehyde for 15 minutes before washing in PBS, and stored at 4°C for fewer than 48h prior to imaging. For each time point, greater than 100 cells were scored for polarity. The assay was repeated at least 2 times for each genotype. For release assays with Rdi1 expression induced under the Gal1 promoter, *pGAL1-RDI1* cells were grown overnight in 4% raffinose media, to which 4% galactose was added at the appropriate time point relative to the addition of □ factor such that addition of glucose 30 minute prior to release from alpha factor would end the induction.

Microscopy and live cell imaging

Imaging of cells expressing GFP-Cdc42, Bem1-GFP and Cdc24-GFP was performed on a PerkinElmer Ultraview spinning disk confocal microscope including a Zeiss Axiovert 200 M inverted microscope, attached to a Yokogawa spinning disk confocal and Hamamatsu EM-CCD C9100 camera with Perkin Elmer Volocity Acquisition software, or a similar system with Metamorph Acquisition software. Images of were collected as a series of optical sections, with a step size of 0.5 µm. Image J software (v. 1.37, http://rsb.info.nih.gov/ij/) was used to process the images. Final images are maximum projections that have been background subtracted and contrast-adjusted for clarity.

For live-cell movies of GFP-Cdc42, cells were arrested in G1 via pheremone for 1.5h, and released into LatA-containing synthetic complete (SC) media for 30 minutes prior to slide preparation on a 1% agarose, 100µM LatA pad. Z-stack images were acquired at 2m time intervals with 0.7 µm between slices. Maximum z-projections of each time point were generated and cells showing polar cap formation and disappearance within a single movie were

identified, and the intensity of the polar cap were measured and plotted over time. These were corrected for bleaching and smoothed via a rolling average of three timepoints, then fitted to Gaussian curves in OriginPro. The duration of the cap is reported as the full width half maximum of the Gaussian fit. For live movies of Cdc24-GFP cycling mid log phase cells were immobilized on 1% agarose in SC complete media.

Bem1 polarity analysis

Maximum projections of Bem1-GFP fluorescence images from the experiment in Figure 2H were background subtracted and processed using the ImageJ "smooth" function to remove noise. Unbudded cells were circled and the maximum and average pixel intensities were calculated for a total of 520 cells per genotype. The Bem1 polarity was calculated as the maximum pixel intensity divided by the average intensity per each cell.

Cdc24-GFP Profile analysis

Two channel z-stack images of cells expressing Cdc24-GFP and mCherry-Cdc42 were background subtracted and maximum projections were generated. A cortex mask of the cell was then generated from the mCherry-Cdc42 channel using a custom macro based on the "Li Dark" thresholding algorithm in ImageJ (Li and Tam, 1998). The mask was applied to the Cdc24-GFP channel and the average intensity of the masked region in 10° increments around the cortex was calculated using a custom plugin to generate a cortical intensity profile Cdc24-GFP. This was completed for at least 25 cells, including all visibly polarized cells from each of several images. The profiles were aligned by maximum value, and each was normalized to the average intensity of the cortex in the 180° region opposite the peak. The normalized curves were averaged. Statistical analysis was performed on peak (0°) values.

Cdc42 Activation Biosensor imaging and analysis

Cells were grown to mid log phase prior to analysis. Polarized cells were imaged on a PerkinElmer Ultraview spinning disk confocal microscope including an inverted Zeiss 200 m microscope, a Yokagawa CSU-X1spinning-disc confocal system, a Hamamatsu ORCA-R2 CCD (2x2 bin), and a PhotoKinesis accessory, using Volocity (Perkin Elmer) acquisition software. Cells were imaged at maximum speed for a total of 42 frames, with 488nm laser power 7% and exposure 100-300 ms depending on biosensor expression level per cell. mCherry throughout the cell was bleached following frame 20, using 1 iteration 568 laser 100%. mCherry fluoresence was checked following acquisition to ensure complete bleaching. Controls indicated no significant bleaching of GFP by 568 excitation, nor crosstalk of mCherry fluorescence into the GFP channel. Analysis was performed using ImageJ software. The first two frames following bleaching (frames 21-22) were discarded due to potential delay of 568 laser shut off. The sum of the full time series was then used to create a cortex mask of the cell, using a custom macro based on the "Li Dark" thresholding algorithm in ImageJ (Li and Tam, 1998). The mask was applied to the series and the average intensity of the masked region in 10° increments around the cortex was calculated at each time point using a custom plugin. The average intensity and the standard deviation intensity of each 10° increment before and after bleach were calculated in R Studio. The standard deviations of all 10° increments before and after bleach were averaged, and cells whose average standard deviation was greater than 10% of its average cortical fluorescence were discarded. Intensity profiles of remaining cells were then aligned such that polar cap center was located at 0°. FRET efficiency was calculated for each 10° segment in remaining cells as 100*(Post bleach-Prebleach)/Prebleach. FRET

efficiencies for each 10° increment were then averaged over at least 25 cells, as in the plot in **Fig. 3E**. The "Peak" FRET efficiency (**Fig. 3F**) was determined as the average of the 30° region containing the 10° increment of highest average FRET efficiency among aligned profiles.

Statistical analysis

Statistical differences between two sets of data were analyzed with a two-tailed unpaired Student t-test.

Acknowledgements

The authors thank J. Zhu, W. Mulla, V. Ramalingam, J. Lange, W. Bradford, S. Ramachandran, G. Rancati, S. Wai, and X. Fan (all current or former Stowers Institute members) for experimental assistance and valuable discussion, and D. Lew (Duke University) for the plasmid DLB3170. This work was supported by NIH grant GM-RO1-057063.

Chapter 4.

Preliminary data on Cdc42 microdomains in the presence of Rdi1 feedback

Introduction

The key finding from our work on the mechanism for actin-dependent polarization presented in Chapter 2 is that microdomains of slow membrane diffusion of Cdc42 within the polar cap are crucial to maintaining high concentration of Cdc42 in the cap during actin dependent polarization. Our complementary work presented in Chapter 3 showed that extraction and recycling of Cdc42 by Rdi1 is key to actin independent polarization, while boosting of Cdc24 GEF activity by Bem1 binding (among other mechanisms) is important for both actin independent and (to a lesser degree) actin dependent polarization. In the preliminary work presented in this chapter, I will examine how Cdc42 microdomains correlate with components implicated in the actin independent polarization pathway.

Results and discussion

Using the Pearson correlation analysis method described in Chapter 2, I began by examining spatiotemporal correlation of Cdc24-GFP with mCherry-Cdc42 in *RDI1* cells with and without LatA. Cdc42 microdomains persisted in the presence of Rdi1-mediated exchange (see red kymographs, Fig 1a-b), and regions of high Cdc24 were spatiotemporally correlated with Cdc42 microdomains (Figs 1a-b, Fig 1e) in both treated and untreated cells. Turning to Bem1, I was surprised to find that although Bem1-GFP was highly spatiotemporally correlated with mCherry-Cdc42 when actin structures were present, the correlation was lost when cells were treated with LatA (Fig 2$P < 0.005$). This suggests that although the interaction of Bem1 with Cdc42 is necessary for localization to the cap, the interaction may not be enduring. It also underscores the lack of requirement for Bem1 feedback for actin independent polarization, as even wild type Bem1 does not cofluctuate with Cdc42 when actin is depolymerized.

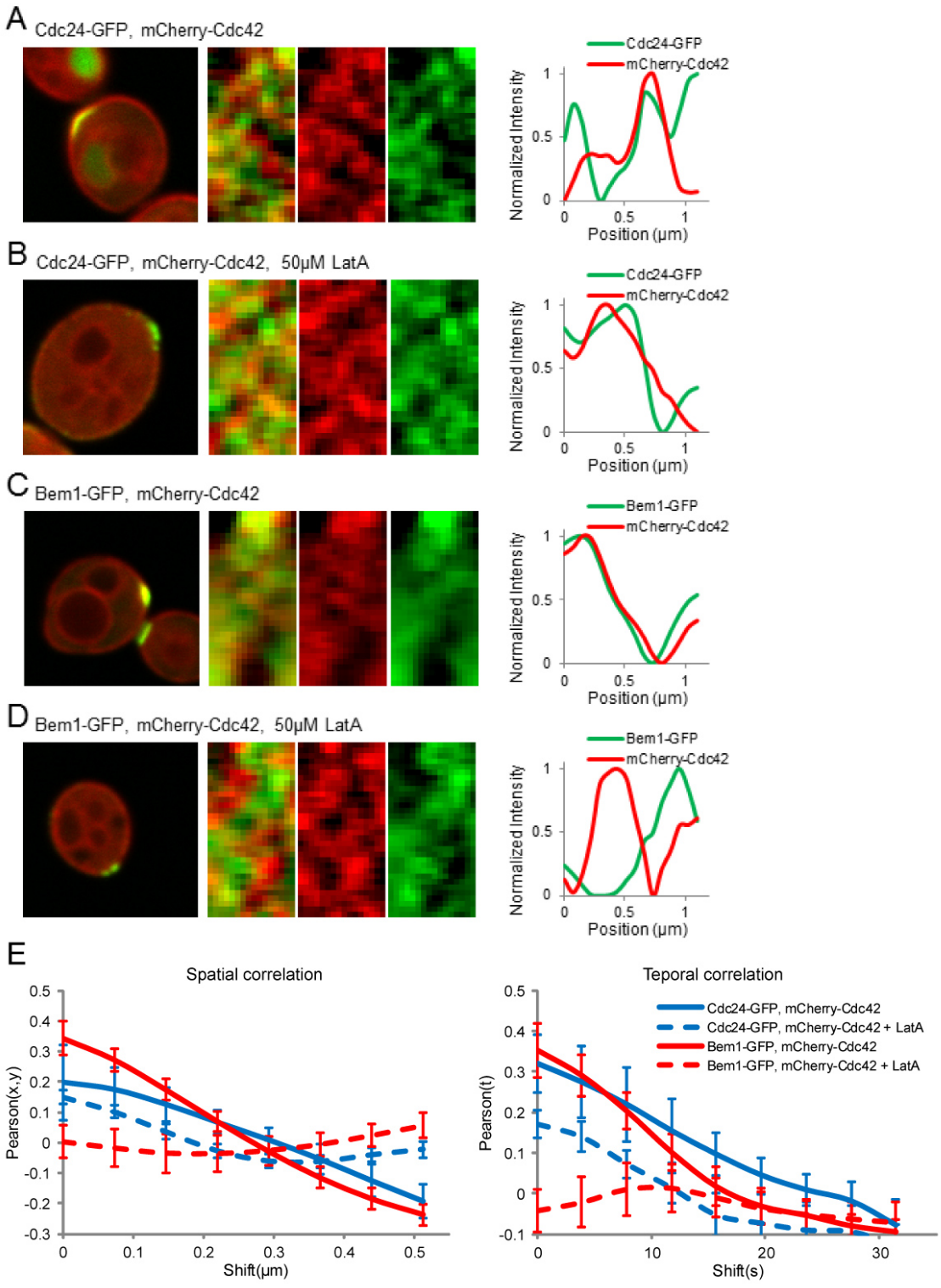

Figure 1. Correlation of Cdc24-GFP and Bem1-GFP with mCherry Cdc42 in microdomains at the polar cap. A-D. Representative polarized cells and kymographs for analysis. Leftmost panel shows sum projection of time series, followed composite kymograph, mCherry-Cdc42 channel kymograph and

Cdc24-GFP (A and B) or Bem1-GFP (C and D) kymographs. Plot at right shows GFP and mCherry intensity at different positions x at a single timepoint in the kymograph. **E**. Pearson curves for spatial (left) and temporal (right) correlation averaged over n>5 cells. Error bars indicate SE.

Wondering if a loss of spatiotemporal correlation with mCherry-Cdc42 in LatA was common to other components of the polar cap, I analyzed strains expressing GFP-tagged versions of the PAK Cla4, the adaptor molecule Boi1, the GAP Bem2 and the phosphotidylserine probe Lact-C2. None of these showed significantly decreased correlation with mCherry-Cdc42 in LatA-treated versus untreated cells (Fig 2). Why then does Bem1 lose localization to microdomains following LatA treatment? It may be that localization of Bem1 to microdomains is due to its interaction with the exocyst complex component Sec15 (France et al., 2006), which would be consistent both with Bem1's strong localization to microdomains (which appear to be centers of exocytosis) and its strong dependence on actin.

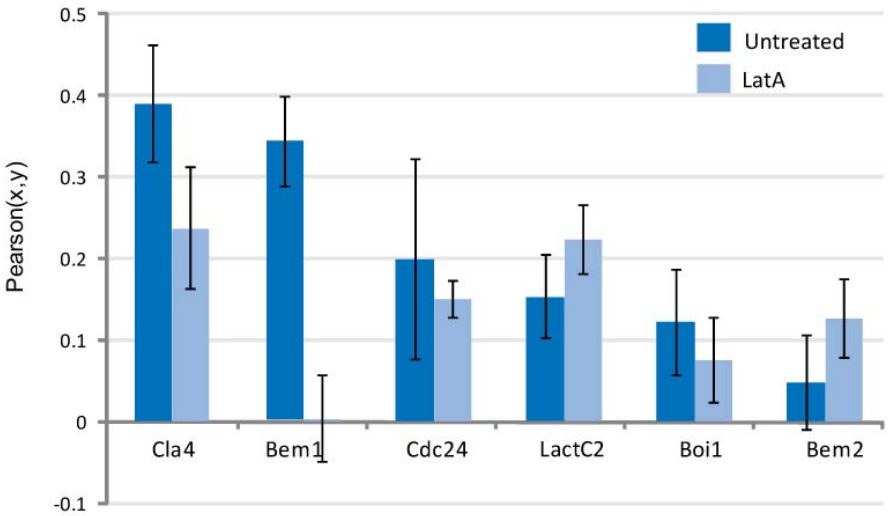

Figure 2. Actin dependence of peak spatial correlation of mCherry-Cdc42 with components of the polar cap. Measurements are for correlation at x=0 spatial shift for indicated polar components tagged with GFP. n > 5 cells for each measurement. Error bars indicate SE.

Comparison of spatiotemporal correlation of various polar components with Cdc42 (Fig 3) revealed an intriguing trend: components associated with Cdc42 signaling (including Cla4, Bem1, and Cdc24) showed the highest correlation, while the GAPs Rga1, Bem2, and Bem3 showed the lowest. This observation is consistent with the idea that microdomains serve as centers of Cdc42 signaling. It is also reminiscent of the suggestion that GAPs may be players in the process of Rdi1 extraction of Cdc42, as has been recently argued (Freisinger et al., 2013). These ideas inspire further investigation, and suggest that analysis of the dynamic substructure of the polar cap may be a fruitful area of future research.

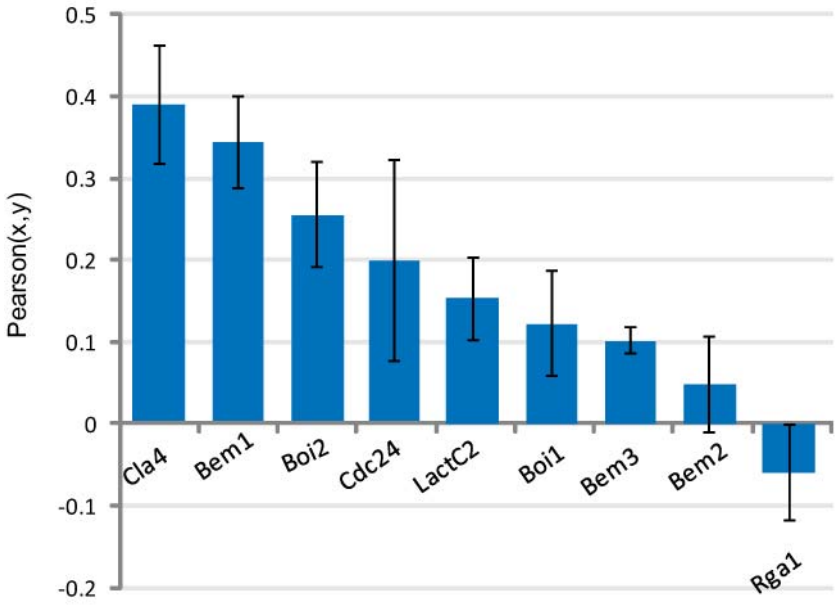

Figure 3. Peak spatial correlation of mCherry-Cdc42 with various components of the polar cap. Measurements are for correlation at x=0 spatial shift for indicated polar components tagged with GFP. n > 5 cells for each measurement. Error bars indicate SE.

Chapter 5.

Summary and Discussion

Summary

In this work, we set out to gain mechanistic insight into the process of cell polarization in budding yeast. It was previously known that yeast polarize via two distinct but coupled mechanisms, one dependent on actin structures and the other independent of actin but dependent on the adaptor Bem1 and the GDI Rdi1. The actin-dependent mechanism was thought to entail a feedback loop wherein a stochastic accumulation active Cdc42-GTP at the cortex initiates nucleation of polarized actin cables, upon which additional Cdc42 is transported to the nascent cap and deposited by exocytic vesicles. A key question central to the feasibility of the proposed feedback was whether the membrane deposited together with Cdc42 by the exocytic vesicles would have an overall dilutive effect on the concentration of Cdc42 at the cap.

The results of our study on membrane flux in actin-dependent polarization are presented in Chapter 2. Reasoning that crucial mechanistic details of actin-dependent feedback loop were yet unknown, we investigated the structure of the polar cap using timelapse confocal imaging with a highly sensitive detector. We were surprised to find that Cdc42 distribution was heterogeneous within the cap, and that regions of high Cdc42 ("microdomains") were strongly correlated with markers for exocytosis and anticorrelated with markers for endocytosis. Although fluorescence correlation spectroscopy and calibrated imaging showed that the concentration of Cdc42 on exocytic vesicles was similar to that at the polar cap, and therefore had positive rather than negative effect on Cdc42 concentration at sites of exocytosis, modeling indicated that the high diffusion rates previously measured for Cdc42 would not allow the persistent level of heterogeneity of Cdc42 distribution exhibited at microdomains. Indeed,

photobleaching experiments revealed that Cdc42 diffusion within the plasma membrane was significantly slowed at microdomains, and computational modeling indicated that these regions of slow diffusion had a concentrating effect on Cdc42, crucial to the support of polarization by actin feedback. Cdc42 microdomains correlated positively with a marker for phosphotidylserine (PS), an acidic phospholipid present on secretory vesicles that was recently shown to be required for robust cell polarity. Supporting a role for Cdc42-PS interactions in microdomain function, introduction of a mutation predicted to disrupt the interaction resulted in an increase in Cdc42 diffusion and a decrease in cap strength.

Actin independent polarization was thought to occur via a feedback loop mediated by the adaptor Bem1. In the proposed mechanism for Bem1-mediated polarization, a stochastic accumulation of Cdc42-GTP would recruit Bem1 complex containing the GEF Cdc24. The GEF would subsequently activate nearby Cdc42, increasing the size of the cap. In the work presented in Chapter 3, we critically tested the proposed loop by testing the capacity of cells to undergo actin independent polarization when individual steps in the loop were disrupted. We found that neither Bem1 feedback nor Bem1 polar localization was required; instead, Bem1 functions primarily to boost GEF activity of Cdc24 through heterotypic interactions of their PB1 domains. The Bem1-Cdc24 interaction was required for actin independent polarization, and measurements of GEF activity as indicated by FRET of a Cdc42 activation biosensor suggested that GEF activity was significantly decreased in cells with the Bem1-Cdc24 interaction disrupted. Expression of a PB1-deleted version of Cdc24 previously found to be constitutively active restored GEF activity in these cells, and, importantly, was also sufficient to partially rescue actin independent polarization. Much of the data supporting the Bem1 feedback model consisted

of genetic interactions of Bem1 with the Rsr1, a Ras-like GTPase required for proper bud site selection in both axial and bipolar patterning. The synthetic lethality of *bem1Δ* with *rsr1Δ* was interpreted as to show a requirement for Bem1 feedback in the absence of spatial cues, however, comparison of *rsr1Δ* cells with cells deleted for upstream bud scar landmarks showed that Rsr1 has patterning-independent roles in localization of Cdc24 as well as maintenance of polar cap stability, which could provide an alternate explanation for the genetic interaction.

Our findings regarding the function of Bem1 pointed to a lack of requirement for sharply localized GEF activity for polarization. Considering that the existence of the GDI Dissociation Factor (GDF) which could break up the diffusible Cdc42-Rdi1 complex had been proposed, we wondered targeted localization feedback of the GDI complex (via a GDF-like downstream effector of Cdc42) would be sufficient to generate polarization in the absence of localized GEF. Turning to mathematical modeling, we found that such a mechanism was feasible if Rdi1 and Cdc42 were maintained within a narrow balance. To test this prediction, we measured the capacity of cells to polarize in LatA after differing periods of induction of Rdi1. Qualitatively supporting the model, we found that cells were only able to polarize efficiently when Rdi1 induction was within a narrow range.

Discussion

Dual functions of Rsr1 in polarization and patterning

Why should Rsr1 have a patterning-independent role in polarization? In wild type cycling cells, the markers for the bud scar signal are deposited near the time of cell division, and

a zone of Cdc42 inhibition is established by GAP immediately over the resultant scar (Tong et al., 2007). In the following cell cycle, a new polar cap is established at a position adjacent to but not on top of the landmark, which could be anywhere in a ring of equally probable locations and which at the molecular scale is far from the site landmark signaling. This "symmetry breaking" within the patterning region may require a fluidity of signaling by Rsr1, to both guide the Cdc42 polarization module to patterning landmark, and to follow it to establish a single cap at a the new site within the patterning region.

Bem1 feedback and the Bem1-Cdc42 interaction

Previous reports have suggested that Bem1 is required for symmetry breaking, and indeed our results confirm that each of the steps in the Bem1-mediated feedback loop (Bem1 recruitment by $Cdc42^{GTP}$, Cdc24 recruitment and activation by Bem1) does occur during endogenous polarization. However, we also find that Bem1 is not necessary for actin-dependent symmetry breaking, and that Bem1 is necessary for Rdi1-dependent symmetry breaking only in its capacity for boosting GEF activity rather than for feedback. What then is the purpose of Bem1 feedback and the Bem1-Cdc42 interaction? One possibility is that Bem1 feedback may function to localize Cdc24 activity specifically to the cap. Spatially limiting Cdc24 activation may help reduce the occurrence or duration of transient multicap states, which have been previously observed in both *bem1Δ* and *rsr1Δ* cells (Howell et al., 2012; Wedlich-Soldner et al., 2004). Unresolved multicap states can lead to multiple buds, or in less severe cases a delay in bud formation which would confer a proliferative disadvantage. A second explanation for the Bem1-Cdc42 interaction is a possible requirement for Bem1 for polarized localization of

Cdc24 in the formation of mating projections: Bem1 has been shown to be required for shmoo formation (Chenevert et al., 1994), and it is unlikely that Rsr1 (as part of the bud scar signaling pathway) would be available to facilitate Cdc24 polarization in pheromone response.

Boosting GEF activity through Bem1 interaction

Although Bem1 feedback is not required for symmetry breaking, Bem1 binding is important for activation of the GEF Cdc24. How might Bem1 work to boost GEF activity? It may be that as previously suggested, Cdc24 exists in an autoinhibited state, with the central catalytic domain shielded by the C-terminal, Bem1-binding PB1 domain (Shimada et al., 2004). Our finding that deletion of the PB1 domain partially rescues actin-independent polarization in Bem1-Cdc24 binding mutants supports this hypothesis, as do our biosensor measurements, which indicate an increase in GEF activity in strains expressing $Cdc24^{\Delta PB1}$. Intriguingly, FCS measurements of species brightness indicate that both Bem1 and Cdc24 exist as monomers when diffusing in the cytosol as mobile species, and the brightness of the species do not increase when both Bem1 and Cdc24 are labeled with GFP, indicating that Bem1 and Cdc24 do not travel as a complex (Chapter 2, Fig S2). Since cortical localization has been shown to be important for GEF activity (Shimada et al., 2004), and it has also been suggested that oligomerization of Cdc24 through its catalytic DH domain also contributes to localization and activity (Mionnet et al., 2008), it may be that Bem1 binding facilitates these other processes at the cortex. In any case, it appears that Bem1 binding is but a single (though important) step in the multilayered and robust system of regulators controlling Cdc24.

Interplay of GEF and Rdi1-dependent localization

Our work supports the hypothesis that actin independent polarization of Cdc42 is mediated by Rdi1 extraction, recycling and targeting. While previous work determined that extraction of Cdc42 from the cortex by Rdi1 is facilitated by modulation of electrostatic interactions of Cdc42 with lipids by the lipid flippase Lem3(Das et al., 2012), it is yet unknown how the Rdi1-Cdc42 complex is broken up, or how Rdi1 recycling leads to targeting of Cdc42 to the cap. Studies in mammalian cells have indicated that GDI-GTPase binding can be modulated by phosphorylation, interaction with certain lipids, or GEF activity among other possibilites, any or all of which could be at work in yeast (Johnson et al., 2009). A suggestive finding is that Rdi1-dependent polarization shows a higher dependence on GEF activity than polarization in the presence of actin: *bem1* mutants resulting in low GEF activity (as measured by the Cdc42 biosensor) are able to polarize only when the actin pathway is available. Taken together with the previous observation that Rdi1-dependent but not actin-dependent polarization requires GTPase cycling of Cdc42(Wedlich-Soldner et al., 2003), this suggests that Cdc24 may be directly involved in the mechanism for Rdi1-dependent Cdc42 localization. Based on the observation that Rdi1 may preferentially extract $Cdc42^{GDP}$ rather than $Cdc42^{GTP}$, it was previously proposed that the GEF could act as an effective shield against Cdc42 extraction at the cap by rapidly converting randomly deposited $Cdc42^{GDP}$ to $Cdc42^{GTP}$, preventing further extraction (Goryachev and Pokhilko, 2008; Kozubowski et al., 2008). Alternatively, Cdc24 could actively direct Rdi1 feedback: GEF-catalyzed GDP/GTP exchange could lead to break-up of the Rdi1-Cdc42 complex, resulting in directed feedback of $Cdc42^{GTP}$ to areas of high Cdc24, as suggested in a recent publication(Freisinger et al., 2013). It is possible however that, like the actin-dependent

mechanism, Rdi1-dependent Cdc42 localization is mechanistically distinct from GEF localization and activity, and that Rdi1 targeting is mediated by a separate $Cdc42^{GTP}$-dependent mechanism. In that case, it may be simply that localization feedback by Rdi1 serves to increase local concentration of $Cdc42^{GDP}$ but not $Cdc42^{GTP}$ (if Rdi1 complexes preferentially with the GDP-bound form), or, if both active and inactive Cdc42 is recycled, that the balance of targeting and diffusion of the highly dynamic Rdi1-dependent polarization is not sufficient to achieve high local concentration of Cdc42GTP when GEF is low, as we illustrate in Figure 7 of Chapter 3. In either of these cases, the GEF activity requirement would be raised to compensate for reduced localization of $Cdc42^{GTP}$ in the Rdi1-dependent pathway relative to the actin-dependent pathway.

Conclusion

In summary, the work presented here indicates that yeast polarization is accomplished through a layered and robust series of parallel and overlapping mechanisms. Activation and localization of Cdc42 are achieved through distinct pathways, both of which are necessary for initiation of cellular symmetry breaking. Because it is essential for yeast to polarize once and only once each cell cycle, it makes sense that tiny, stochastic accumulations of $Cdc42^{GTP}$ which may occur at inopportune moments should not be sufficient to initiate symmetry breaking. When the time is right, however, a series of robust and overlapping activation mechanisms act to “pull the trigger” on the polarization module, initiating polarization of Cdc42 and ultimately cell growth.

References

Adams, A.E., D.I. Johnson, R.M. Longnecker, B.F. Sloat, and J.R. Pringle. 1990. CDC42 and CDC43, two additional genes involved in budding and the establishment of cell polarity in the yeast Saccharomyces cerevisiae. *J. Cell Biol.* 111:131-142.

Allen, L.H., and A. Aderem. 1995. A role for MARCKS, the alpha isozyme of protein kinase C and myosin I in zymosan phagocytosis by macrophages. *J Exp Med*. 182:829-840.

Altschuler, S.J., S.B. Angenent, Y. Wang, and L.F. Wu. 2008. On the spontaneous emergence of cell polarity. *Nature*. 454:886-889.

Anderson, R.G., and K. Jacobson. 2002. A role for lipid shells in targeting proteins to caveolae, rafts, and other lipid domains. *Science*. 296:1821-1825.

Ayscough, K.R., J. Stryker, N. Pokala, M. Sanders, P. Crews, and D.G. Drubin. 1997. High Rates of Actin Filament Turnover in Budding Yeast and Roles for Actin in Establishment and Maintenance of Cell Polarity Revealed Using the Actin Inhibitor Latrunculin-A. *The Journal of Cell Biology*. 137:399-416.

Bender, A., and J.R. Pringle. 1989. Multicopy suppression of the cdc24 budding defect in yeast by CDC42 and three newly identified genes including the ras-related gene RSR1. *Proceedings of the National Academy of Sciences*. 86:9976-9980.

Bender, L., H.S. Lo, H. Lee, V. Kokojan, V. Peterson, and A. Bender. 1996. Associations among PH and SH3 domain-containing proteins and Rho-type GTPases in Yeast. *J. Cell Biol.* 133:879-894.

Bi, E., and H.-O. Park. 2012. Cell Polarization and Cytokinesis in Budding Yeast. *Genetics*. 191:347-387.

Bose, I., J.E. Irazoqui, J.J. Moskow, E.S. Bardes, T.R. Zyla, and D.J. Lew. 2001a. Assembly of scaffold-mediated complexes containing Cdc42p, the exchange factor Cdc24p, and the effector Cla4p required for cell cycle-regulated phosphorylation of Cdc24p. *J Biol Chem*. 276:7176-7186.

Bose, I., J.E. Irazoqui, J.J. Moskow, E.S.G. Bardes, T.R. Zyla, and D.J. Lew. 2001b. Assembly of Scaffold-mediated Complexes Containing Cdc42p, the Exchange Factor Cdc24p, and the Effector Cla4p Required for Cell Cycle-regulated Phosphorylation of Cdc24p. *J. Biol. Chem.* 276:7176-7186.

Boyd, C., T. Hughes, M. Pypaert, and P. Novick. 2004. Vesicles carry most exocyst subunits to exocytic sites marked by the remaining two subunits, Sec3p and Exo70p. *J Cell Biol*. 167:889-901.

Brach, T., T. Specht, and M. Kaksonen. 2011. Reassessment of the role of plasma membrane domains in the regulation of vesicular traffic in yeast. *J Cell Sci*. 124:328-337.

Brandman, O., J. Ferrell, James E., R. Li, and T. Meyer. 2005. Interlinked fast and slow positive feedback loops drive reliable cell decisions. *Science*. 310:496-498.

Burke, D., D. Dawson, and T. Stearns. 2000. Methods in yeast genetics: a Cold Spring Harbor Laboratory course manual. Cold Spring Harbor Laboratory Press, Plainview, N.Y.

Buttery, S.M., S. Yoshida, and D. Pellman. 2007. Yeast formins Bni1 and Bnr1 utilize different modes of cortical interaction during the assembly of actin cables. *Mol Biol Cell*. 18:1826-1838.

Butty, A.-C., N. Perrinjaquet, A. Petit, M. Jaquenoud, J.E. Segall, K. Hofmann, C. Zwahlen, and M. Peter. 2002a. A positive feedback loop stabilizes the guanine-nucleotide exchange factor Cdc24 at sites of polarization. *The EMBO Journal*. 21:1565-1576.

Butty, A.C., N. Perrinjaquet, A. Petit, M. Jaquenoud, J.E. Segall, K. Hofmann, C. Zwahlen, and M. Peter. 2002b. A positive feedback loop stabilizes the guanine-nucleotide exchange factor Cdc24 at sites of polarization. *Embo J*. 21:1565-1576.

Calderon de Anda, F., A. Gärtner, L.-H. Tsai, and C.G. Dotti. 2008. Pyramidal neuron polarity axis is defined at the bipolar stage. *Journal of Cell Science*. 121:178-185.

Casamayor, A., and M. Snyder. 2002. Bud-site selection and cell polarity in budding yeast. *Current Opinion in Microbiology*. 5:179-186.

Chant, J., and I. Herskowitz. 1991. Genetic control of bud site selection in yeast by a set of gene products that constitute a morphogenetic pathway. *Cell*. 65:1203-1212.

Chant, J., M. Mischke, E. Mitchell, I. Herskowitz, and J.R. Pringle. 1995. Role of Bud3p in producing the axial budding pattern of yeast. *The Journal of Cell Biology*. 129:767-778.

Cheung, A.Y., and H.M. Wu. 2008. Structural and signaling networks for the polar cell growth machinery in pollen tubes. *Annu Rev Plant Biol*. 59:547-572.

Da Silva, J.S., and C.G. Dotti. 2002. Breaking the neuronal sphere: regulation of the actin cytoskeleton in neuritogenesis. *Nat Rev Neurosci*. 3:694-704.

Das, A., B.D. Slaughter, J.R. Unruh, W.D. Bradford, R. Alexander, B. Rubinstein, and R. Li. 2012a. Flippase-mediated phospholipid asymmetry promotes fast Cdc42 recycling in dynamic maintenance of cell polarity. *Nat Cell Biol*. 14:304-310.

Das, A., B.D. Slaughter, J.R. Unruh, W.D. Bradford, R. Alexander, B. Rubinstein, and R. Li. 2012b. Flippase-mediated phospholipid asymmetry promotes fast Cdc42 recycling in dynamic maintenance of cell polarity. *Nat Cell Biol*. 14:304-310.

Dent, E.W., S.L. Gupton, and F.B. Gertler. 2011. The Growth Cone Cytoskeleton in Axon Outgrowth and Guidance. *Cold Spring Harbor Perspectives in Biology*. 3.

DerMardirossian, C., and G.M. Bokoch. 2005. GDIs: central regulatory molecules in Rho GTPase activation. *Trends in Cell Biology*. 15:356-363.

Drees, B., C. Brown, B.G. Barrell, and A. Bretscher. 1995. Tropomyosin is essential in yeast, yet the TPM1 and TPM2 products perform distinct functions. *J. Cell Biol.* 128:383-392.

El-Benna, J., P.M.-C. Dang, M.-A. Gougerot-Pocidalo, J.-C. Marie, and F. Braut-Boucher. 2009. p47phox, the phagocyte NADPH oxidase/NOX2 organizer: structure, phosphorylation and implication in diseases. *Exp Mol Med.* 41:217–225.

Etienne-Manneville, S. 2004a. Cdc42--the centre of polarity. *J Cell Sci*. 117:1291-1300.

Etienne-Manneville, S. 2004b. Cdc42 - the centre of polarity. *J Cell Sci*. 117:1291-1300.

Evangelista, M., K. Blundell, M.S. Longtine, C.J. Chow, N. Adames, J.R. Pringle, M. Peter, and C. Boone. 1997a. Bni1p, a yeast formin linking cdc42p and the actin cytoskeleton during polarized morphogenesis. *Science*. 276:118-122.

Evangelista, M., K. Blundell, M.S. Longtine, C.J. Chow, N. Adames, J.R. Pringle, M. Peter, and C. Boone. 1997b. Bni1p, a Yeast Formin Linking Cdc42p and the Actin Cytoskeleton During Polarized Morphogenesis. *Science*. 276:118-122.

Evangelista, M., D. Pruyne, D.C. Amberg, C. Boone, and A. Bretscher. 2002. Formins direct Arp2/3-independent actin filament assembly to polarize cell growth in yeast. *Nat Cell Biol*. 4:32-41.

Evangelista, M., S. Zigmond, and C. Boone. 2003. Formins: signaling effectors for assembly and polarization of actin filaments. *J Cell Sci*. 116:2603-2611.

Fairn, G.D., M. Hermansson, P. Somerharju, and S. Grinstein. 2011. Phosphatidylserine is polarized and required for proper Cdc42 localization and for development of cell polarity. *Nat Cell Biol*. 13:1424-1430.

Freisinger, T., B. Klünder, J. Johnson, N. Müller, G. Pichler, G. Beck, M. Costanzo, C. Boone, R.A. Cerione, E. Frey, and R. Wedlich-Söldner. 2013. Establishment of a robust single axis of cell polarity by coupling multiple positive feedback loops. *Nat Commun*. 4:1807.

Fujimura-Kamada, K., T. Hirai, and K. Tanaka. 2012. Essential Role of the NH2-Terminal Region of Cdc24 Guanine Nucleotide Exchange Factor in Its Initial Polarized Localization in Saccharomyces cerevisiae. *Eukaryotic Cell*. 11:2-15.

Fujita, A., M. Lord, T. Hiroko, F. Hiroko, T. Chen, C. Oka, Y. Misumi, and J. Chant. 2004. Rax1, a protein required for the establishment of the bipolar budding pattern in yeast. *Gene*. 327:161-169.

Fujita, A., C. Oka, Y. Arikawa, T. Katagai, A. Tonouchi, S. Kuhara, and Y. Misumi. 1994. A yeast gene necessary for bud-site selection encodes a protein similar to insulin-degrading enzymes. *Nature*. 372:567-570.

Gao, L., and A. Bretscher. 2009. Polarized Growth in Budding Yeast in the Absence of a Localized Formin. *Mol. Biol. Cell*:E09-03-0194.

Gao, X.-D., L.M. Sperber, S.A. Kane, Z. Tong, A.H.Y. Tong, C. Boone, and E. Bi. 2007. Sequential and Distinct Roles of the Cadherin Domain-containing Protein Axl2p in Cell Polarization in Yeast Cell Cycle. *Molecular Biology of the Cell*. 18:2542-2560.

Garcia-Mata, R., E. Boulter, and K. Burridge. 2011. The 'invisible hand': regulation of RHO GTPases by RHOGDIs. *Nat Rev Mol Cell Biol*. 12:493-504.

Goehring, N.W., P.K. Trong, J.S. Bois, D. Chowdhury, E.M. Nicola, A.A. Hyman, and S.W. Grill. 2011. Polarization of PAR Proteins by Advective Triggering of a Pattern-Forming System. *Science*. 334:1137-1141.

Goryachev, A.B., and A.V. Pokhilko. 2006. Computational Model Explains High Activity and Rapid Cycling of Rho GTPases within Protein Complexes. *PLoS Comput Biol*. 2:e172.

Goryachev, A.B., and A.V. Pokhilko. 2008. Dynamics of Cdc42 network embodies a Turing-type mechanism of yeast cell polarity. *FEBS Letters*. 582:1437-1443.

Gosser, Y.Q., T.K. Nomanbhoy, B. Aghazadeh, D. Manor, C. Combs, R.A. Cerione, and M.K. Rosen. 1997. C-terminal binding domain of Rho GDP-dissociation inhibitor directs N-terminal inhibitory peptide to GTPases. *Nature*. 387:814-819.

Govindan, B., R. Bowser, and P. Novick. 1995. The role of Myo2, a yeast class V myosin, in vesicular transport. *J Cell Biol*. 128:1055-1068.

Greenberg, M.L., and D. Axelrod. 1993. Anomalously slow mobility of fluorescent lipid probes in the plasma membrane of the yeast Saccharomyces cerevisiae. *J Membr Biol*. 131:115-127.

Gulli, M.-P., M. Jaquenoud, Y. Shimada, G. Niederhäuser, P. Wiget, and M. Peter. 2000a. Phosphorylation of the Cdc42 Exchange Factor Cdc24 by the PAK-like Kinase Cla4 May Regulate Polarized Growth in Yeast. *Molecular Cell*. 6:1115-1167.

Gulli, M.P., M. Jaquenoud, Y. Shimada, G. Niederhauser, P. Wiget, and M. Peter. 2000b. Phosphorylation of the Cdc42 exchange factor Cdc24 by the PAK-like kinase Cla4 may regulate polarized growth in yeast. *Mol Cell*. 6:1155-1167.

Harlan, J.E., P.J. Hajduk, H.S. Yoon, and S.W. Fesik. 1994. Pleckstrin homology domains bind to phosphatidylinositol-4,5-bisphosphate. *Nature*. 371:168-170.

Heider, M.R., and M. Munson. 2012. Exorcising the Exocyst Complex. *Traffic*.

Hodgson, L., O. Pertz, and K.M. Hahn. 2008. Design and Optimization of Genetically Encoded Fluorescent Biosensors: GTPase Biosensors. *In* Methods in Cell Biology. Vol. Volume 85. F.S. Kevin, editor. Academic Press. 63-81.

Howell, Audrey S., M. Jin, C.-F. Wu, Trevin R. Zyla, Timothy C. Elston, and Daniel J. Lew. 2012. Negative Feedback Enhances Robustness in the Yeast Polarity Establishment Circuit. *Cell*. 149:322-333.

Howell, A.S., N.S. Savage, S.A. Johnson, I. Bose, A.W. Wagner, T.R. Zyla, H.F. Nijhout, M.C. Reed, A.B. Goryachev, and D.J. Lew. 2009. Singularity in Polarization: Rewiring Yeast Cells to Make Two Buds. *Cell*. 139:731-743.

Irazoqui, J.E., A.S. Gladfelter, and D.J. Lew. 2003a. Scaffold-mediated symmetry breaking by Cdc42p. *Nat Cell Biol*. 5:1062-1070.

Irazoqui, J.E., A.S. Gladfelter, and D.J. Lew. 2003b. Scaffold-mediated symmetry breaking by Cdc42p. *Nat Cell Biol*. 5:1062-1070.

Irazoqui, J.E., A.S. Howell, C.L. Theesfeld, and D.J. Lew. 2005. Opposing Roles for Actin in Cdc42p Polarization. *Mol. Biol. Cell*. 16:1296-1304.

Ito, H., Y. Fukuda, K. Murata, and A. Kimura. 1983. Transformation of intact yeast cells treated with alkali cations. *Journal of Bacteriology*. 153:163-168.

Ito, T., Y. Matsui, T. Ago, K. Ota, and H. Sumimoto. 2001. Novel modular domain PB1 recognizes PC motif to mediate functional protein–protein interactions. *The EMBO Journal*. 20:3938–3946.

Itoh, R.E., K. Kurokawa, Y. Ohba, H. Yoshizaki, N. Mochizuki, and M. Matsuda. 2002. Activation of Rac and Cdc42 Video Imaged by Fluorescent Resonance Energy Transfer-Based Single-Molecule Probes in the Membrane of Living Cells. *Molecular and Cellular Biology*. 22:6582-6591.

Iwase, M., J. Luo, S. Nagaraj, M. Longtine, H.B. Kim, B.K. Haarer, C. Caruso, Z. Tong, J.R. Pringle, and E. Bi. 2006. Role of a Cdc42p effector pathway in recruitment of the yeast septins to the presumptive bud site. *Mol Biol Cell*. 17:1110-1125.

Johnson, J.L., J.W. Erickson, and R.A. Cerione. 2009. New Insights into How the Rho Guanine Nucleotide Dissociation Inhibitor Regulates the Interaction of Cdc42 with Membranes. *Journal of Biological Chemistry*. 284:23860-23871.

Johnston, G.C., J.A. Prendergast, and R.A. Singer. 1991. The Saccharomyces cerevisiae MYO2 gene encodes an essential myosin for vectorial transport of vesicles. *J. Cell Biol.* 113:539-551.

Jonsdottir, G.A., and R. Li. 2004. Dynamics of yeast Myosin I: evidence for a possible role in scission of endocytic vesicles. *Curr Biol*. 14:1604-1609.

Jose, M., S. Tollis, D. Nair, J.-B. Sibarita, and D. McCusker. 2013. Robust polarity establishment occurs via an endocytosis-based cortical corralling mechanism. *The Journal of Cell Biology*. 200:407-418.

Kang, P.J., E. Angerman, C.-H. Jung, and H.-O. Park. 2012. Bud4 mediates the cell-type-specific assembly of the axial landmark in budding yeast. *Journal of Cell Science*. 125:3840-3849.

Kang, P.J., E. Angerman, K. Nakashima, J.R. Pringle, and H.-O. Park. 2004a. Interactions among Rax1p, Rax2p, Bud8p, and Bud9p in Marking Cortical Sites for Bipolar Bud-site Selection in Yeast. *Molecular Biology of the Cell*. 15:5145-5157.

Kang, P.J., L. Beven, S. Hariharan, and H.-O. Park. 2010. The Rsr1/Bud1 GTPase Interacts with Itself and the Cdc42 GTPase during Bud-Site Selection and Polarity Establishment in Budding Yeast. *Mol. Biol. Cell*. 21:3007-3016.

Kang, P.J., J.K. Hood-DeGrenier, and H.-O. Park. 2013. Coupling of septins to the axial landmark by Bud4 in budding yeast. *Journal of Cell Science*. 126:1218-1226.

Kang, P.J., B. Lee, and H.-O. Park. 2004b. Specific Residues of the GDP/GTP Exchange Factor Bud5p Are Involved in Establishment of the Cell Type-specific Budding Pattern in Yeast. *Journal of Biological Chemistry*. 279:27980-27985.

Kang, P.J., A. Sanson, B. Lee, and H.-O. Park. 2001. A GDP/GTP Exchange Factor Involved in Linking a Spatial Landmark to Cell Polarity. *Science*. 292:1376-1378.

Karpova, T.S., S.L. Reck-Peterson, N.B. Elkind, M.S. Mooseker, P.J. Novick, and J.A. Cooper. 2000. Role of Actin and Myo2p in Polarized Secretion and Growth of Saccharomyces cerevisiae. *Mol. Biol. Cell*. 11:1727-1737.

Kawasaki, R., K. Fujimura-Kamada, H. Toi, H. Kato, and K. Tanaka. 2003. The upstream regulator, Rsr1p, and downstream effectors, Gic1p and Gic2p, of the Cdc42p small GTPase coordinately regulate initiation of budding in Saccharomyces cerevisiae. *Genes to Cells*. 8:235-250.

Koch, G., K. Tanaka, T. Masuda, W. Yamochi, H. Nonaka, and Y. Takai. 1997. Association of the Rho family small GTP-binding proteins with Rho GDP dissociation inhibitor (Rho GDI) in Saccharomyces cerevisiae. *Oncogene*. 15:417-422.

Kozminski, K.G., L. Beven, E. Angerman, A.H.Y. Tong, C. Boone, and H.-O. Park. 2003. Interaction between a Ras and a Rho GTPase Couples Selection of a Growth Site to the Development of Cell Polarity in Yeast. *Mol. Biol. Cell*. 14:4958-4970.

Kozubowski, L., K. Saito, J.M. Johnson, A.S. Howell, T.R. Zyla, and D.J. Lew. 2008. Symmetry-Breaking Polarization Driven by a Cdc42p GEF-PAK Complex. *Current Biology*. 18:1719-1726.

Ku, C.-J., Y. Wang, Orion D. Weiner, Steven J. Altschuler, and Lani F. Wu. 2012. Network Crosstalk Dynamically Changes during Neutrophil Polarization. *Cell*. 149:1073-1083.

Lamping, E., K. Tanabe, M. Niimi, Y. Uehara, B.C. Monk, and R.D. Cannon. 2005. Characterization of the Saccharomyces cerevisiae sec6-4 mutation and tools to create S. cerevisiae strains containing the sec6-4 allele. *Gene*. 361:57-66.

Larson, S.M., and A.R. Davidson. 2000. The identification of conserved interactions within the SH3 domain by alignment of sequences and structures. *Protein Science*. 9:2170-2180.

Layton, A.T., N.S. Savage, A.S. Howell, S.Y. Carroll, D.G. Drubin, and D.J. Lew. 2011a. Modeling Vesicle Traffic Reveals Unexpected Consequences for Cdc42p-Mediated Polarity Establishment. *Current Biology*. 21:184-194.

Layton, A.T., N.S. Savage, A.S. Howell, S.Y. Carroll, D.G. Drubin, and D.J. Lew. 2011b. Modeling vesicle traffic reveals unexpected consequences for Cdc42p-mediated polarity establishment. *Curr Biol*. 21:184-194.

Li, C.H., and P.K.S. Tam. 1998. An Iterative Algorithm for Minimum Cross Entropy Thresholding. *Pattern Recognition Letters*. 18:771-776.

Li, R., and G.G. Gundersen. 2008. Beyond polymer polarity: how the cytoskeleton builds a polarized cell. *Nat Rev Mol Cell Biol*. 9:860-873.

Lin, Q., R.N. Fuji, W. Yang, and R.A. Cerione. 2003. RhoGDI Is Required for Cdc42-Mediated Cellular Transformation. *Current Biology*. 13:1469-1479.

Lingwood, D., and K. Simons. 2010. Lipid rafts as a membrane-organizing principle. *Science*. 327:46-50.

Liu, H., and A. Bretscher. 1992. Characterization of TPM1 disrupted yeast cells indicates an involvement of tropomyosin in directed vesicular transport. *J. Cell Biol.* 118:285-299.

Malinska, K., J. Malinsky, M. Opekarova, and W. Tanner. 2003. Visualization of protein compartmentation within the plasma membrane of living yeast cells. *Mol Biol Cell*. 14:4427-4436.

Marco, E., R. Wedlich-Soldner, R. Li, S.J. Altschuler, and L.F. Wu. 2007a. Endocytosis optimizes the dynamic localization of membrane proteins that regulate cortical polarity. *Cell*. 129:411-422.

Marco, E., R. Wedlich-Soldner, R. Li, S.J. Altschuler, and L.F. Wu. 2007b. Endocytosis Optimizes the Dynamic Localization of Membrane Proteins that Regulate Cortical Polarity. *Cell*. 129:411-422.

McCaffrey, L.M., and I.G. Macara. 2009. Widely Conserved Signaling Pathways in the Establishment of Cell Polarity. *Cold Spring Harbor Perspectives in Biology*. 1.

Mogilner, A., J. Allard, and R. Wollman. 2012. Cell polarity: quantitative modeling as a tool in cell biology. *Science*. 336:175-179.

Mori, Y., A. Jilkine, and L. Edelstein-Keshet. 2011. Asymptotic and Bifurcation Analysis of Wave-Pinning in a Reaction-Diffusion Model for Cell Polarization. *SIAM Journal on Applied Mathematics*. 71:1401-1427.

Mulholland, J., D. Preuss, A. Moon, A. Wong, D. Drubin, and D. Botstein. 1994. Ultrastructure of the yeast actin cytoskeleton and its association with the plasma membrane. *J Cell Biol*. 125:381-391.

Mullins, R.D. 2010. Cytoskeletal mechanisms for breaking cellular symmetry. *Cold Spring Harb Perspect Biol*. 2:a003392.

Munro, E., and B. Bowerman. 2009. Cellular Symmetry Breaking during Caenorhabditis elegans Development. *Cold Spring Harbor Perspectives in Biology*. 1.

Nern, A., and R.A. Arkowitz. 2000. Nucleocytoplasmic shuttling of the Cdc42p exchange factor Cdc24p. *J Cell Biol*. 148:1115-1122.

Newpher, T.M., R.P. Smith, V. Lemmon, and S.K. Lemmon. 2005. In vivo dynamics of clathrin and its adaptor-dependent recruitment to the actin-based endocytic machinery in yeast. *Dev Cell*. 9:87-98.

Nomanbhoy, T.K., and R.A. Cerione. 1996. Characterization of the Interaction between RhoGDI and Cdc42Hs Using Fluorescence Spectroscopy. *Journal of Biological Chemistry*. 271:10004-10009.

Norambuena, A., and M.A. Schwartz. 2011. Effects of integrin-mediated cell adhesion on plasma membrane lipid raft components and signaling. *Mol Biol Cell*. 22:3456-3464.

Novick, P., C. Field, and R. Schekman. 1980. Identification of 23 complementation groups required for post-translational events in the yeast secretory pathway. *Cell*. 21:205-215.

Onsum, M.D., and C.V. Rao. 2009. Calling heads from tails: the role of mathematical modeling in understanding cell polarization. *Current Opinion in Cell Biology*. 21:74-81.

Orlando, K., and W. Guo. 2009. Membrane organization and dynamics in cell polarity. *Cold Spring Harb Perspect Biol*. 1:a001321.

Orlando, K., X. Sun, J. Zhang, T. Lu, L. Yokomizo, P. Wang, and W. Guo. 2011. Exo-endocytic trafficking and the septin-based diffusion barrier are required for the maintenance of Cdc42p polarization during budding yeast asymmetric growth. *Mol Biol Cell*. 22:624-633.

Otsuji, M., S. Ishihara, C. Co, K. Kaibuchi, A. Mochizuki, and S. Kuroda. 2007. A Mass Conserved Reaction–Diffusion System Captures Properties of Cell Polarity. *PLoS Comput Biol*. 3:e108.

Ozbudak, E.M., A. Becskei, and A. van Oudenaarden. 2005. A System of Counteracting Feedback Loops Regulates Cdc42p Activity during Spontaneous Cell Polarization. *Developmental cell*. 9:565-571.

Park, H.-O., and E. Bi. 2007a. Central Roles of Small GTPases in the Development of Cell Polarity in Yeast and Beyond. *Microbiology and Molecular Biology Reviews*. 71:48-96.

Park, H.-O., E. Bi, J.R. Pringle, and I. Herskowitz. 1997a. Two active states of the Ras-related Bud1/Rsr1 protein bind to different effectors to determine yeast cell polarity. *Proceedings of the National Academy of Sciences*. 94:4463-4468.

Park, H.-O., P.J. Kang, and A.W. Rachfal. 2002. Localization of the Rsr1/Bud1 GTPase Involved in Selection of a Proper Growth Site in Yeast. *Journal of Biological Chemistry*. 277:26721-26724.

Park, H.O., and E. Bi. 2007b. Central roles of small GTPases in the development of cell polarity in yeast and beyond. *Microbiol Mol Biol Rev*. 71:48-96.

Park, H.O., E. Bi, J.R. Pringle, and I. Herskowitz. 1997b. Two active states of the Ras-related Bud1/Rsr1 protein bind to different effectors to determine yeast cell polarity. *Proc Natl Acad Sci U S A*. 94:4463-4468.

Parton, R.G., and J.F. Hancock. 2004. Lipid rafts and plasma membrane microorganization: insights from Ras. *Trends Cell Biol*. 14:141-147.

Peterson, J., Y. Zheng, L. Bender, A. Myers, R. Cerione, and A. Bender. 1994. Interactions between the bud emergence proteins Bem1p and Bem2p and Rho- type GTPases in yeast. *J. Cell Biol.* 127:1395-1406.

Prescianotto-Baschong, C., and H. Riezman. 1998. Morphology of the yeast endocytic pathway. *Mol Biol Cell*. 9:173-189.

Pruyne, D., A. Legesse-Miller, L. Gao, Y. Dong, and A. Bretscher. 2004. Mechanisms of polarized growth and organelle segregation in yeast. *Annual Review of Cell and Developmental Biology*. 20:559-591.

Pruyne, D.W., D.H. Schott, and A. Bretscher. 1998. Tropomyosin-containing Actin Cables Direct the Myo2p-dependent Polarized Delivery of Secretory Vesicles in Budding Yeast. *J. Cell Biol.* 143:1931-1945.

Richman, T., K. Toenjes, S. Morales, K. Cole, B. Wasserman, C. Taylor, J. Koster, M. Whelihan, and D. Johnson. 2004. Analysis of cell-cycle specific localization of the Rdi1p RhoGDI and the structural determinants required for Cdc42p membrane localization and clustering at sites of polarized growth. *Curr Genet*. 45:339-349.

Roemer, T., K. Madden, J. Chang, and M. Snyder. 1996. Selection of axial growth sites in yeast requires Axl2p, a novel plasma membrane glycoprotein. *Genes & Development*. 10:777-793.

Rosen, A., K.F. Keenan, M. Thelen, A.C. Nairn, and A. Aderem. 1990. Activation of protein kinase C results in the displacement of its myristoylated, alanine-rich substrate from punctate structures in macrophage filopodia. *J Exp Med*. 172:1211-1215.

Rubinstein, B., B.D. Slaughter, and R. Li. 2012. Weakly nonlinear analysis of symmetry breaking in cell polarity models. *Physical Biology*. 9:045006.

Sagot, I., S.K. Klee, and D. Pellman. 2002. Yeast formins regulate cell polarity by controlling the assembly of actin cables. *Nat Cell Biol*. 4:42-50.

Sanders, S.L., M. Gentzsch, W. Tanner, and I. Herskowitz. 1999. O-Glycosylation of Axl2/Bud10p by Pmt4p Is Required for Its Stability, Localization, and Function in Daughter Cells. *The Journal of Cell Biology*. 145:1177-1188.

Sanders, S.L., and I. Herskowitz. 1996. The BUD4 protein of yeast, required for axial budding, is localized to the mother/BUD neck in a cell cycle-dependent manner. *The Journal of Cell Biology*. 134:413-427.

Savage, N.S., A.T. Layton, and D.J. Lew. 2012. Mechanistic mathematical model of polarity in yeast. *Molecular Biology of the Cell*. 23:1998-2013.

Schott, D., J. Ho, D. Pruyne, and A. Bretscher. 1999. The COOH-Terminal Domain of Myo2p, a Yeast Myosin V, Has a Direct Role in Secretory Vesicle Targeting. *J. Cell Biol.* 147:791-808.

Seetapun, D., and D.J. Odde. 2010. Cell-Length-Dependent Microtubule Accumulation during Polarization. *Current Biology*. 20:979-988.

Shimada, Y., M.P. Gulli, and M. Peter. 2000. Nuclear sequestration of the exchange factor Cdc24 by Far1 regulates cell polarity during yeast mating. *Nat Cell Biol*. 2:117-124.

Shimada, Y., P. Wiget, M.-P. Gulli, E. Bi, and M. Peter. 2004a. The nucleotide exchange factor Cdc24p may be regulated by auto-inhibition. *EMBO J*. 23:1051-1062.

Shimada, Y., P. Wiget, M.-P. Gulli, E. Bi, and M. Peter. 2004b. The nucleotide exchange factor Cdc24p may be regulated by auto-inhibition. *The EMBO Journal* 23:1051–1062.

Shimada, Y., P. Wiget, M.P. Gulli, E. Bi, and M. Peter. 2004c. The nucleotide exchange factor Cdc24p may be regulated by auto-inhibition. *Embo J*. 23:1051-1062.

Slaughter, B.D., A. Das, J.W. Schwartz, B. Rubinstein, and R. Li. 2009a. Dual modes of cdc42 recycling fine-tune polarized morphogenesis. *Dev Cell*. 17:823-835.

Slaughter, B.D., A. Das, J.W. Schwartz, B. Rubinstein, and R. Li. 2009b. Dual Modes of Cdc42 Recycling Fine-Tune Polarized Morphogenesis. *Developmental cell*. 17:823-835.

Slaughter, B.D., and R. Li. 2010. Toward quantitative "in vivo biochemistry" with fluorescence fluctuation spectroscopy. *Mol Biol Cell*. 21:4306-4311.

Slaughter, B.D., S.E. Smith, and R. Li. 2009c. Symmetry Breaking in the Life Cycle of the Budding Yeast. *Cold Spring Harbor Perspectives in Biology*. 1.

Slaughter, B.D., S.E. Smith, and R. Li. 2009d. Symmetry breaking in the life cycle of the budding yeast. *Cold Spring Harb Perspect Biol*. 1:a003384.

Slaughter, B.D., J.R. Unruh, A. Das, S.E. Smith, B. Rubinstein, and R. Li. 2013. Non-uniform membrane diffusion enables steady-state cell polarization via vesicular trafficking. *Nat Commun*. 4:1380.

Slaughter, B.D., J.R. Unruh, and R. Li. 2011. Fluorescence fluctuation spectroscopy and imaging methods for examination of dynamic protein interactions in yeast. *Methods Mol Biol*. 759:283-306.

Spira, F., N.S. Mueller, G. Beck, P. von Olshausen, J. Beig, and R. Wedlich-Soldner. 2012. Patchwork organization of the yeast plasma membrane into numerous coexisting domains. *Nat Cell Biol*. 14:640-648.

Stahelin, R.V., D. Karathanassis, D. Murray, R.L. Williams, and W. Cho. 2007. Structural and Membrane Binding Analysis of the Phox Homology Domain of Bem1p: BASIS OF PHOSPHATIDYLINOSITOL 4-PHOSPHATE SPECIFICITY. *J. Biol. Chem.* 282:25737-25747.

Takizawa, P.A., J.L. DeRisi, J.E. Wilhelm, and R.D. Vale. 2000. Plasma membrane compartmentalization in yeast by messenger RNA transport and a septin diffusion barrier. *Science*. 290:341-344.

Thompson, N.L. 1991. Fluorescence Correlation Spectroscopy. *In* Topics in Fluorescence Spectroscopy Vol. 1. J.R. Lakowicz, editor. 337-378.

Tiedje, C., I. Sakwa, U. Just, and T. Höfken. 2008. The Rho GDI Rdi1 Regulates Rho GTPases by Distinct Mechanisms. *Molecular Biology of the Cell*. 19:2885-2896.
Toenjes, K.A., M.M. Sawyer, and D.I. Johnson. 1999. The guanine-nucleotide-exchange factor Cdc24p is targeted to the nucleus and polarized growth sites. *Curr Biol*. 9:1183-1186.
Togawa, A., J. Miyoshi, H. Ishizaki, M. Tanaka, A. Takakura, H. Nishioka, H. Yoshida, T. Doi, A. Mizoguchi, N. Matsuura, Y. Niho, Y. Nishimune, S.-i. Nishikawa, and Y. Takai. 1999. Progressive impairment of kidneys and reproductive organs in mice lacking Rho GDI. 18:5373-5380.
Tong, Z., X.-D. Gao, A.S. Howell, I. Bose, D.J. Lew, and E. Bi. 2007. Adjacent positioning of cellular structures enabled by a Cdc42 GTPase-activating proteinâ€“mediated zone of inhibition. *The Journal of Cell Biology*. 179:1375-1384.
Turing, A.M. 1952. The Chemical Basis of Morphogenesis. *Philosophical Transactions of The Royal Society of London*. 237:37-72.
Valdez-Taubas, J., and H.R. Pelham. 2003. Slow diffusion of proteins in the yeast plasma membrane allows polarity to be maintained by endocytic cycling. *Curr Biol*. 13:1636-1640.
van Drogen-Petit, A., C. Zwahlen, M. Peter, and A.M.J.J. Bonvin. 2004. Insight into Molecular Interactions Between Two PB1 Domains. *Journal of Molecular Biology*. 336:1195-1210.
van Steensel, B., E.P. van Binnendijk, C.D. Hornsby, H.T. van der Voort, Z.S. Krozowski, E.R. de Kloet, and R. van Driel. 1996. Partial colocalization of glucocorticoid and mineralocorticoid receptors in discrete compartments in nuclei of rat hippocampus neurons. *J Cell Sci*. 109 (Pt 4):787-792.
Wai, S.C., S.A. Gerber, and R. Li. 2009. Multisite Phosphorylation of the Guanine Nucleotide Exchange Factor Cdc24 during Yeast Cell Polarization. *PLoS ONE*. 4:e6563.
Wedlich-Soldner, R., S. Altschuler, L. Wu, and R. Li. 2003a. Spontaneous Cell Polarization Through Actomyosin-Based Delivery of the Cdc42 GTPase. *Science*. 299:1231-1235.
Wedlich-Soldner, R., S. Altschuler, L. Wu, and R. Li. 2003b. Spontaneous cell polarization through actomyosin-based delivery of the Cdc42 GTPase. *Science*. 299:1231-1235.
Wedlich-Soldner, R., and R. Li. 2008. Yeast and fungal morphogenesis from an evolutionary perspective. *Seminars in Cell & Developmental Biology*. 19:224-233.
Wedlich-Soldner, R., S.C. Wai, T. Schmidt, and R. Li. 2004a. Robust cell polarity is a dynamic state established by coupling transport and GTPase signaling. *J. Cell Biol.* . 166:889-900.
Wedlich-Soldner, R., S.C. Wai, T. Schmidt, and R. Li. 2004b. Robust cell polarity is a dynamic state established by coupling transport and GTPase signaling. *J Cell Biol*. 166:889-900.
Winters, M.J., and P.M. Pryciak. 2005. Interaction with the SH3 Domain Protein Bem1 Regulates Signaling by the Saccharomyces cerevisiae p21-Activated Kinase Ste20. *Mol. Cell. Biol.* 25:2177-2190.
Wu, H., C. Turner, J. Gardner, B. Temple, and P. Brennwald. 2010. The Exo70 subunit of the exocyst is an effector for both Cdc42 and Rho3 function in polarized exocytosis. *Mol Biol Cell*. 21:430-442.
Yamaguchi, Y., K. Ota, and T. Ito. 2007. A Novel Cdc42-interacting Domain of the Yeast Polarity Establishment Protein Bem1: Implications for modulation of mating pheromone signaling. *J. Biol. Chem.* 282:29-38.
Yeung, T., G.E. Gilbert, J. Shi, J. Silvius, A. Kapus, and S. Grinstein. 2008. Membrane phosphatidylserine regulates surface charge and protein localization. *Science*. 319:210-213.

Zahner, J.E., H.A. Harkins, and J.R. Pringle. 1996. Genetic analysis of the bipolar pattern of bud site selection in the yeast Saccharomyces cerevisiae. *Molecular and Cellular Biology*. 16:1857-1870.

Zajac, A., X. Sun, J. Zhang, and W. Guo. 2005. Cyclical Regulation of the Exocyst and Cell Polarity Determinants for Polarized Cell Growth. *Mol. Biol. Cell*. 16:1500-1512.

Zhang, X., K. Orlando, B. He, F. Xi, J. Zhang, A. Zajac, and W. Guo. 2008. Membrane association and functional regulation of Sec3 by phospholipids and Cdc42. *J Cell Biol*. 180:145-158.

Zheng, Y., A. Bender, and R.A. Cerione. 1995a. Interactions among Proteins Involved in Bud-site Selection and Bud-site Assembly in Saccharomyces cerevisiae. *J. Biol. Chem.* 270:626-630.

Zheng, Y., A. Bender, and R.A. Cerione. 1995b. Interactions among proteins involved in bud-site selection and bud-site assembly in Saccharomyces cerevisiae. *J Biol Chem*. 270:626-630.

Ziman, M., D. Preuss, J. Mulholland, J.M. O'Brien, D. Botstein, and D.I. Johnson. 1993. Subcellular localization of Cdc42p, a Saccharomyces cerevisiae GTP-binding protein involved in the control of cell polarity. *Mol Biol Cell*. 4:1307-1316.